Characterisation of Membranes Using Electrochemical Impedance Spectroscopy (EIS) and Computational Fluid Dynamics (CFD)

JJ Smit • GP Greyvenstein

Report to the Water Research Commission
by the
Department of Chemical and Mechanical Engineering
Potchefstroom University for CHE

WRC Report No 529/1/97

CHARACTERISATION OF MEMBRANES USING ELECTRO-CHEMICAL IMPEDANCE SPECTROSCOPY (EIS) AND COMPUTATIONAL FLUID DYNAMICS (CFD)

Final Report to the
Water Research Commission

by

J J Smit and G P Greyvenstein

Department of Chemical and Mechanical Engineering
Potchefstroom University for CHE
Private Bag X6001
Potchefstroom 2520

WRC Project No. 529/1/97
ISBN 1 86845 273 5

EXECUTIVE SUMMARY

CHARACTERISATION OF MEMBRANES USING ELECTRO-CHEMICAL IMPEDANCE SPECTROSCOPY (EIS) AND COMPUTATIONAL FLUID DYNAMICS (CFD).

by

J.J. SMIT and G.P. GREYVENSTEIN

Potchefstroom University for CHE.
Departments of Chemical and Mechanical
Engineering, P.U. for CHE., Private bag X6001
Potchefstroom 2520

A. EXECUTIVE SUMMARY

A.1 INTRODUCTION AND MOTIVATIONAL STATEMENT

The characterisation of membranes or other porous materials is normally undertaken by means of invasive methods such as scanning electron microscopy, mercury porosimetry, bubble point effects and permeability effects. There is currently no method available to determine membrane characteristics such as porosity, permeability, tortuosity compaction etc. before, during and after usage.

This investigation attempts to quantify membrane characteristics (such as porosity) by means of the Electrochemical Impedance Spectroscopy (EIS) and Computational Fluid Dynamics (CFD). The report is therefore presented in two parts pertaining to EIS and CFD respectively. The EIS section of this report endeavours to model a membrane/electrolyte system as an electrical circuit containing a number of capacitances and resistances (conductances).

This would enable the flow of mass through a membrane to be simulated to a "flow" of electrons. If this simulation can be successfully modeled it implies that the flow dynamic (hydrodynamic) characteristics of mass transfer could be equivalated by the flow dynamics of electrical charge (electrons). From such an equivalation between EIS and CFD it would consequently be possible to equivalate and measure parameters such as permeability, compaction, fouling and concentration polarisation directly as electrical variables.

These variables could then by equivalation (dimensional analysis) be translated to their physical counterparts (membrane thickness, tortuosity, compaction) or their hydrodynamic (permeability, flow density, hydraulic resistance) counterparts.

The synergism of simultaneous EIS and CFD investigations is immediately obvious but some detail is necessary to describe the envisaged interaction of the two techniques:-

EIS employs an alternating current between two electrode pairs to generate impedance spectra over a frequency range in an electrolyte. If any discontinuity in the flow path of electrons is experienced this can be "seen" on the impedance spectra. If this discontinuity is a porous membrane, very specific capacitance (C) and impedances (R) can be identified, measured and subsequently modeled in an electric circuit. The RC-components of this circuit can now be measured electrically and with great accuracy in either a flow mode (like in RO or UF) or under static conditions.

CFD, on the other hand, was developed separately to yield profiles of trans-membrane variables, intra-membrane variables and membrane proximity variables such as for example.

- pressure-gradient, permeability (trans-membrane)
- compaction, tortuosity, porosity (intramembrane)
- concentration-gradient, density profile, viscosity profile, velocity profile etc. (membrane-proximity)

It is obvious that there must be a close relationship between the hydraulic resistance for example and the electrical resistance. Furthermore electrical capacity could be equivalated to porosity and/or retention time of flow through the porous capillaries. It was indeed found (also substantiated in literature) that porosity can be calculated from EIS measurements.

The CFD studies presented here use novel and advanced finite volume analysis to simulate a tubular RO element with permeation from inside to outside diameter. The solution protocol integrates all nonlinear physical relationships in a stepping calculative procedure. A computer disc is available with user friendly selection menu which prompts the selection of tube diameter, feed rate and concentration to yield the range of response variables previously listed.

A.2 THE AIMS OF THIS RESEARCH:-

The research concerning both parts demanded substantial fundamental investigation, development and verification of results.

The CFD procedure called for a large number of internal loop routines integrated with the main program. These were necessary for the iterative convergence of especially the nonlinear relationships between viscosity, density, concentration and osmotic pressure with changes in temperature, axial position and temperature.

The EIS procedure presented more problems mainly associated with this fairly novel application. The following were the main goals for the two-tiered research.

EIS GOALS:

A.2.1 The development of a suitable electrolytic cell with a satisfactory electrode configuration with which to generate the impedance spectra.

A.2.2 The development and quantification of a method which determines the character (hydrophobic or hydrophilic) of membranes for comparison between membranes.

A.2.3 The static modelling of a membrane, in a standard electrolyte, as a resistance/capacitance (RC) electrical circuit of which the RC elements can be measured.

A.2.4 The determination of temperature sensitivity of the R and C elements in the model.

A.2.5 The qualification of the interdependence of the RC-elements on electrolyte type, concentration and active membrane area.

A.2.6 The derivation of certain physical properties of the membrane such as, for example, porosity.

A.2.7 An assessment of further calculative properties to be derived from these electrical measurements.

A.2.8 An assessment of the same goals (A.2.1 - A.2.7) using membranes in the dynamic flow situations called for by RO and UF systems. This would mainly call for an integration between EIS and CFD regarding the equivalation of electric variables to their hydrodynamic flow counterparts.

In summary it is seen that the CFD research was developed fast towards the "integration" point. Being a more fundamental research assignment the EIS-programme is currently not yet advanced to the "integration" stage and still needs substantial fundamental interpretative research. It is also for this reason that the final phase of this combined research effort could not yet be attained.

The first six goals as stated were however attained and could be furthered to other physical parameters as mentioned in A.2.7. The final phase of the research viz the integration of CFD and EIS can only be finalised and its effects realised with further research of a highly applied character. The following are visualised as research products to be derived from continued research.

POTENTIAL RESEARCH PRODUCT 1

The equivalation potential of dynamic parameters such as permeability, fouling, compaction and concentration polarisation to particular electrically measured variables such as capacitance and impedance.

POTENTIAL RESEARCH PRODUCT 2

The potential to relate the directly measurable electrical characteristics as inputs to a control protocol to effect the operation of the membrane in a continuously optimised mode.

POTENTIAL RESEARCH PRODUCT 3

The equivalated hydrodynamic/electrical variables, or combinations, can now be adapted as predictors for membrane conditions (in situ) to indicate and assess adverse, undesirable phenomena such as increased tortuosity, compaction, plastic deformation, and concentration polarisation extremities. The continuous measurement of these variables enhances the control potential as well as the optimisation of pressure driven processes.

POTENTIAL RESEARCH PRODUCT 4

The combined synergism between EIS and CFD will strengthen the effects and the positive aspects of the previous potential products.

A.3 A BRIEF SUMMARY OF RESULTS

The investigation indicates that characterisation of membranes is possible on aspects such as:

- hydrophobicity/hydrophilicity
- porosity measurement.
- determination of the capacitances, impedances and conductances from the electrical RC-modelled circuit.

In this respect the objectives (A.2.1 - A.2.6) were attained. The translation or transformation of these electrical properties to their hydrodynamic counterparts is however not yet completed.

A.4 POSSIBLE TECHNOLOGY TRANSFER

The determination of hydrophobicity/hydrophilicity of a membrane as well as its porosity can now be effected under static conditions.

An extended range of membranes (10 membranes of Russian origin) investigated gave good results on the classification between hydrophobic/hydrophilic discrimination. Some in-depth investigation is however still necessary to clarify peculiarities. Refer to § A.6.1.2.

The concept could be extended and explored for catalyst support media, filter applications, quantification of fouling in general and possible measurement of thickness of the membrane under operating conditions.

A.5 RECOMMENDATIONS

1. The investigation which was executed from a bare concept clearly indicates and motivates the further development of the concept in subsequent research efforts.

2. The detailed transformation between electrochemical responses and their hydrodynamic counter parts have not been demonstrated. Although it was intended as phase 3 of this project (refer to the original proposal p10 B.5.1) the fundamentals of the static qualification and verification were prioritised.

   Subsequent research would therefore have to elucidate this additional potential.

3. Although substantial information was derived from the impedance spectra coupled to the electrochemical double layer theory a vast grey area still exists around the interpretation of all the peculiarities presented on the spectra. This would call for a fundamental assessment of probably the influence of inductance, coupled capacities and could call for a revision of the simple model suggested now.

4. One of the more prominent features for the EIS-spectra indicates that the multilayer of membranes like the RO types could now be "seen" separately and possible modeled. This aspect alone motivates further investigation as it is this layer which imparts the properties to the membrane in most cases like RO and the discriminative ED membranes.

A.6 HIGHLIGHTS OF RESULTS TO BE READ WITH EXECUTIVE SUMMARY

The following aspects are highly condensed results presented to illustrate and substantiate the most important results mentioned in the "Executive Summary".

A.6.1 CONDENSED EIS RESULTS:-

A.6.1.1 ELECTROCHEMICAL MODEL AND DISCRIMINATION POTENTIAL

From EIS spectra a simplified model was selected to represent the system response as an electrical circuit with RC-components as follows:-

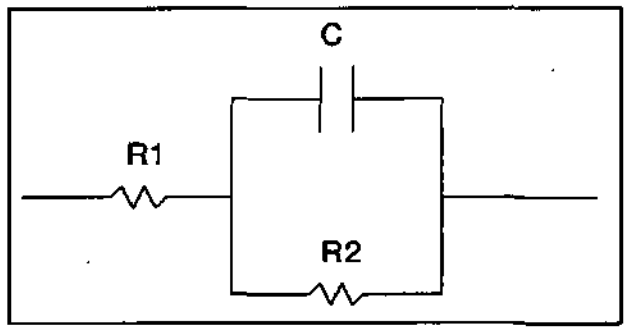

R_1 = resistive component of the impedance of the electrolyte

R_2 = resistive component of the impedance of the membrane

C = capacitance of the membrane

These RC-values were obtained from the Nyquist plot of the impedance spectra in the following way:-

- the Bode plot yields the magnitude(Z) and the phase angle(ϕ) vs frequency(ω)

- from this information the Nyquist plot can be drawn which yields the R_1 and $R_1 + R_2$ values when the imaginary part of the impedance is zero.

$$|-Z''| = 0 \text{ yields } |Z'| = R_1 \text{ or } R_1 + R_2$$

where R_1 = electrolyte resistance

R_1+R_2 = electrolyte + membrane resistance

The result of a typical calculation and plot sequence is shown in figures A1 and A2 below for a Celgard hydrophobic and hydrophilic membrane as well as on figures A.3 and A.4 for two selected Russian membranes. The Russian membranes also consisted of a hydrophobic and a hydrophilic sample respectively.

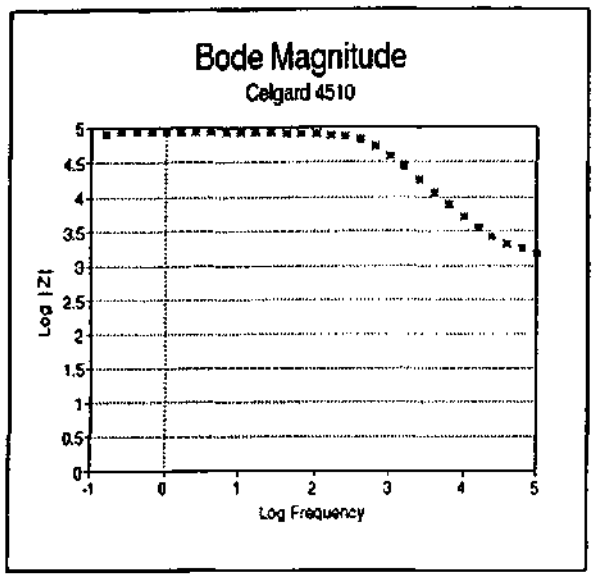

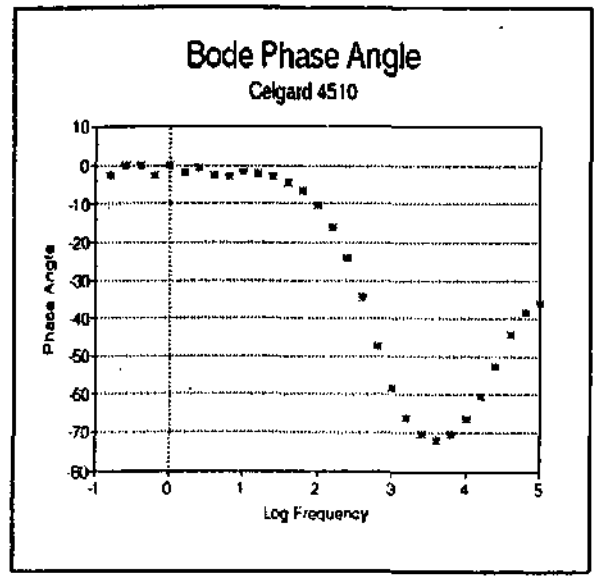

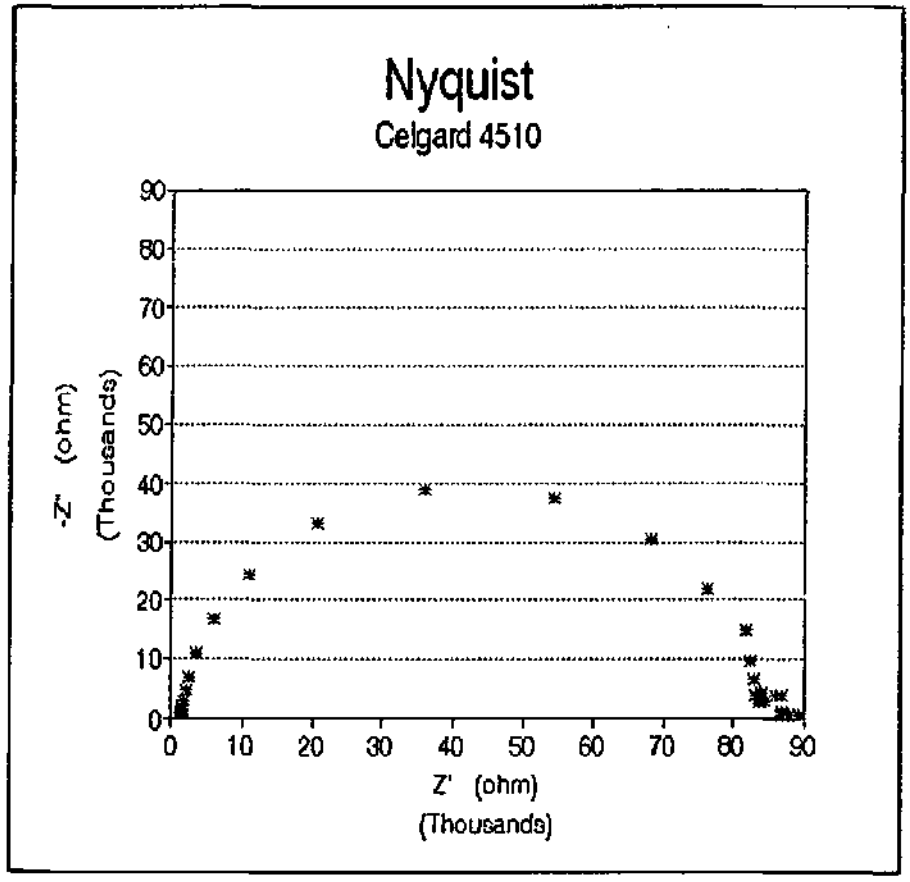

Figure A1 Bode- and Nyquist plots for the Celgard 4510 hydrophobic membrane.

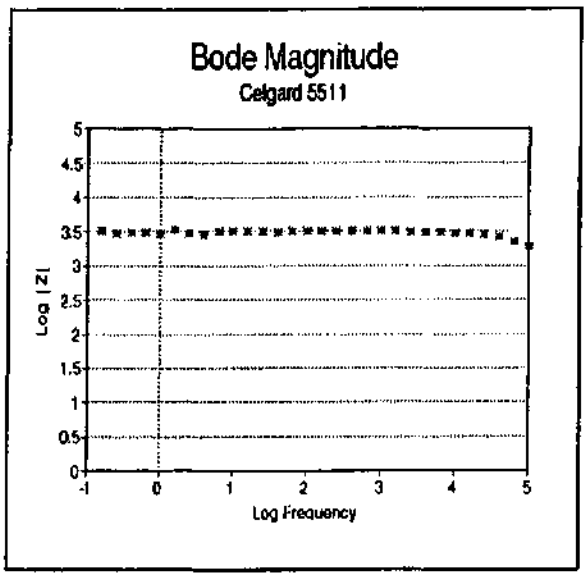

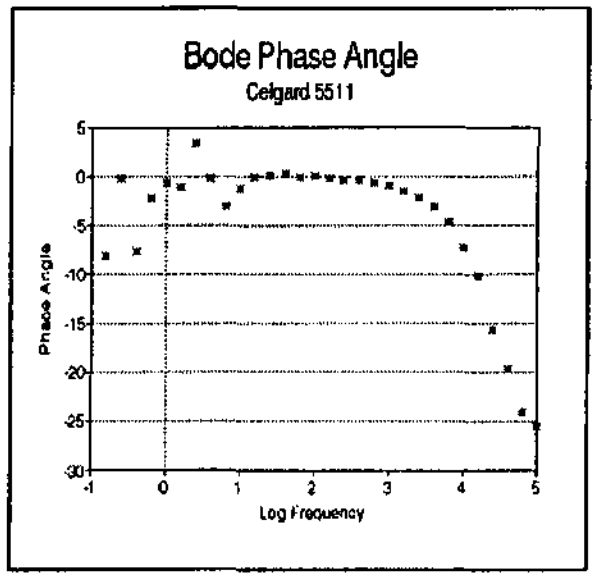

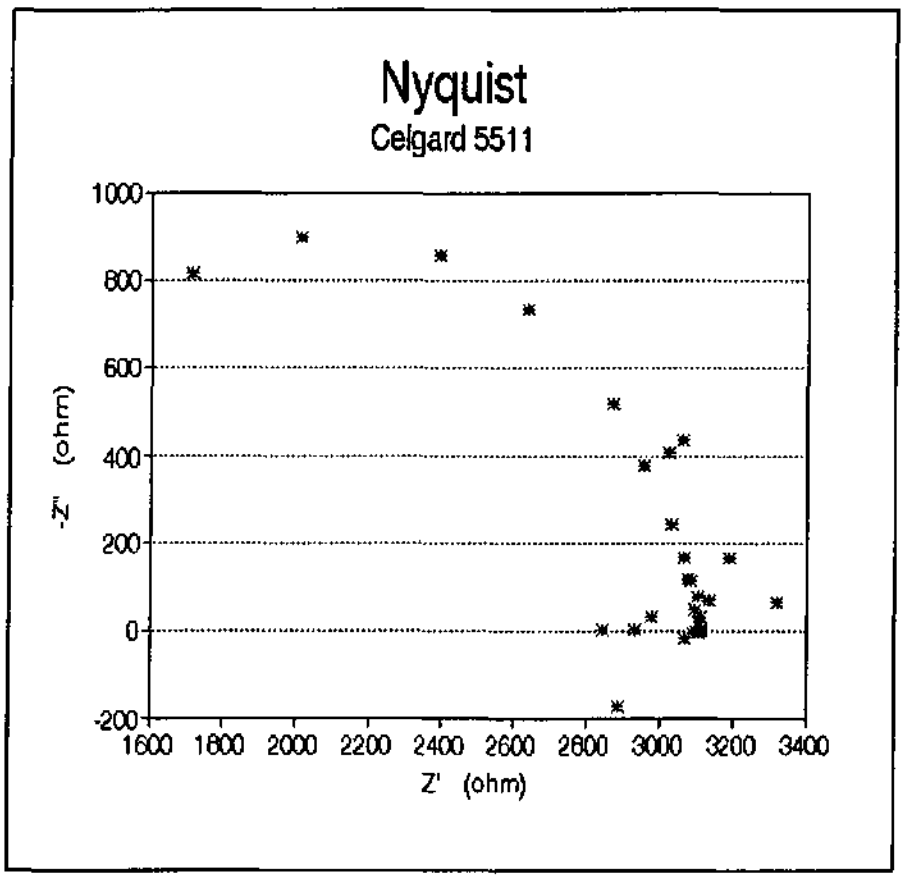

Figure A2 Bode- and Nyquist plots for the Celgard 5511 hydrophilic membrane.

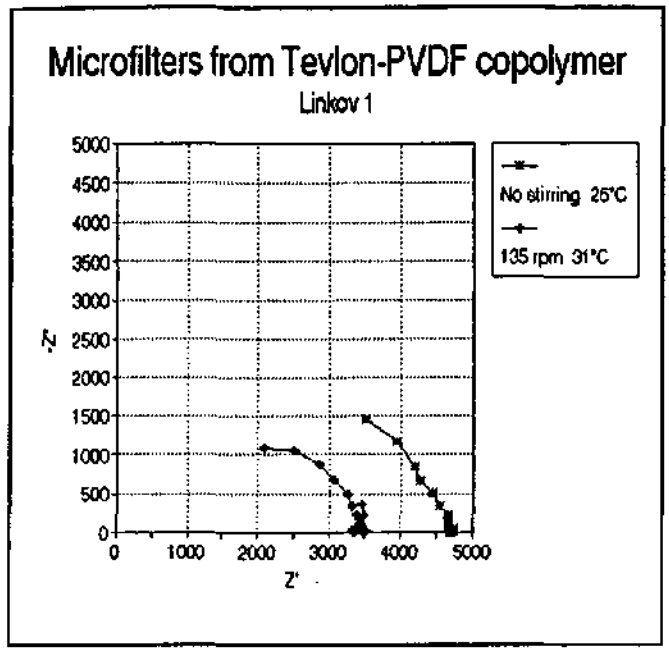

Figure A3 EIS spectrum of hydrophilic membrane

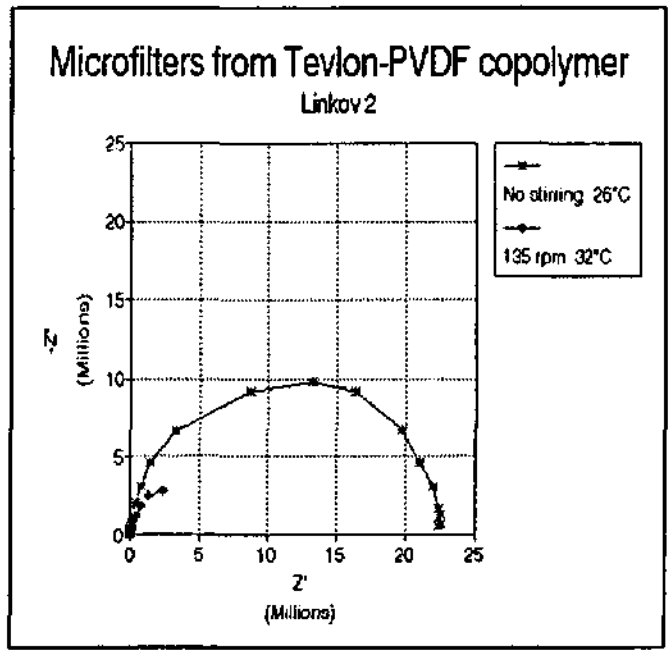

Figure A4 EIS spectrum of hydrophobic membrane

From an inspection of figures A3 and A4 it can be clearly seen that a substantial difference exists between the resistance values of the hydrophobic and the hydrophilic membrane types.

A.6.1.2 THE COMPARISON OF RC VALUES FOR TEN DIFFERENT MEMBRANES FROM RUSSIAN ORIGIN.

Referring to Table A.1 it is immediately obvious that substantial differences occur in the values of especially R_2 and C between the different membranes at different temperatures and at different agitation in the cell. The membrane descriptions are as follows.

TABLE OF RUSSIAN MEMBRANES AS SUPPLIED BY V. LINKOV

TABLE 10B

MEMBRANES OF RUSSIAN ORIGIN CHARACTERISED BY EIS

No	Type	Pore Size(μ)	Flux $l.m^{-2}hr^{-1}$	Temp °C	Rejec-tion(%)	P(MPa)	Medium %NaCl	HL/HB
1	MF(PVDF)	0.4	15000	< 80				HL
2	MF(PVDF)	0.15		< 80				HB
3	UF(PA)	kD/50	60-1560		> 95			HL
4	RO(PA)		100	50	90	3	0.5	HL
5	UF(PA)	kD/10	60-1560		95			HL
6	UF(PS)	kD/100						HL
7	UF(PVDF)		1000	< 80				HB
8	UF(PVDF)	0.09	35					HL
9	UF(PSA)	kD/50	120		99.7			HL
10	UF(PSA)		100		95			HL

PVDF	Polyvinylideneflouride	MF	Micro filtration
UF	Ultrafiltration	PA	Polyamide
PSA	Polysulphonamide	RO	Reverse Osmosis
HL	Hydrophilic	HB	Hydrophobic

TABLE 10
EIS RESULTS OF RUSSIAN MEMBRANES

NO STIRRING

	Time (hr)	0	1		2		3	
1	25 °C						26 °C	
	R1	2370	R1	2140	R1	1942	R1	1900
	R2	3575	R2	3363	R2	3161	R2	2776
	C	6.297E-10	C	5.358E-10	C	4.933E-10	C	5.375E-10
2	25°C						26°C	
	R1	4370	R1	3896	R1	3872	R1	3804
	R2	10363869	R2	18959232	R2	20048608	R2	21606399
	C	9.897E-10	C	1.059E-09	C	1.109E-09	C	1.136E-09
3	25°C						26°C	
	R1	2492	R1	2273	R1	2260	R1	2110
	R2	2967	R2	2993	R2	2752	R2	2706
	C	7.353E-10	C	6.441E-10	C	6.933E-10	C	6.774E-10
4	25°C						26°C	
	R1	2736	R1	2185	R1	2119	R1	2041
	R2	3287	R2	3170	R2	2836	R2	2720
	C	8.495E-10	C	5.328E-10	C	6.118E-10	C	6.182E-10
5	25°C						26°C	
	R1	2555	R1	2288	R1	2184	R1	2161
	R2	3912	R2	3641	R2	3440	R2	3377
	C	5.984E-10	C	5.249E-10	C	5.166E-10	C	5.312E-10

TABLE 10 (Continue)

EIS RESULTS OF RUSSIAN MEMBRANES

NO STIRRING

	Time (hr)	0	1		2		3	
6	24°C						25°C	
	R1	2589	R1	2516	R1	2421	R1	1131
	R2	3837	R2	3636	R2	3507	R2	4569
	C	6.91E-10	C	6.609E-10	C	6.398E-10	C	6.196E-10
7	25°C						25°C	
	R1	5647	R1	5036	R1	5059	R1	4993
	R2	2118183	R2	1520873	R2	1659073	R2	1741057
	C	1.926E-09	C	1.999E-09	C	2.046E-09	C	2.084E-09
8	24°C						25°C	
	R1	2548	R1	2490	R1	2425	R1	2352
	R2	3341	R2	3015	R2	2897	R2	2792
	C	8.33E-10	C	7.572E-10	C	7.706E-10	C	7.271E-10
9	23°C						25°C	
	R1	2687	R1	2548	R1	2354	R1	2431
	R2	3463	R2	3334	R2	3391	R2	3177
	C	1.113E-09	C	9.885E-10	C	8.112E-10	C	8.729E-10
10	25°C						26°C	
	R1	2819	R1	2515	R1	2597	R1	2463
	R2	3043	R2	2916	R2	2712	R2	2657
	C	8.416E-10	C	8.367E-10	C	9.193E-10	C	8.785E-10

TABLE 10 (Continue)

EIS RESULTS OF RUSSIAN MEMBRANES

STIRRING 135 r.p.m.

	Time (hr)	0	1		2		3	
1	26°C						31°C	
	R1	1627	R1	1476	R1	1384	R1	1285
	R2	2827	R2	2610	R2	2390	R2	2159
	C	9.686E-10	C	9.69E-10	C	1.011E-09	C	1.032E-09
2	26°C						32°C	
	R1	3455	R1	3261	R1	3049	R1	3028
	R2	9108536	R2	8731632	R2	8360625	R2	7417223
	C	1.165E-09	C	2.229E-09	C	2.676E-09	C	2.7E-09
3	26°C						32°C	
	R1	2003	R1	1743	R1	1608	R1	1471
	R2	2806	R2	2528	R2	2257	R2	1996
	C	1.331E-09	C	1.081E-09	C	1.068E-09	C	1.071E-09
4	26°C						32°C	
	R1	2047	R1	1964	R1	1774	R1	1668
	R2	2937	R2	2740	R2	2442	R2	2243
	C	1.138E-09	C	1.077E-09	C	1.046E-09	C	1.07E-09
5	26°C						30°C	
	R1	2289	R1	2145	R1	2036	R1	1974
	R2	3345	R2	3177	R2	2898	R2	2753
	C	1.115E-09	C	1.084E-09	C	1.104E-09	C	1.133E-09

TABLE 10 (Continue)

EIS RESULTS OF RUSSIAN MEMBRANES

STIRRING 135 r.p.m.

	Time (hr)	0	1		2		3	
6	25°C						30°C	
	R1	2226	R1	2082	R1	1504	R1	1570
	R2	3662	R2	3512	R2	3299	R2	2927
	C	1.135E-09	C	1.061E-09	C	1.585E-09	C	1.365E-09
7	25°C						30°C	
	R1	3757	R1	3981	R1	4010	R1	3862
	R2	1877623	R2	803806	R2	269521	R2	214122
	C	2.075E-09	C	4.181E-09	C	7.028E-09	C	7.814E-09
8	25°C						30°C	
	R1	2258	R1	1908	R1	1741	R1	1609
	R2	2927	R2	2532	R2	2270	R2	2057
	C	1.388E-09	C	1.132E-09	C	1.144E-09	C	1.168E-09
9	25°C						30°C	
	R1	2302	R1	2188	R1	2149	R1	2047
	R2	3527	R2	3291	R2	2997	R2	2866
	C	1.406E-09	C	1.128E-09	C	1.574E-09	C	1.234E-09
10	26°C						30°C	
	R1	2313	R1	2120	R1	1907	R1	1780
	R2	3035	R2	2888	R2	2495	R2	2272
	C	1.274E-09	C	1.153E-09	C	1.251E-09	C	1.214E-09

A.6.1.3 THE CALCULATION OF POROSITY FROM EIS-SPECTRA.

The following calculative sequence illustrates a way of calculating the porosity for a specific membrane.

From the capacitance of the interface C_T, the capacitances C_1 and C_2 lead to the porosity of the membrane from calculation. The following analysis shows how the porosity is calculated. If, adjacent to the membrane, there is a layer in contact with the electrolyte then

$$C_p = \frac{A_{pore}\epsilon_\omega\epsilon_0}{d} \qquad (1.1)$$

where C_p is the capacitance of the electrolyte filled pores. Here d is the thickness, ϵ_0 is the permittivity of free space and ϵ_ω , and ϵ_m are the dielectric constant for water and the polymer membrane respectively.

A_{pore} = total area of the pores and A_{pore} = (A)(p) where p is the porosity and A is the area of the membrane.

The conductance of the membrane bulk (phase 2) is taken as approaching zero.
Phase 1 has a capacitance $C_{(skin\ layer)}$.
Then

$$C_{(skinlayer)} = \frac{(A_{skin})(\epsilon_m)(\epsilon_0)}{d} \qquad (1.2)$$

where A_{skin} = A = total skin area.
The total skin area, excluding pores, will be given by (1-p)(A).

Total capacitance

$$C_1 = C_p + C_{skin} = \frac{[(\epsilon_\omega)(\epsilon_0)(A)(p)] + [(\epsilon_m)(\epsilon_0)(1 - p)A]}{d} \quad (1.3)$$

Calculation of the porosity, p (in %), is from:

$$p = \frac{\left(\frac{dC_1}{\epsilon_0 A} - \epsilon_m \right)}{(\epsilon_\omega - \epsilon_m)} \quad (1.4)$$

A.6.1.4 SPECTRUM OF TWO-PHASE MODEL AS SEEN BY EIS.

There are two possible two-phase models namely,

(1) double layer/membrane skin

(2) membrane skin/membrane bulk

The two different double layers, i.e. NaF and KC*l*, hardly differ in their EIS spectrum data. With a hydrophobic membrane and 150 mg/l KC*l* solution the value of C_T is about 3.0×10^{-9} F/m^2 and with 150 mg/l NaF solution the value of C_T is about 3.6×10^{-9} F/m^2. The value of C_T is not very different whether a hydrophobic or hydrophilic membrane is used. The actual value of C_T = 0.546 μF/m^2 was experimentally determined in the system 15 mg/l KC*l* solution / hydrophobic membrane. It was calculated that the value of C_1, (phase 1) would have to be between 20 and 200 μF/m^2 to yield C_T = 0.546 μF/m^2. Thus the model(l) is not being seen. Model(2) where C_1 is far less conducting than the double layer capacity of 36000 μF/m^2 is the correct model. The hydrophilic membrane, shows an incomplete Nyquist plot over the frequency range 1 - 10^5 Hz and this implies that the bulk membrane/skin layer may only be seen at even higher frequencies where C_1 should be fairly large as predicted.

In dilute electrolyte solutions the two-phase model is more likely to resemble the actual situation than in concentrated solutions where a three-phase model might be more correct.

It can consequently be expected that an improved resolution of the spectra for double layer investigation could be derived, increasing the spectra to frequencies beyond 10^6 Hz. This might indeed yield valuable information on especially anisotropic (multilayer) membranes (RO) or charge selective membranes (or species selective membranes) with (ED).

A.6.1.5 A CONCISE SUMMARY OF CFD IVESTIGATION.

This report deals with the development of a numerical model to simulate the transfer processes in a cylindrical membrane. The model predicts the radial and axial distribution of velocity components and ion concentration as well as the axial variation of pressure. The ion concentration at the wall was used to predict the osmotic pressure which, together with the inside and outside pressures, determine the driving force for reverse osmosis. With the driving force known, the permeate and ion fluxes through the membrane are calculated. These fluxes are functions of axial position. The model also takes the variation in diameter due to pressure loading into consideration.

The basic model was tested by comparing it with an approximate analytical method. It was found that the results of the two methods agree very well. The model was also applied to a membrane and it is shown that the model behaves qualitatively correct.

An investigation was being done to determine the effect of inlet pressure, inlet velocity, diameter and length-to-diameter ratio on separation efficiency. It was shown that separation efficiency decreases with diameter, velocity and inlet concentration while it increases with length-to-diameter ratio. Separation increases with inlet pressure up to a certain value and then decreases.

This study showed that the numerical model can successfully predict the transfer of mass and momentum in a cylindrical membrane, taking all the fundamental transfer mechanisms into account.

TABLE OF CONTENTS

A. EXECUTIVE SUMMARY A2

A.1 INTRODUCTION AND MOTIVATIONAL STATEMENT A2

A.2 THE AIMS OF THIS RESEARCH:- A4

A.3 A BRIEF SUMMARY OF RESULTS A6

A.4 POSSIBLE TECHNOLOGY TRANSFER A7

A.5 RECOMMENDATIONS A7

A.6 HIGHLIGHTS OF RESULTS TO BE READ WITH EXECUTIVE SUMMARY A8

A.6.1 CONDENSED EIS RESULTS:- A8

A.6.1.1 ELECTROCHEMICAL MODEL AND DISCRIMINATION POTENTIAL A8

A.6.1.2 THE COMPARISON OF RC VALUES FOR TEN DIFFERENT MEMBRANES FROM RUSSIAN ORIGIN. A13

A.6.1.3 THE CALCULATION OF POROSITY FROM EIS-SPECTRA. A18

A.6.1.4 SPECTRUM OF TWO-PHASE MODEL AS SEEN BY EIS. A19

A.6.1.5 A CONCISE SUMMARY OF CFD IVESTIGATION. A20

B. GENERAL INTRODUCTION 1

B.1 MOTIVATION 1

B.2 A CONCISE DESCRIPTION OF THE EIS PROCEDURE 5

B.2.1 THE ELECTROCHEMICAL DOUBLE-LAYER AND RELATED THEORIES 5

B.2.2 THE EIS APPLICATION TO MEMBRANES AND A LITERATURE SURVEY OF ITS USE 6

B.2.3 A THEORETICAL OVERVIEW ON EIS APPLICATION FOR CHARACTERISATION OF POROUS MEDIA. 7

B.2.3.1 TEMPERATURE DEPENDENCE OF (EIS) SPECTRA 8

B.2.3.2 CAPACITY OF THE DOUBLE LAYER - A THEORETICAL EXTRACT 9

B.2.3.3 EFFECT OF CATION AND ANION VARIATION ON THE CALCULATION OF DOUBLE LAYER CAPACITANCE. 14

B.2.3.3.1 INNER LAYER 14

B.2.3.3.2 CAPACITY OF THE INNER LAYER AS A FUNCTION OF CONCENTRATION 15

B.2.3.3.3 CAPACITANCE OF INDIVIDUAL CATIONS AND ANIONS 16

B.2.3.4 CONDUCTANCE OF THE DOUBLE-LAYER 17

B.2.3.5 VARIATION OF CAPACITANCE WITH TEMPERATURE 23

B.2.3.6 CONDUCTANCE VARIATION OF THE DOUBLE LAYER WITH TEMPERATURE 27

B.2.3.7 VARIATION OF CAPACITANCE OF KCl WITH TEMPERATURE 28

B.2.3.8 MODEL OF THE KCl/MEMBRANE INTERFACE 29

B.2.3.9 VARIATION OF MEMBRANE CAPACITANCE 34

B.2.3.10 EFFECT OF C_1 AND$_2$ C VARIATION ON THE CONDUCTANCE OF THE INTERFACE 36

B.2.3.11 TEST OF THE KCl/MEMBRANE THEORY 39

B.2.3.12 STUDY OF THE ELECTROLYTE SIDE OF THE INTERFACE

A23

44

B.2.4 CHARACTERISATION OF MEMBRANES ACCORDING TO R_1, R_2 AND C_T 49

B.2.5 CONCLUSION 62

B.2.5.1. DISCRIMINATION BETWEEN LAYERS CONSTITUTING THE MEMBRANE CAPACITY 62

B.2.5.2 TWO PHASE MODEL OF AN INTERFACE - FREQUENCY DEPENDENCE OF THE CAPACITY AND CONDUCTANCE 63

B.3 NUMERICAL MODEL FOR THE PREDICTION OF THE TRANSFER PROCESSES IN A CYLINDRICAL MEMBRANE 67

B.3.1. INTRODUCTION 67

B.3.2 PURPOSE 68

B.3.3. GOVERNING EQUATIONS 68

B.3.3.1. ASSUMPTIONS 68

B.3.3.2. COORDINATE SYSTEM 69

B.3.3.3. PARTIAL DIFFERENTIAL EQUATIONS 70

B.3.3.4. SIMPLIFIED PARTIAL DIFFERENTIAL EQUATIONS 72

B.3.3.5. OVERALL CONTINUITY EQUATION AND DENSITY 75

B.3.3.6. EQUATION FOR THE WALL VELOCITY 77

B.3.3.7. TRANSPORT COEFFICIENT FOR THE MASS FRACTION EQUATION 78

B.3.3.8. DETERMINATION OF INSIDE TUBE DIAMETER. 79

B.3.4. NUMERICAL MODEL 80

B.3.4.1. INTRODUCTION 80

B.3.4.2. DISCRETIZATION OF THE MOMENTUM EQUATION 80

B.3.4.3. DISCRETIZED CONTINUITY EQUATION 83

B.3.4.4. DISCRETIZED MASS FRACTION EQUATION 85

B.3.4.5. SOLUTION ALGORITHM 89
B.3.4.6. VERIFICATION OF THE METHOD 92
B.3.4.6.1. VELOCITIES AND PRESSURES 92
B.3.4.6.2. CONCENTRATION 96
B.3.5. APPLICATION 97
B.3.5.1. INTRODUCTION 97
B.3.5.2. EXAMPLE CALCULATION 98
B.3.5.2.1. DIMENSIONS, OPERATING CONDITIONS AND STRUCTURAL PROPERTIES 98
B.3.5.2.2. MEMBRANE CONSTANTS 99
B.3.5.2.3. GRID SIZE 102
B.3.5.2.4. RESULTS 102
B.3.5.3. INVESTIGATION INTO THE EFFECT OF GEOMETRY AND OPERATING CONDITIONS ON SEPARATION EFFICIENCY 109
B.3.5.3.1. INTRODUCTION 109
B.3.5.3.2. SEPARATION EFFICIENCY 109
B.3.5.3.3. DISCUSSION OF RESULTS 110
SUMMARY AND CONCLUTION 115
B.3.6.1. SUMMARY 115
B.3.6.2. DETAIL INTERPRETATION OF THE ENHANCEMENTS PROVIDED BY THIS STUDY 116

REFERENCES Pertaining to CFD. 118

REFERENCES Pertaining to EIS 120

PROGRAM LISTING 121

LIST OF FIGURES

Figure A1 Bode- and Nyquist plots for the Celgard 4510 hydrophobic membrane. A10

Figure A2 Bode- and Nyquist plots for the Celgard 5511 hydrophilic membrane. A11

Figure A3 EIS spectrum of hydrophilic membrane A12

Figure A4 EIS spectrum of hydrophobic membrane A12

Figure 1 Proposed model of the electrode-solution, double-layer region. 6

Figure 2 HHC contactor 7

Figure 3 Integral capacity C^i of the compact double-layer against the charge on the electrode for potassium chloride in contact with mercury at 25 °C. Comparison with the differential capacity $C_{M\text{-}2}$ for potassium fluoride. 15

Figure 4 Variations of the capacity of the compact double layer with the charge on the electrode. Calculated from data for 0.916 *M* sodium fluoride as reported by Grahame . 16

Figure 5 Calculation of double layer capacitance as a function of concentration at 0 °C for the potassium chloride/membrane interface. 24

Figure 6 Calculation of the double layer capacitance as a function of concentration at 25 °C for the potassium chloride/membrane interface. 24

Figure 7 Calculation of the double layer capacitance as a function of concentration at 45 °C for the potassium chloride/membrane interface. 25

Figure 8 Calculation of the double-layer capacitance as a function of concentration at 45 °C for the potassium chloride / membrane interface. 25

Figure 9 Double layer capacitance, the temperature dependence at various frequencies. Membrane capacitance assumed to be temperature independent at 2 $\mu F/m^2$ 26

Figure 10 The variation of conductance with temperature at various frequencies $C_m = 2\ \mu F/m^2$. 28

Figure 11 Capacitance of the double layer/membrane at 25 °C, as a function of frequency, keeping the membrane capacitance fixed at 2 $\mu F/m^2$, $G_1 = 0.58\ S/m^2$, $G_2 = 6.0\ S/m^2$. Dependence of the magnitude of C_1 (double layer) on the overall capacitance of the system. KCl concentration = 15 mg/l. 32

Figure 12 Variation of capacitance and conductance with frequency at 25 °C. 33

Figure 13 Capacitance of the double layer/membrane at 0°C as a function of frequency; $C_2 = 2\ \mu F/m^2$, $G_1 = 0.58\ S/m^2$, $G_2 = 6.0\ S/m^2$. Dependence of the magnitude of C_1 on the overall capacity of the system. KCl concentration = 15 mg/l. 33

Figure 14 Capacitance of the double layer as a function of frequency, variation of the membrane capacitance C_2. C_1 is kept constant at 3600 μF/m². The KCl concentration = 15 mg/l. 35

Figure 15 Capacitance of the double layer as a function of frequency, variation of the membrane capacitance C_2 while C_1 has a fixed value of 36000 μF/m². KCl concentration = 15 mg/l. 36

Figure 16 The effect of the double layer capacitance on the conductance of the phases at the interface. Values of C_1 as shown for a 15 mg/l KCl solution at 25 °C. C_2 = 2 μF/m², G_1 = 0.58 S/m², G_2 = 6.0 S/m². 37

Figure 17 The effect of membrane capacitance variation on the interfacial conductance of the phases for a 15 mg/l KCl concentration. C_1 = 3600 μF/m². 38

Figure 18 The effect of membrane capacitance variation on the interfacial conductance of the phases for a 15 mg/l KCl concentration with C_1 = 36 000 μF/m². 39

Figure 19 Electrochemical impedance profile for a simple electrochemical system. 40

Figure 20 Computer plotted Nyquist diagram for 15 mg/l KCl at 25 °C / Celgard 4510 Hydrophobic membrane where the capacitance C_T has been calculated. Resistances R_1 and R_2 are calculated in addition. 41

Figure 21 EIS spectrum of membrane 1 56

Figure 22 EIS spectrum of membrane 2 56

Figure 23 EIS spectrum of membrane 3 57

Figure 24 EIS spectrum for membrane 4 57

Figure 25 EIS spectrum of membrane 5 58

Figure 26 EIS spectrum of membrane 6 58

Figure 27 EIS spectrum of membrane 7 59

Figure 28 EIS spectrum of membrane 8 59

Figure 29 EIS spectrum of membrane 9 60

Figure 30 EIS spectrum of membrane 10 60

Figure 31 Capacitance vs frequency for 15 mg/l KCl solution. 64

Figure 32 Conductance vs frequency for 15 mg/l KCl, C_1 = 200 μF/m², C_2 = 2 μF/m². 64

Figure 33 Resistance of membrane. 65

Figure 34 The orthogonal curvilinear axi-symmetrical coordinate system. 70

Figure 3.2 Varying diameter tube with boundary fitting orthogonal curvilinear axi-symmetrical grid. 72

Figure 4.1 Control volume for the discretization of the momentum equation. 81

Figure 4.2 Control volume for the discretization of the continuity equation. 83

Figure 4.3 Staggered grid with control volume used for the concentration equation. 85

Figure 4.4 Control volume and grid arrangement next to the wall for the concentration equation. 87

Figure 4.5 Comparison of centreline velocities. 93

Figure 4.6 Comparison of velocity profiles at different axial positions. 94

Figure 4.7 Variation of pressure along the axis of the tube. 95

Figure 4.8 Comparison of concentration profiles in the fully developed region. 97

Figure 5.1 Variation of pressure, osmotic pressure and effective pressure difference with axial distance. 103

Figure 5.2 Variation of the salt mass fraction at the wall with axial distance. 103

Figure 5.3 Percentage increase in diameter as function of axial distance. 104

Figure 5.4 Variation of the wall velocity along the length of the tube. 105

Figure 5.5 Variation of axial mass flow along the length of the tube. 106

Figure 5.6 Variation of rejection coefficient with axial distance. 107

Figure 5.7 Variation of concentration, axial velocity, and radial velocity over the radius at the outlet of the tube. 108

Figure 5.8 Separation efficiency versus L/D for different diameters at p_{in} = 60 Bar, u_{in} = 1 m/s, and ϕ_{in} = 0.02. 111

Figure 5.9 Separation efficiency versus inlet pressure for u_{in} = 1 m/s, ϕ_{in} = 0,02, D = 0,5 mm and L/D = 5000. 112

Figure 5.10 Separation efficiency versus inlet concentration for p_{in} = 60 Bar, u_{in} = 1 m/s, D = 0,5 mm and L/D = 5000. 113

Figure 5.11 Separation efficiency versus inlet velocity for p_{in} = 60 Bar, ϕ_{in} = 0,02, D = 0,5 mm and L/D = 5000. 114

LIST OF TABLES

Membranes of Russian origin characterised by EIS A13
EIS results of Russian membranes A14

TABLE 1 NaF Capacitance values 13

TABLE 2 Actual KCl Capacitance values. 14

TABLE 3 Typical Concentrations of Na^+ and F^- in the plane of closest approach for NaF solutions. 18

TABLE 4 Conductance of KCl solution at various temperatures 22

TABLE 5 EIS results of Celgard 4510 hydrophobic membrane with KCl systems at ±25 °C 45

TABLE 6 EIS results of Celgard 4510 hydrophobic membrane with NaF system at ± 25 °C 46

TABLE 7 EIS results of Celgaurd 5511 hidrophilic membrane with KCl system at ± 25 °C 48

TABLE 8 Inner- and outer layer capacities 49

TABLE 9 Comparison of hydrophobic and hydrophilic membranes 50

TABLE 10B Membranes of Russian origin characterised by EIS 51

TABLE 10 EIS results of Russian membranes 52

TABLE 11 Range of values for each membrane type in 15 mg/ℓ KCl 61

LIST OF ACRONYMS AND ABBREVIATIONS

CFD	Computational Fluid Dynamics
EIS	Electrochemical Impedance Spectroscopy
HCC	Hydrodynamically Characterised Cell
HFF	Hollow Fine Fibre
IHP	Inner Helmholtz Plane
NF	Nanofiltration
OHP	Outer Helmholtz Plane
RO	Reverse Osmosis
UF	Ultrafiltration
ac	alternating current
dc	direct current

NOMENCLATURE

A	Area (m^2)
C	Capacitance (Farad)
E	Potential (Volt)
F	Faraday
P	Charge density (Coulomb/m^3)
R	Resistance (Ohm)
T	Absolute temperature (K)
d	Thickness (m)
f	F/(RT)
k	Conductance of electrolyte
p	Porosity (%)
q	Charge (Coulomb)
t	Temperature (°C)
x	Distance (m)
z	Valency of ion

GREEK LETTERS

σ	Charge density
ϵ	Dielectric constant
Λ	Equivalent conductance
ω	Frequency
Ω	Ohm
ϕ	Potential at distance x
π	pi
Δ	Temperature coefficient

SUPERSCRIPTS

s	Solution bulk
i	Species i
z	Valency

SUBSCRIPTS

i	Species i
1	Inner
2	Outer
skin	Skin layer

B. GENERAL INTRODUCTION

B.1 MOTIVATION

Characterization of porous media (including all types of membranes) is normally done by physical description and physical measurements obtained through various procedures. These procedures vary from the measurements of porosity, permeability, electrical resistance, geometry and tensile strength. These methods yield fairly reliable physical properties for these media. These procedures are however invasive and involve the destruction of the membrane (e.g. electron microscopy). There is clearly a need for non-invasive characterisation before, during and after usage of the membrane.

The investigation into the adherence of thin layers on substrates and the corrosion rates of various materials by Electrochemical Impedance Spectroscopy (EIS) seems to be a technique which could fruitfully be applied to the characterisation of porous media. This conceptual idea was investigated and the first cursory measurements indicated that substantial data could be derived from the impedance, and capacitance properties which are normally obtained from EIS experimentation.

Having arrived at this visualisation of the concept further discussion with various people within the WRC as well as independent consultants led the way to the possible combination of EIS and Computational Fluid Dynamics (CFD). The rationale for coupling EIS/CFD lies in the fact that EIS is a flow of electrons (or charge) which could be quantified by physical measurement of amperes.

The derivative properties from electric current such as resistance (impedance) and capacitance, could therefore be measured directly by the very well developed and standardised EIS techniques. The analogy between EIS and CFD lies in the fact that fluid flow could possibly be equivalated to a flow of electrons.

Similarly the derivative properties associated with fluid dynamics could now, possibly, be equivalated with the previously mentioned counterparts in the electrical discipline such as resistance. Should this be feasible it would be possible to obtain electrochemical measurements remotely, on both sides of a functioning membrane. These measured properties, under operating conditions, could then be equivalated to their respective counterparts in the fluid dynamics of, for example, a reverse osmosis process.

A substantial amount of information is expected to emerge from this possibility and the most obvious would be an enhanced control protocol for membrane processes in general.

As a general perspective on the potential of these projects, the successful development, application and translation of the principle of alternating current impedance could be applied to various different unit processes where interphase and interfacial modelling is required.

The initial project proposal visualised the full integration of EIS/CFD as a final phase of the project. This would have had to be executed, dynamically, in a reverse osmosis cell under operating conditions. The design and development of high pressure electrodes required for these experiments were however prioritised lower than the detailed, fundamental qualifications of the EIS process on different membranes under "no load" conditions.

The theory and its conformation to experimental values obtained from this research, as well as from literature, were therefore foremost in the research program, and were consequently researched as first priority.

Concerning CFD, a detailed derivation of almost all possible variables was obtained. The research method relied on the powerful numerical technique of finite volume, numerical analysis including a discrete "stepping" protocol to render the program feasible on a P.C.

A properly configured diskette is supplied to illustrate the program results which could be utilised for Hollow Fine Fibres (HFF) with diameters as small as 100μm diameter through tubules up to tubes of 10mm diameter. For the selection of any particular diameter with a selection of conditions, RO, UF or NF membranes could be modelled to yield virtually all variables.

These include variables such as permeability, pressure drop, compaction, transmembrane pressure, hydraulic resistance, flow velocities, concentration profiles, density and viscosity variation etc. Although the CFD analysis was undertaken to assist and facilitate the eventual "translation" between electrically and hydrodynamically derived properties, it has proven to be valuable in its own rights. The CFD protocol presented here could now also be utilised to optimise all flow schemes associated with pressure-driven separation processes such as RO, UF and NF. As an example it can now be used to optimise the flow tapering of modules in multimodule plant as well as internal tapering of a shell-and-tube flow arrangement.

To facilitate a sensible presentation of both the EIS and the CFD parts of the project they will be discussed separately. An integration with envisaged perspectives for the combination of EIS and CFD would be presented in a different section.

In summary the aims and objectives of thus study can be listed as follows for the EIS part of the project.

1. The assessment of the repeatability of RC-responses to EIS with a membrane interposed in the electrical impedance circuit. This also entails the development, construction and qualification of a cell in which to perform the EIS experiments.

2. The identification and quantification of RC-values obtained from EIS experimentation.

3. The development of a model circuit to simulate the membrane electrically.

4. The comparison of the simulation model with other model(s) reported in literature (Coster's model).

5. The quantification of the independent variables such as electrolyte type and concentration, frequency of the alternating current, and temperature.

6. The interpretation and calculation of directly measurable membrane characteristics such as resistive impedance and capacitance.

7. The calculation of derived characteristics such as porosity for different membranes.

The aims and objectives for the CFD part of the project are as follows:

The development of a general CFD protocol to enable calculation of the response variables from selected input variables for geometry, pressure, concentration and flow rate to typical reverse osmosis membranes. A cylindrical configuration, permeating from the inside bore was used as model.

B.2 A CONCISE DESCRIPTION OF THE EIS PROCEDURE

To utilise the EIS-technique for purposes of membrane characterisation it is necessary to describe the interphase between the electrochemical double layer theory and the EIS procedure.

B.2.1 THE ELECTROCHEMICAL DOUBLE-LAYER AND RELATED THEORIES

Any charged electrode, submerged in an electrolyte, is thought to give rise to several "layers" immediately adjacent to the electrode. The innermost layer contains solvent and other species (ions and molecules) which are said to be specifically adsorbed onto the electrode surface. This inner layer is called the compact, Helmholtz or Stern layer. The locus of the electrical centres of these adsorbed species is called the Inner Helmholtz plane (IHP) at a distance of x_1 from the electrode. The charge density ($\mu C/cm^2$) of adsorbed species in the IHP is σ_i.

Solvated ions can only approach the electrode to within a distance of x_2 measured from the electrode. The locus of centres of these nearest solvated species is called the Outer Helmholtz plane (OHP). The interaction of the solvated ions with the charged electrode involves only long-range electrostatic forces so that their interaction is independent of the chemical properties of the ions. The ions in the OHP are said to be non-specifically adsorbed. These ions in the OHP are distributed in a 3-dimentional region which is called the diffuse layer, extending from the OHP into the adjacent electrolyte solution.

The excess charge in the diffuse layer is σ_d so that the total excess charge density on the solution side of the double layer σ_s, is given by:-

$\sigma_s = \sigma_i + \sigma_d = \sigma_e$ = electrode charge density

The thickness of the diffuse layer depends on the ionic concentration in the electrolytic solution and is of the order of 30 nm (max) for concentrations of 10^{-2} M. A typical

schematic model is shown in Figure 1 with a characteristic (static) potential profile.

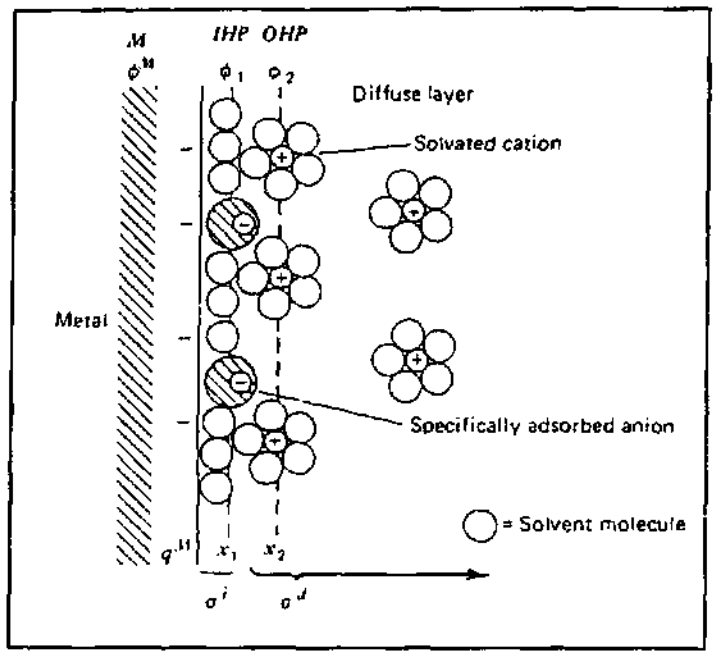

Figure 1 Proposed model of the electrode-solution, double-layer region.

It is obvious that this dc presentation would be substantially more complex when an ac source is used. This will have to be explained in the next section in which the capacitance and impedance effects on the double layer is accentuated by using an alternating (sinusoidal) source at variable frequencies (ω). A very fundamental visualization of the EIS technique is the fact that the application of alternating current to this system facilitates and enables us to "see" and measure the different layers' capacities, impedances and admittances. To exploit these facilities the following theoretical background was collated from literature [1].

B.2.2 THE EIS APPLICATION TO MEMBRANES AND A LITERATURE SURVEY OF ITS USE.

The applications of the EIS technique for the investigation of surface phenomena like corrosion is extensively described in literature [1] [2] [3] [4]. Although these publications describe the EIS technique as applied to metal/electrolyte interfaces the current research

applied the EIS technique to a membrane/electrolyte interface.

Impedance spectra were generated utilising an automatic system which included a Solartron Model 1255 Frequency Response Analyzer (FRA) and an EG&G PARC Model 273 Potentiostat/Galvanostat controlled by an IBM personal computer. A four electrode system was used comprising of two working and two reference electrodes, one set on either side of the membrane. Only two electrolytes were used namely KC*l* and NaF at various concentrations.

B.2.3 A THEORETICAL OVERVIEW ON EIS APPLICATION FOR CHARACTERISATION OF POROUS MEDIA.

In order to compare the experimentally obtained EIS spectra of the KC*l*/hydrophobic and the KC*l*/hydrophilic membranes with theory, calculation of the double layer capacitance and impedance need to be done. These values obtained should then be tested and verified experimentally in a simple model. To translate the application of the EIS technique from the traditional corrosion applications it was necessary to develop and design a Hydrodynamically Characterised Cell (HCC) to contain the necessary electrodes and electrolytes. This HCC is shown in Figure 2.

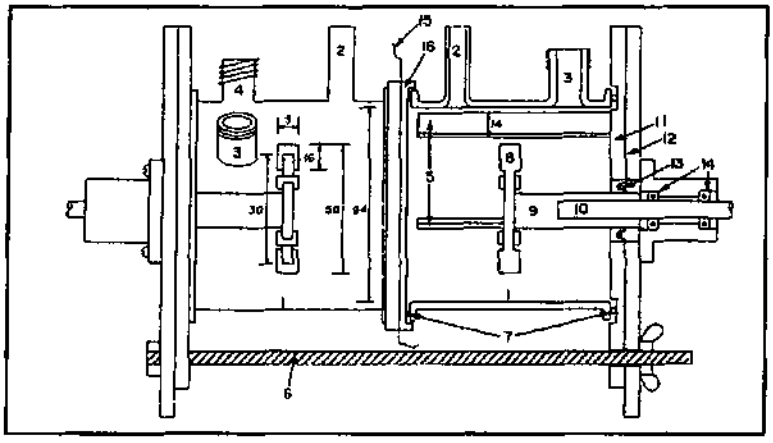

Figure 2 HHC contactor

The HCC is equiped with ports for the electrodes, sampling and temperature

measurement. An impeller is provided in each compartment for effective agitation and the membrane is interposed between the two compartments. The EIS spectra were now obtained for different membranes while varying the electrolyte concentration, electrolyte type and the temperature. The spectra were plotted via a curve-fitting facility to yield the Bode and Nyquist plots for the various cases. Once this data is captured, various manipulations yielded the impedance, (or resistances at zero frequency), as well as the capacitances. This determination was done by graphical extrapolation discussed in the experimental results section.

B.2.3.1 TEMPERATURE DEPENDENCE OF (EIS) SPECTRA

It was anticipated that EIS spectra of the membrane/solution interphase will be a function of temperature. This is a consequence of the marked temperature dependence of both capacity and specific conductance of ionic salt solutions. Calculation of these quantities in relevance to the electrical double layer is possible.

The theoretical background is summarised. A multiphase model of the interphase is necessary to calculate the porosity data of the membrane. Temperature is the variable that has been identified as the major source of errors in the measured parameters obtained by EIS.

Thus the calculated temperature variations need to be known in order to determine the confidence limits of experimental data obtained by EIS.

The complex impedance response on the membrane system was obtained by applying a low voltage sinusoidal excitation signal (± 10 mV) over a wide frequency range (typically 0,01 Hz to 200 000 Hz), using an appropriate dc bias or rest potential. Response data obtained were statistically analysed and a non-linear least squares curve-fitting procedure enabled the modelling of the system as an equivalent electrical circuit. This circuit contains RC elements which could now be interpreted as electrical properties of the physical "layers" from the electrochemical double layer theory.

The elegance of the EIS technique, therefore, lies in the fact that specific values for the RC-components can now be deduced from these measurements and used to simulate the physical system.

A literature survey revealed a dearth of activity in the field of synthetic membrane characterisation by EIS.

The most interesting research was that of Coster *et al*, [2] [3] [4] which dealt with an EIS investigation of two types of polysulphone anisotropic membranes for which he determined the capacitances and conductances of both the skin layer and the substrate.

The theory and relationships between the various parameters must however be summarised so as to effect a well founded basis for subsequent development for practical use.

B.2.3.2 CAPACITY OF THE DOUBLE LAYER - A THEORETICAL EXTRACT

The parameters obtained from EIS spectra are the impedance and capacitance of a typical RC-network. Although the double layer capacity theory is traditionally applied to the electrode/solution interface the membrane/solution interface differs only in its ability to transfer charge. It will have different physical constants, for example, refractive index and dielectric constant.

At the membrane/solution interface an equal and opposite charge, q, develops and this results in a parallel plate capacitor.

The integral capacity C^i at the potential E (with respect to a reference electrode, in this case Ag/AgC*l*) is defined as:-

$$q = C^i(E - E_{ref}) \qquad (2.1)$$

Since C^i is a function of E it is appropriate to define a differential capacity .

$$C = \left(\frac{\partial q}{\partial E}\right)_{T,P} \tag{2.2}$$

If the perturbation used in EIS is only a few millivolts, the variation of C with potential may be ignored.

Denoting C_i (not to be confused with C^i - integral capacity) as the concentration of ions at point x from the membrane and C^s_i as the concentration of ions in the bulk of the solution,

$$C_i = C_i^s e^{-z_i f \phi} \tag{2.3}$$

with

$$f = \frac{F}{RT} \tag{2.4}$$

where z_i is the ionic valency of ion i and ϕ is the potential at x with respect to the potential ϕ_s in the bulk solution.

For convenience ϕ_s is set at zero while x is the distance from the electrode which may have any value, however small for the moment.

Assuming that the work done to bring ion i from outside the double layer at coordinate x is ($z_i f\phi$) then equation (2.3) corresponds to a Boltzman distribution,

$$\frac{d^2\phi}{dx^2} = -\frac{4\pi P}{\epsilon} \tag{2.5}$$

where P = charge density per unit volume and ϵ is the dielectric constant.

$$P = \sum z_i F C_i \tag{2.6}$$

Combining equations (2.3), (2.5) and (2.6) gives

$$\frac{d^2\phi}{dx^2} = -\frac{4\pi}{\epsilon}\sum z_i F C_i^s e^{-z_i f\phi} \qquad (2.7)$$

At this stage the assumption that ϵ is independent of x allows the equation (2.7) to be solved.

Multiplying both sides of (2.7) by $2(d\phi/dx)$ and integrating with the limits $\phi \to o$ and $d\phi/dx \to o$ for $x \to \infty$ the following equation is obtained:-

$$\left(\frac{d\phi}{dx}\right)^2 = \frac{8\pi RT}{\epsilon}\sum C_i^s\left(e^{-z_i f\phi} - 1\right) \qquad (2.8)$$

The Gauss theorem relates the charge per unit area, q, to $d\phi/dx$.

$$4\pi q = -\epsilon\left(\frac{d\phi}{dx}\right)_{x_2} \qquad (2.9)$$

where subscripts 1 and 2 refer to the inner and outer layers of the double layer respectively. Combining (2.8) and (2.9) and substituting $x = x_2$, $\phi = \phi_2$.

$$q = \pm\left[\frac{RT\epsilon}{2\pi}\sum C_i^s\left(e^{-z_i f\phi_2} - 1\right)\right]^{\frac{1}{2}} \qquad (2.10)$$

Equation (2.10) allows the calculation of q as a function of ϕ. This equation may be expressed in the following form for a 1:1 electrolyte such as KC*l* or NaF of concentration C^s.

$$q \simeq +2A\sinh\left(\frac{f\phi_2}{2}\right) \qquad (2.11)$$

where

$$A = +\left(\frac{RT\epsilon C^s}{2\pi}\right)^{\frac{1}{2}} \tag{2.12}$$

For an aqueous solution at 25 °C,

$$q = 11.74(C^s)^{\frac{1}{2}}\sinh(19.46\phi_2) \tag{2.13}$$

where q is in microcoulomb/cm^2, C^s is in mole/dm^3 and ϕ in volt.

It is now convenient to divide the double layer into two regions: a compact double layer between the membrane and the plane of closest approach (co-ordinate 2) and the diffuse double layer extending from the plane of closest approach to the bulk of the solution.

The potential difference ϕ_m between the membrane and solution may now be partitioned into

$$\phi_m = (\phi_m - \phi_2) + \phi_2 \tag{2.14}$$

where ϕ_2 is the potential in the plane of closest approach. Subscript 1 would apply for a second plane which is even closer to the electrode.

Differentiating ϕ_m with respect to q gives,

$$\frac{\partial\phi_m}{\partial q} = \frac{\partial(\phi_m - \phi_2)}{\partial q} + \frac{\partial\phi_2}{\partial q} \tag{2.15}$$

or by definition;

$$\frac{1}{C} = \frac{1}{C_{m-2}} + \frac{1}{C_{2-s}} \tag{2.16}$$

where C is the double layer differential capacity and C_{m-2} and C_{2-s} correspond to the compact and diffuse double layers respectively.

Thus the double layer is modelled as two capacitors in series.

Capacitance $C_{2\text{-}s}$ is obtained by differentiating equation (2.10) with respect to ϕ_2. The units of $C_{2\text{-}s}$ are microfarads/cm^2, with ϕ_2 in volt and C^s in mole/dm^3.

Values for $C_{m\text{-}2}$ and $C_{2\text{-}s}$ are available at various temperatures from literature.

$C_{2\text{-}s}$ increases with the square root of concentration (equation 2.10). With KC*l* solutions, the point of zero charge shifts with electrolyte concentration whereas for NaF the point of zero charge is independent of electrolyte concentration [5]. Hence NaF solutions were used as reference solutions for the double layer capacitance values used in calculations of theoretical EIS curves.

The KC*l* capacitance values are very close to those of the NaF as seen from Tables 1 and 2.

TABLE 1

NaF Capacitance values

[NaF] Normality	C (μF/cm^2)			
	0 °C	25 °C	45 °C	65 °C
0.001	7.5	6.0	5.0	4.8
0.01	19.0	18.0	17.0	16.5
0.1	32.5	32.0	31.0	30.0
0.7953	44.2	43.0	42.0	40.5

TABLE 2 Actual KCl Capacitance values.	
[KCl] Normality	C ($\mu F/cm^2$) 25 °C
0.001	6.0
0.01	16.0
0.1	32.0
1.0	39.6

B.2.3.3 EFFECT OF CATION AND ANION VARIATION ON THE CALCULATION OF DOUBLE LAYER CAPACITANCE.

B.2.3.3.1 INNER LAYER

Having considered the case, in the calculations so far, where the inner layer remains charge free there are differences due to changing the electrolyte from sodium or potassium fluoride to potassium chloride.

It is necessary to have some idea of the magnitude of the capacitance in changing the structure of the double layer so that the results of EIS spectra may be interpreted in a reasonable manner.

Figure 3 [5] shows that the inner layer capacities of KF and KCl as a function of charge (i.e. a non adsorbed and an adsorbed anion) are not appreciably different in capacity values. Less than 1 $\mu F/cm^2$ capacitance difference is observed over the range of q = +10 to -8 $\mu C/cm^2$.

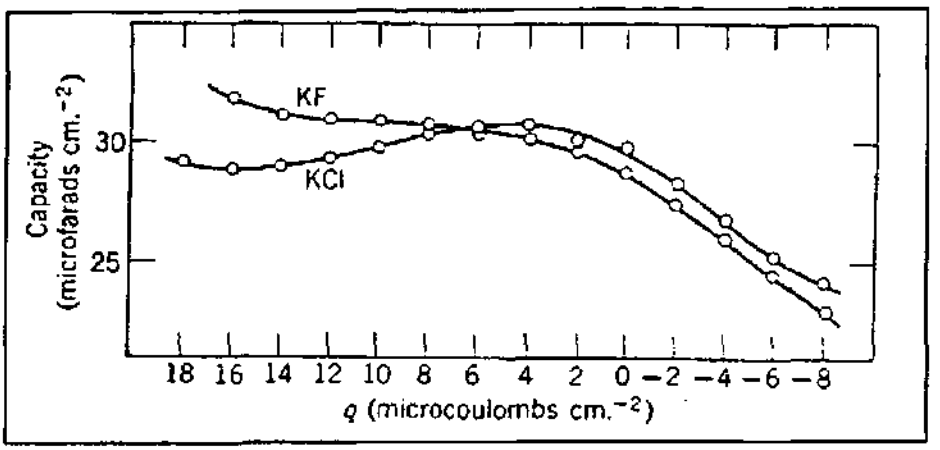

Figure 3 Integral capacity C' of the compact double-layer against the charge on the electrode for potassium chloride in contact with mercury at 25 °C. Comparison with the differential capacity $C_{M\cdot2}$ for potassium fluoride.

As errors in EIS spectra are probably greater than the measured errors between KF and KCl electrolytes it is not always possible to give meaningful interpretations to certain systems of membranes and salt solutions where large levels of noise are present or where the time dependence of the results is dramatic.

B.2.3.3.2 CAPACITY OF THE INNER LAYER AS A FUNCTION OF CONCENTRATION

At constant temperature the inner layer capacity C° has been found to be a function of charge density q and independent of concentration; certainly in the case of sodium fluoride.

The variation (Figure 4) of C° with charge density is marked and thus if the potential of modulation is large, q may depart from the q = ± 1 - 2 μC/cm^2 and the double layer capacity cannot be accurately defined.

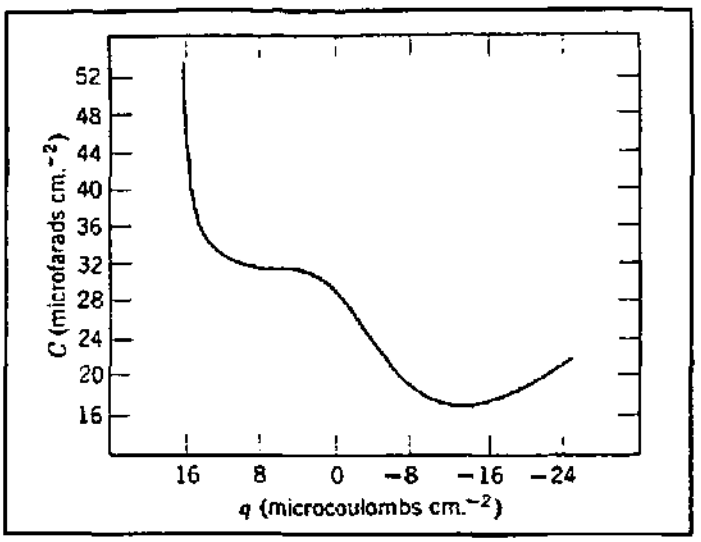

Figure 4 Variations of the capacity of the compact double layer with the charge on the electrode. Calculated from data for 0.916 *M* sodium fluoride as reported by Grahame.

B.2.3.3.3 CAPACITANCE OF INDIVIDUAL CATIONS AND ANIONS.

From the results of Devanathan [6] the values of capacitance for various potassium salts have been calculated.

The following results were quoted for the anions of F, *Cl*, Br and I which had capacities of 46.8, 35.2, 32.6 and 29.5 μF/cm^2 respectively. A lack of marked dependence of the differential capacity on the nature of the cation has been thoroughly investigated by Grahame [8].

This is useful from the point of view of variation of the membrane/electrolyte system and thus changes in the EIS spectra may be expected to be easier to interpret.

B.2.3.4 CONDUCTANCE OF THE DOUBLE-LAYER

While values of the bulk solution conductivity of electrolytes are available in the literature and may be calculated as a function of temperature, conductances of the compact and diffuse double layer are required for modelling purposes.

In order to calculate the conductivity of the double layer, the ionic concentrations in the plane of closest approach and ionic contributions that anions and cations make to the total charge on the solution side need to be evaluated.

The ionic concentration C_i^2 in the plane of closest approach
is given by:

$$C_i^2 = C_i^s e^{-z_i f \phi_2} \qquad (2.17)$$

$C_i^2 \neq C_i^s$ when $z_i\phi_2 \neq 0$. As $\phi_2 > 0$ when $E > E_z$ and $\phi < 0$ where $E < E_z$, cations are attracted for $E < E_z$ and are repelled when $E > E_z$ in the absence of specific absorptions.

The calculated concentrations of anions and cations that are typical are shown for NaF in Table 3, at various potentials.

The effect of concentration should thus be seen in the calculated capacity of the double layer.

It would be anticipated that this data may be extrapolated to the case actually present, i.e. only a small applied potential close to 0 vs. the Ag/AgC*l* reference electrode.

TABLE 3

Typical Concentrations of Na^+ and F^- in the plane of closest approach for NaF solutions.

Potential vs. Ag/AgCl (V)	Bulk concentration Molarity	Potential ϕ_2 (V)	$[Na^+]$ C_2 Molarity	$[F^-]$ C_2 Molarity
-1.75	0.001	-0.241	11.8	8.46E-8
	0.01	-0.184	13.1	7.62E-6
	0.1	-0.128	14.8	6.76E-4
	1	-0.074	18.1	5.52E-2
-1.35	0.001	-0.22	5.27	1.90E-7
	0.01	-0.164	6.04	1.63E-5
	0.1	-0.109	7.03	1.42E-3
	1	-0.058	9.62	0.104
-0.95	0.001	-0.187	1.45	6.89E-7
	0.01	-0.15	1.90	5.26E-5
	0.1	-0.083	2.53	3.96E-3
	1	-0.039	4.56	0.219
-0.55	0.001	-0.066	1.31E-2	7.64E-5
	0.01	-0.041	5.00E-2	2.00E-3
	0.1	-0.021	0.221	4.42E-2
	1	-0.0085	1.41	0.718
-0.45	0.001	0.141	5.75E-4	1.73E-3
	0.01	0.134	5.93E-3	1.69E-2
	0.1	0.067	7.70E-2	0.130
	1	0.0024	0.911	1.10

A differential capacity, it will be recalled, is $\left(\frac{\partial q}{\partial E}\right)$ and the contributions that cations and anions have to total charge on the solution side of the electrolyte/membrane interface require elaboration.

A derivation after Grahame shows that the ionic components are

$$q_{+}^{2-s} = \int_{x_2}^{\infty}(P_{+} - z_{+}FC^{s})dx \tag{2.18}$$

and

$$q_{-}^{2-s} = \int_{x_2}^{\infty}(P_{-} - z_{-}FC^{s})dx \tag{2.19}$$

where P_+ and P_- are charge densities per unit volume of electrolyte solution.

$$P = \sum z_i FC_i \tag{2.20}$$

and

$$C_i = C_i^{s} e^{-z_i f\phi} \tag{2.21}$$

then

$$P_{-} = z_{-}FC^{s}e^{-z_{-}f\phi} \tag{2.22}$$

thus

$$q_{+}^{2-s} = z_{+}FC^{s}\int_{x_2}^{\infty}(e^{-z_{+}f\phi} - 1)dx \tag{2.23}$$

Rewriting equation (2.23) in the following form eliminates the variable x and integration with respect to ϕ gives:

$$q_+^{2-s} = z_+ FC^s \int_{x_2}^{\infty} \left(e^{-2z_+ f\phi} - 2e^{-z_+ f\phi} + 1\right)^{\frac{1}{2}} dx$$
$$= z_+ FC^s \int_{x_2}^{\infty} \left(\left(e^{z_+ f\phi} + e^{-z_+ f\phi} - 2\right)e^{-z_+ f\phi}\right)^{\frac{1}{2}} dx \qquad (2.24)$$

For a z-z electrolyte of concentration c^s.

$$q = +2A \sinh\left(\frac{zf\phi_2}{2}\right) \qquad (2.25)$$

where

$$A = \left(\frac{RT\epsilon C^s}{2\pi}\right)^{\frac{1}{2}} \qquad (2.26)$$

This may be rewritten as:

$$q = A\left(e^{\left(\frac{z_+ f\phi}{2}\right)} - e^{\left(\frac{-z_+ f\phi}{2}\right)}\right)$$
$$= A\left(e^{z_+ f\phi} + e^{z_+ f\phi} - 2\right)^{\frac{1}{2}} \qquad (2.27)$$

Equation (2.24) may thus be recognised as of the same form as equation (2.27) and equation (2.24) now becomes.

$$q_+^{2-s} = -z_+ F \int_{x_2}^{\infty} q\left(\frac{2\pi C^s}{\epsilon RT} e^{-z_+ f\phi}\right)^{\frac{1}{2}} dx \qquad (2.28)$$

The charge q on the membrane per unit area is related to $d\phi/dx$ by the Gauss theorem

$$4\pi q = -\epsilon\left(\frac{d\phi}{dx}\right)_{x_2} \qquad (2.29)$$

Substituting for q in equation 2.28 yields:-

$$q_{+}^{2-s} = -z_{+}F\int_{\phi_2}^{0}\left(\frac{\epsilon C^{s}}{8\pi RT}e^{-z_{+}f\phi}\right)^{\frac{1}{2}}d\phi \qquad (2.30)$$

Performing the integration where A was defined by equations (2.25) gives:-

$$q_{+}^{2-s} = A\left(e^{\frac{-z_{+}f\phi_2}{2}} - 1\right) \qquad (2.31)$$

In a similar manner q_{-}^{2-s} may be derived

$$q_{-}^{2-s} = -A\left(e^{\frac{-z_{-}f\phi_2}{2}} - 1\right) \qquad (2.32)$$

At the point of zero charge it may be deduced that

$$q_{+}^{2-s} = q_{-}^{2-s} = 0 \qquad (2.33)$$

As part of the temperature dependence of the conductivity parameter G_m, the quantity G_e figures in the model of the membrane/electrolyte interface where G_e is the conductivity of the bulk solution electrolyte. To investigate the conductivity of the compact and diffuse double layers, one needs to know the conductivity of the bulk electrolyte solution firstly, as a function of temperature.

The following analysis shows how the conductance data at various temperatures was arrived at. At any concentration the conductivity may be calculated from the following equations.

$$\Lambda_t = \frac{1000k}{c} \qquad (2.34)$$

where c is the bulk solution concentration, k is the conductance of the electrolyte and Λ

is the equivalent conductance of the solution at a given temperature t.

A relationship between temperature and the equivalent conductance of a strong electrolyte is given by.

$$\Lambda_t = \Lambda_{180}[1 + \Delta(t - 18°C)] \qquad (2.35)$$

where Δ is the temperature coefficient.

Factors which determine the shape of the temperature versus equivalent conductance curve are (i) an increase in the viscosity of the solution and corresponding decrease in the mobility of the ions with a decrease in temperature and (ii) a decrease in dissociation of the electrolyte with rising temperature. The temperature coefficient of conductance may be positive or negative accordingly depending on which factor predominates. The temperature-conductance curve thus exhibits a maximum.

For potassium chloride solutions the best values of conductance, as data at selected temperatures, are the following by Jones and Prendergast [10] in Table 4.

From the values in Table 4, the conductance at any concentration and at various temperatures may be calculated by extrapolation.

TABLE 4
Conductance of KCl solution at various temperatures.

Concentration Moles (g/1000g solution)	**Conductance** (Ω^{-1} cm^{-1})			
	0 °C	18 °C	20 °C	25 °C
1.0 N 71.3828	0.065430	0.098201	0.010202	0.111733
0.1 N 7.4334	0.007154	0.111919	0.116676	0.012886
0.01 N 0.7466	0.000775	0.001223	0.001276	0.0014114

The conductance G_e of the bulk solution may differ appreciably from that of the double layer as the concentration of current carrying species is different. The conductance of the double layer may be calculated from the bulk solution concentration at any given temperature.

B.2.3.5 VARIATION OF CAPACITANCE WITH TEMPERATURE.

In a three-phase model of the double-layer/membrane interface, with C_1 and C_2 in series with the membrane, the Bode and Nyquist plots may be computed for the KCl//membrane system.

This model may then be fitted to the experimental results obtained. In order to observe the effect of temperature on the capacitance, a series of curves of capacitance with frequency at various temperature were calculated so that during experiments it could be known in advance whether small temperature differences could lead to significant experimental errors.

For the Celgard membranes it was assumed that there was no surface difference over the total membrane area.

The calculated double layer capacities as a function of concentration are shown in Figures 5 to 8 and the equations used to fit the data, obtained at various temperatures by Grahame[7], are shown on the graphs themselves. There was no single equation which fitted the data over the whole temperature range.

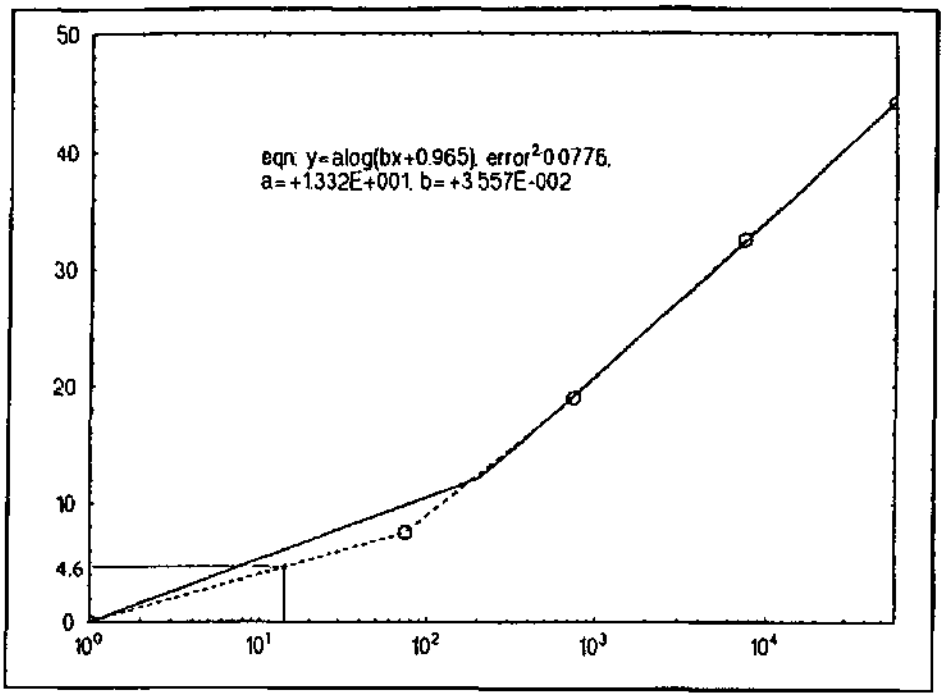

Figure 5 Calculation of double layer capacitance as a function of concentration at 0°C for the potassiumchloride/membrane interface.

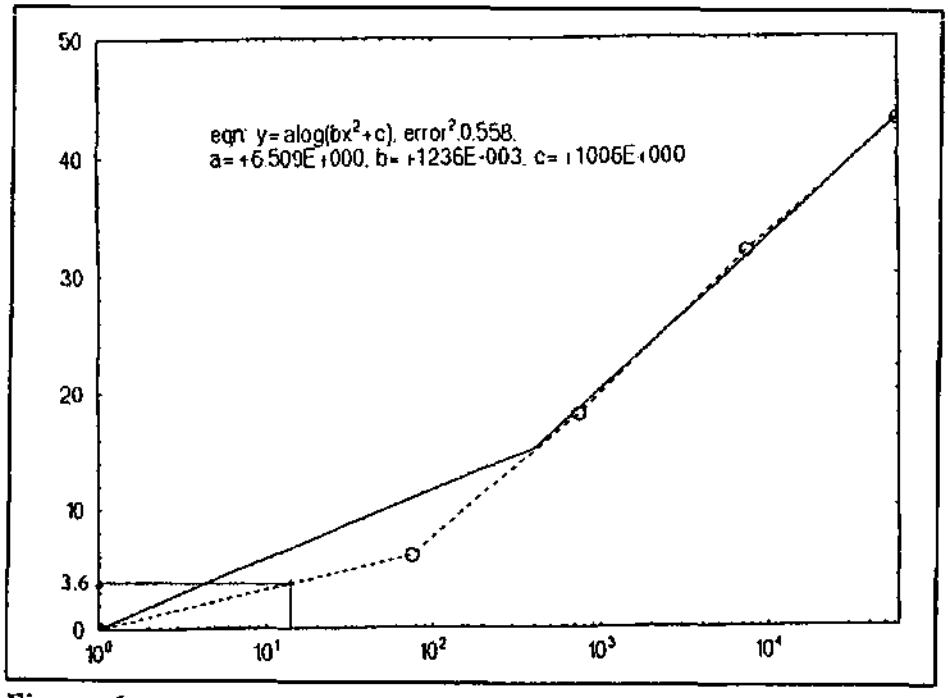

Figure 6 Calculation of the double layer capacitance as a function of concentration at 25°C for the potassiumchloride/membrane interface.

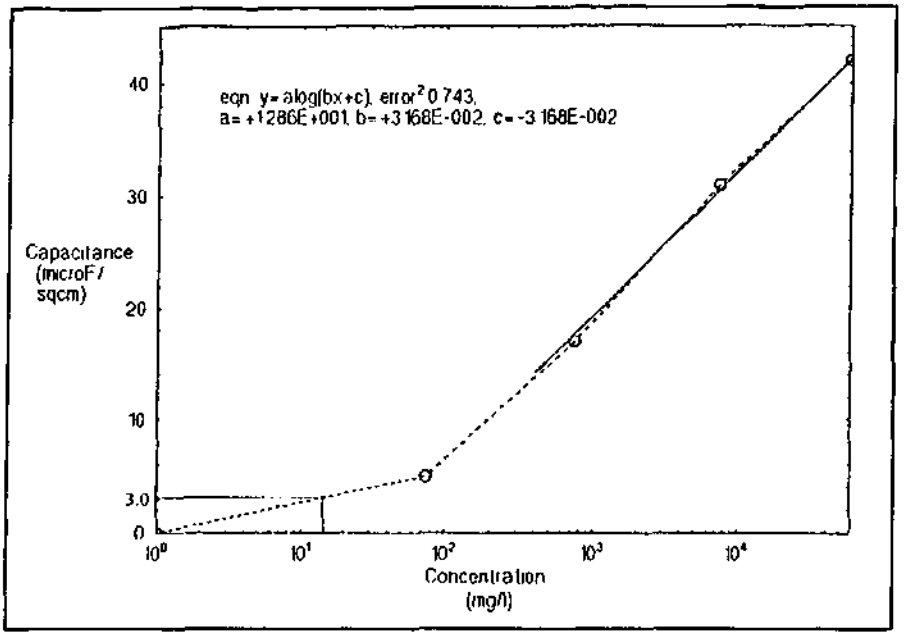

Figure 7 Calculation of the double layer capacitance as a function of concentration at 45°C for the potassiumchloride/membrane interface.

Using a concentration of 15 mg/ℓ KCl it may be seen that the absolute value of the double layer capacitance over the frequency range 1000 to 10000 Hz hardly varies at all at frequencies greater the 3000 Hz whereas at 1000 Hz the value of this capacitance varies from 0.046 F/m^2 at 0 °C to 0.028 F/m^2 at 25 °C (Figures 5 to 8).

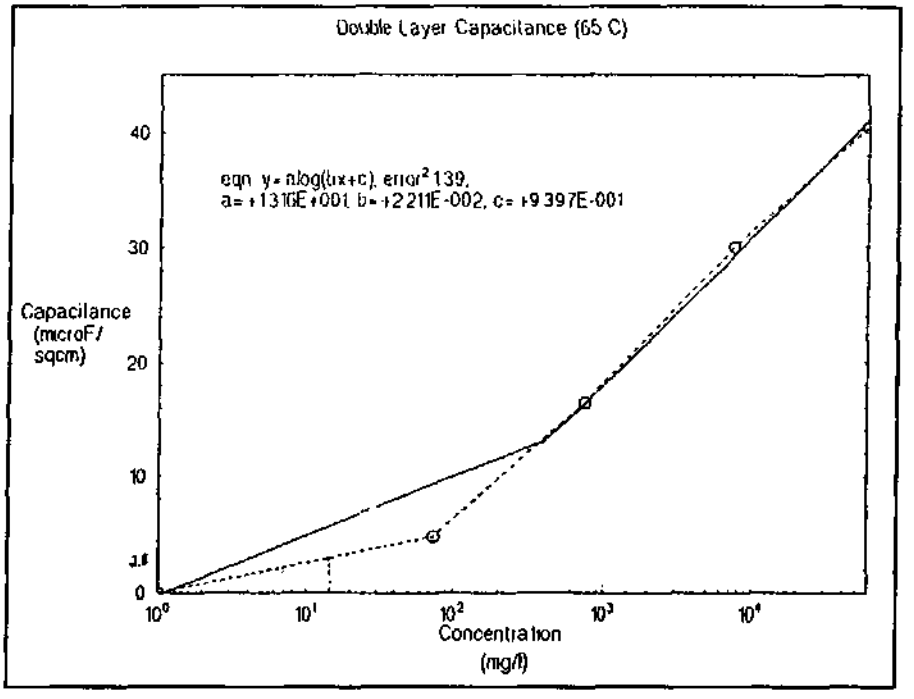

Figure 8 Calculation of the double-layer capacitance as a function of concentration at 45°C for the potassium chloride / membrane interface.

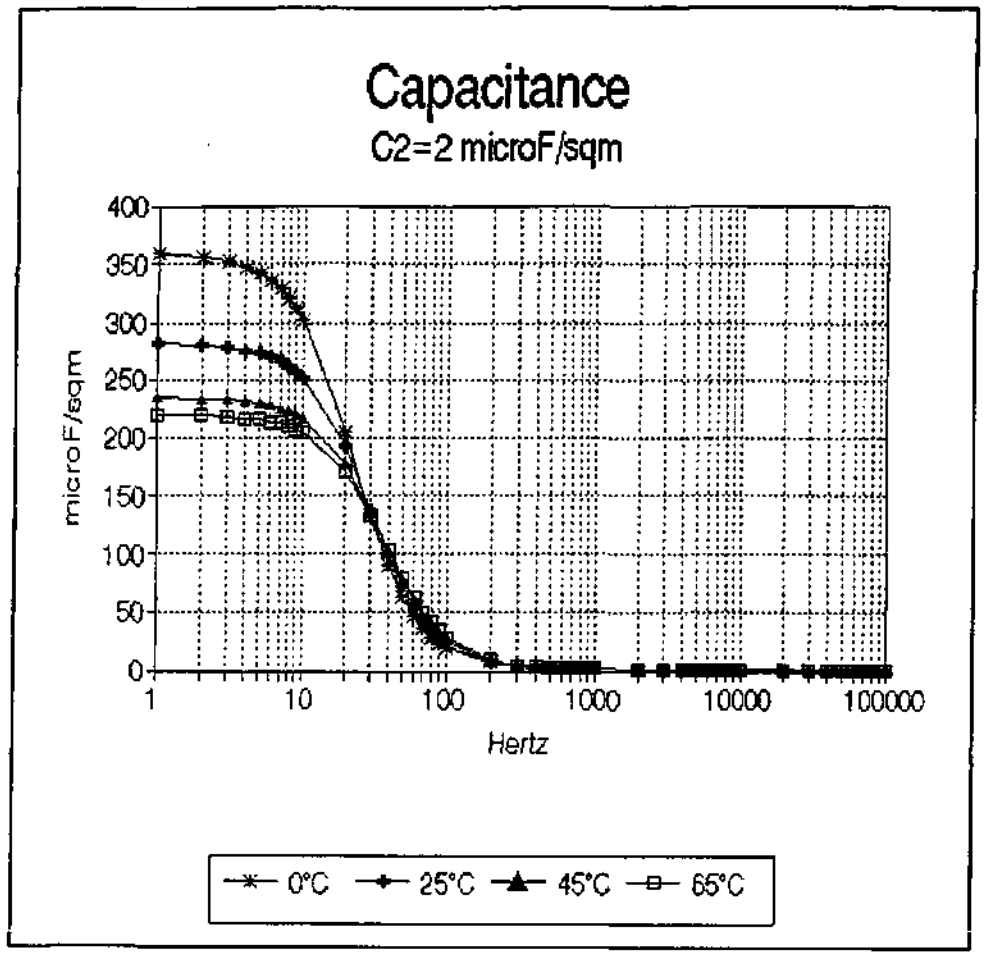

Figure 9 Double layer capacitance, the temperature dependence at various frequencies. Membrane capacitance assumed to be temperature independent at 2 $\mu F/m^2$

Although from Figure 9 it can be seen that there is not a linear relationship between capacitance and temperature over the two twenty degree ranges spanned, the variation of a few degrees in temperature does not change the capacitance much at the higher temperature (i.e. 45 °C to 65 °C). At lower temperature there is a larger variation in capacitance.

The effect of the magnitude of the double layer capacitance on the shape of the EIS spectrum will thus not be so pronounced at the higher frequencies where double layer relaxation is at values greater than 3000 Hz.

Calculations using various double layer capacitance values at 0 °C and 25 °C will be covered in a subsequent section. Only the effect of temperature on the magnitude of the capacitance is described here.

At higher concentrations, for example 1000 mg/ℓ KC*l*, the computed capacitance of the double layer varies from 21 μF/cm^2 at 0 °C to 19 μF/cm^2 at 45 °C and thus there is much less percentage variation in the capacitance values over the temperature range than at the low concentration of 15 mg/ℓ KC*l* where the range of capacitance over the same temperature varied from 4.6 μF/cm^2 to 3.0 μF/cm^2 respectively.

Clearly, temperature effects are more important at low ionic salt concentrations.

B.2.3.6 CONDUCTANCE VARIATION OF THE DOUBLE LAYER WITH TEMPERATURE

Continuing with the same three phase layer of the KC*l*/membrane interface the conductance G_1 as a function of frequency may be computed at various temperatures. In similar manner Figure 10 shows that the conductance reaches a limiting value at about 3000 Hz and that the influence of temperature on this variable is not as sensitive as was found to be the case for capacitance.

For a concentration of 15 mg/ℓ KC*l* only a small decrease in the conductance results from a 0 °C to 65 °C variations in temperature. Certain assumptions have to be made in these calculations; the main one being that the conductance of the membrane is relatively temperature independent.

It should be noted that the double layer conductance as computed is very different from the temperature dependence of bulk solution 15 mg/ℓ KC*l*. As may be seen from Table 4 (in the conductance).

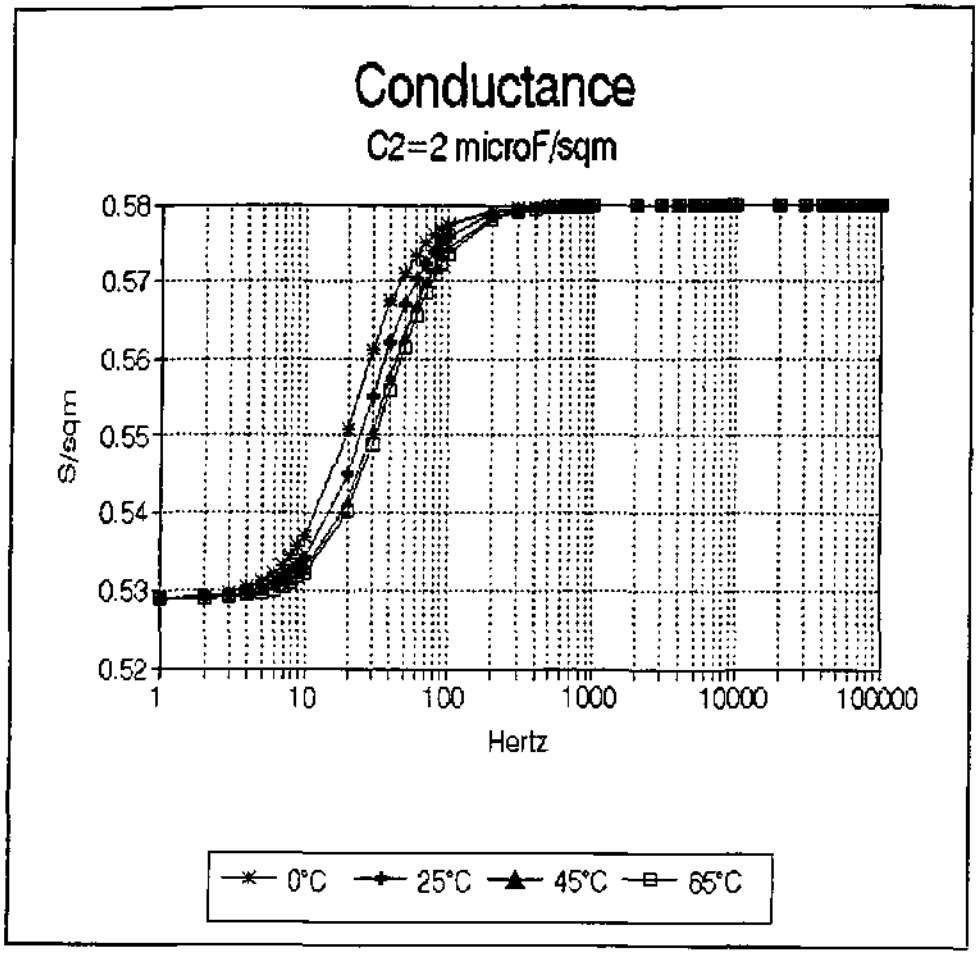

Figure 10 The variation of conductance with temperature at various frequencies $C_m = 2\ \mu F/m^2$.

B.2.3.7 VARIATION OF CAPACITANCE OF KCl WITH TEMPERATURE

In the three-phase model of the double-layer/membrane interface with C_1 and C_2 in series with the membrane, the Bode and Nyquist plots may be computed for the KCl/membrane system.

This model may then be fitted to the experimental results obtained. In order to observe the effect of temperature on the capacitance, a series of curves of capacitance with frequency at various temperatures were calculated so that during experiments it could be known in advance whether small temperature differences could lead to significant experimental errors.

For the Celgard membranes it was again assumed that there was no surface differences and that the membrane is uniform and isotropic.

The calculated double layer capacities as a function of concentration are shown in Figures 5 to 8 and the equations used to fit the data obtained at various temperatures by Grahame[7] are shown on the graphs themselves. There was no single equation which fitted the data over the whole temperature range.

Using a concentration of 15mg/ℓ KCl it may be seen that the absolute value of the double layer capacitance over the frequency range 1000 to 10000 Hz hardly varies at all at frequencies greater then 3000 Hz whereas at 1000 Hz the value of this capacitance varies from 0.046 F/m^2 at 0 °C to 0028 F/m^2 at 25 °C.

Although from Figure 9 it can be seen that there is not a linear relationship between capacitance and temperature over the two twenty degree ranges spanned, the variation of a few degrees in temperature does not change the capacitance much at the higher temperature (i.e. 45 °C to 65 °C).

At lower temperatures there is a larger variation in capacitance.

The effect of the magnitude of the double layer capacitance on the shape of the EIS spectrum will thus not be seen as KCl solution concentration increases over the range 0 °C - 25 °C.

B.2.3.8 MODEL OF THE KCℓ/MEMBRANE INTERFACE

Using various values for capacitance and impedance (conductance) in a simple two or three-phase-model, the calculation of a theoretical EIS spectrum with frequency is possible.

The variation of capacitance, C_1 = total double layer capacitance with frequency, affects the shape and magnitude of the entire system at the interface. In order to quantify what is being seen at the membrane/double layer interface a knowledge of the dependence of C_1 and C_2, (in the model shown below) on the capacitance values emerging from the EIS spectra, is necessary.

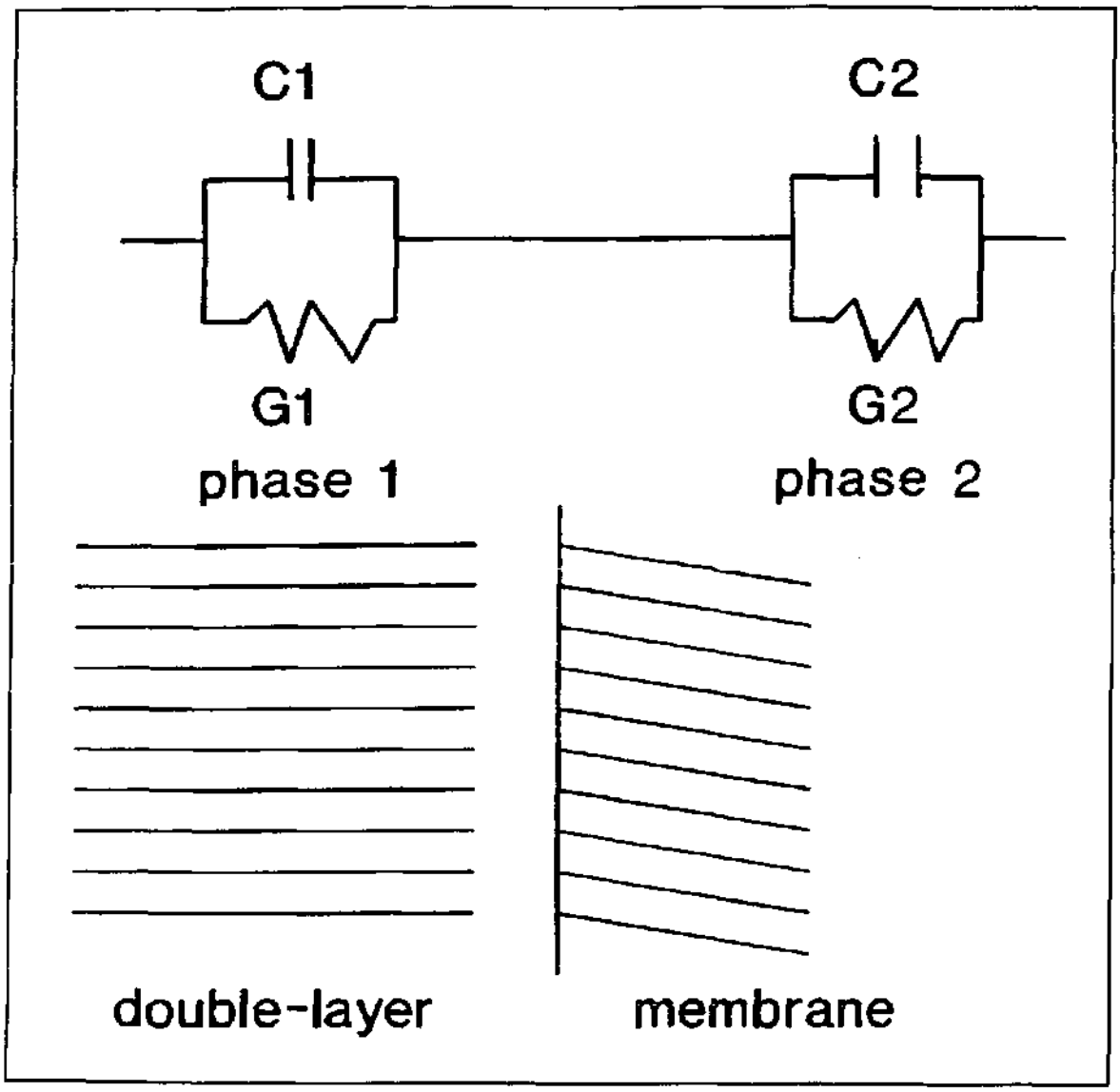

In the EIS technique, the double layer is perturbed at various frequencies and its frequency dependence may be understood by following the shape of the capacitance and conductance curves of the system as C_1 is varied keeping the other parameters constant.

A question now arises: What is the effect of an order of magnitude variation on the EIS obtained value of $C_{dl} = C_1$ = the capacity of the double layer?

Before any fitting of data to the experimentally determined EIS spectra at constant temperature the model needs to be tested to find out the trends of the data.

As the double layer capacitance may vary according to concentration and temperature a range of values has been covered. Figure 11 shows how the overall capacitance for the system responds to changes in C_1 from 36 $\mu F/m^2$ to 3600 $\mu F/m^2$ at 25 °C. It may be recalled from Figure 6 that for a 15 mg/ℓ KCl solution the calculated capacitance C_1 was 3.6 $\mu F/cm^2$ (or 36 000 $\mu F/m^2$). The detail of capacitance versus frequency shown in Figure 12 shows that over the frequency range 1 000 to 10000 Hz there is a value of C_1 which yields a maximum over the range 36 to 36 000 $\mu F/m^2$.

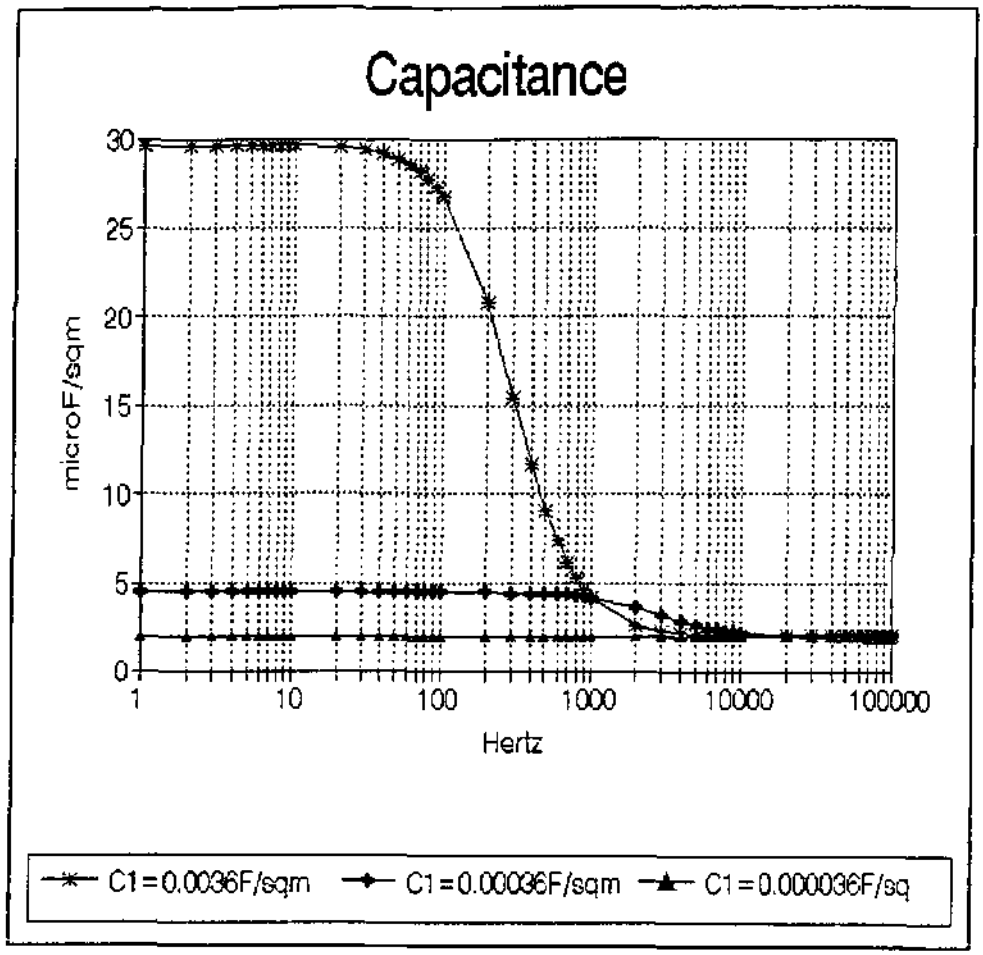

Figure 11 Capacitance of the double layer/membrane at 25 °C, as a function of frequency, keeping the membrane capacitance fixed at 2 $\mu F/m^2$, G_1 = 0.58 S/m, $G_2 = 6.0\ S/m^2$. Dependence of the magnitude of C_1 (double layer) on the overall capacitance of the system. KCl concentration = 15 mg/l.

Thus both high and low values of C_1 yield similar results in the overall capacitance of the KCl/membrane system. By considering other frequency ranges, however, there is fortunately some linearity. Between 100 to 1 000 Hz an increase in the value of C_1 results in a corresponding increase in interface capacity. At 0 °C, (Figure 13) the observation is very similar; the lower frequencies yielding the highest values of capacitance which reaches an asymptotic constant value where the frequency becomes less than 30 Hz or greater than 11 000 Hz.

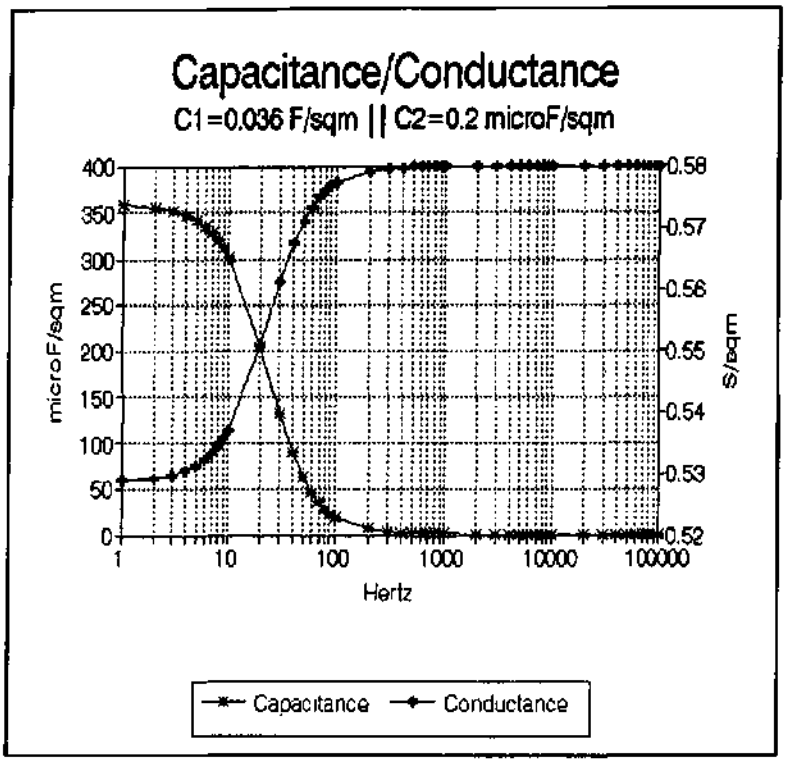

Figure 12 Variation of capacitance and conductance with frequency at 25°C.

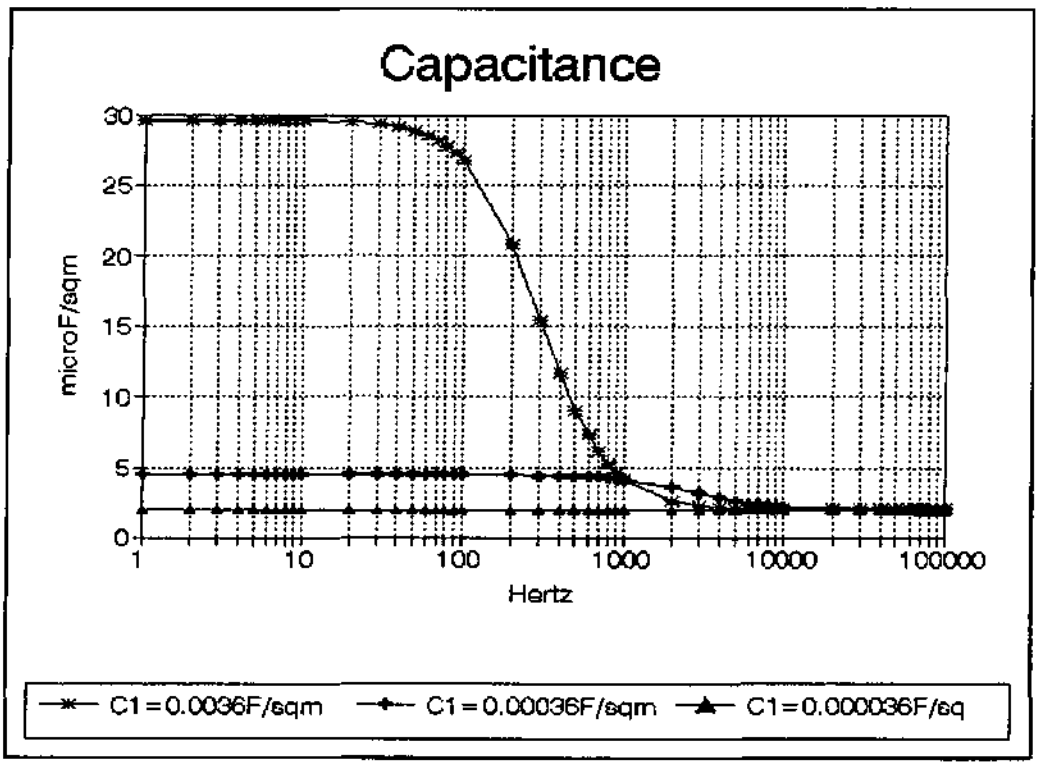

Figure 13 Capacitance of the double layer/membrane at 0 °C as a function of frequency; $C_2 = 2\ \mu F/m^2$, $G_1 = 0.58\ S/m^2$, $G_2 = 6.0\ S/m^2$. Dependence of the magnitude of C_1 on the overall capacity of the system. *KCl* concentration = 15 mg/l.

Another feature of Figure 11 is the observation that the larger the value of C_1, the lower the frequency limit where the slope of the graph changes rapidly prior to reaching an asymptotic value at high frequency.

These points of inflection should enable the observation of the range of C_1 to be estimated in addition to the absolute value in this model. A further feature of these capacitance graphs is the limiting value of the intercept in Figure 13, i.e. 2 $\mu F/m^2$ which is the value of C_2 at high frequency. Thus if the model is correct the experimental graph derived from the EIS spectra should yield an accurate value of C_2.

B.2.3.9 VARIATION OF MEMBRANE CAPACITANCE

In the analysis of the model so far C_1 the double layer capacitance was allowed to vary while C_2 the membrane capacitance was kept constant. In Figure 14, the effect of varying C_2, while C_1 is kept at 3600 $\mu F/m^2$ may be observed. The values of G_1 and G_2 are as before and the effect of varying these parameters will be discussed in a subsequent section.

If a shift in the y-axis value of capacitance of the membrane/KCl system occurs, the larger the value of C_2, then the larger the capacitances which are obtained at very high and very low frequencies.

At high frequency the limiting value of C_2 is observed at C_2 values between 0.2 and 20 $\mu F/m^2$ although at $C_2 = 200$ $\mu F/m^2$ the model does not follow this general finding, but the shape of the curve is the same with the region 100 Hz to 2000 Hz exhibiting the largest variation in the capacitance of the interface.

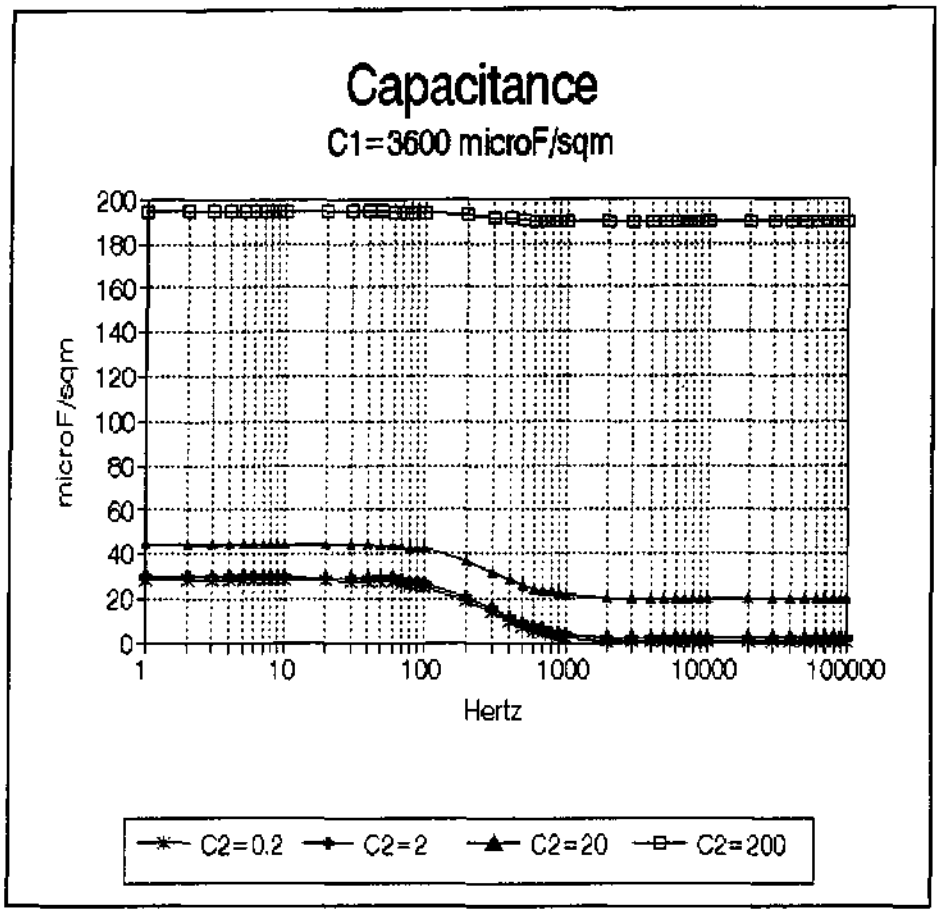

Figure 14 Capacitance of the double layer as a function of frequency, variation of the membrane capacitance C_2. C_1 is kept constant at 3600 μF/m². The KCl concentration = 15 mg/l.

As the value of C_1 calculated from actual double layer measurements at 25 °C was 36 000 μF/m² the capacitance of a system with C_1 = 36 000 μF/m² was computed in Figure 15 where the sensitivity of the capacitance with frequency is illustrated more clearly . A feature here which was not so clearly seen with lower values of C_1 is that at low frequencies less than 100 Hz the capacitance of the interface is not constant as was the case previously. While at high frequencies (greater than 7 000 Hz) this is constant. The change of shape now occurs at very low frequency i.e. 1 - 1 000 Hz after which the capacitance remains effectively constant.

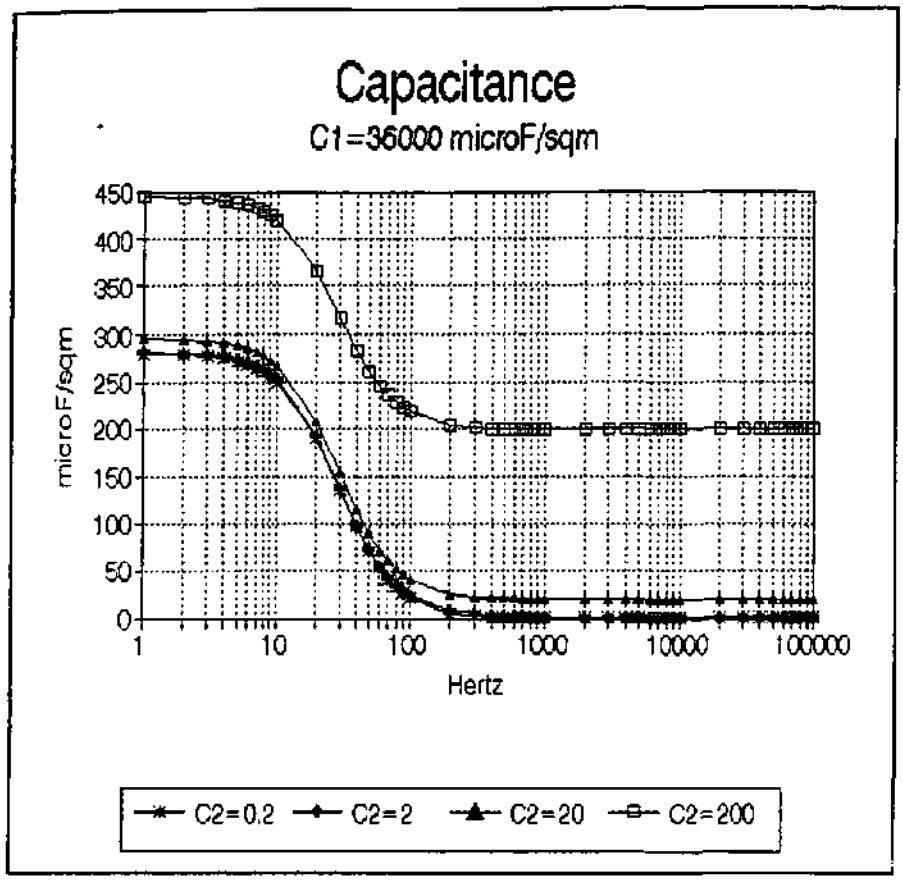

Figure 15 Capacitance of the double layer as a function of frequency, variation of the membrane capacitance C_2 while C_1 has a fixed value of 36000 μF/m². KCl concentration = 15 mg/l.

If Figure 15 is compared with Figure 31, it may be seen that the capacitance of the interface was constant from 1 to 100 Hz. Thus depending on the magnitude of the actual values of C_1 and C_2 they determine the frequency at which the change of shape in the capacitance occurs. This will accordingly be useful in fitting a model to the actual experiment obtained with EIS spectra.

B.2.3.10 EFFECT OF C_1 AND C_2 VARIATION ON THE CONDUCTANCE OF THE INTERFACE

Values of conductance of each phase of the interface also vary with frequency. In Figure 16 the double layer capacitance C_1 is varied over a suitable range from 3600 μF/m² to 36 μF/m² at 25 °C.

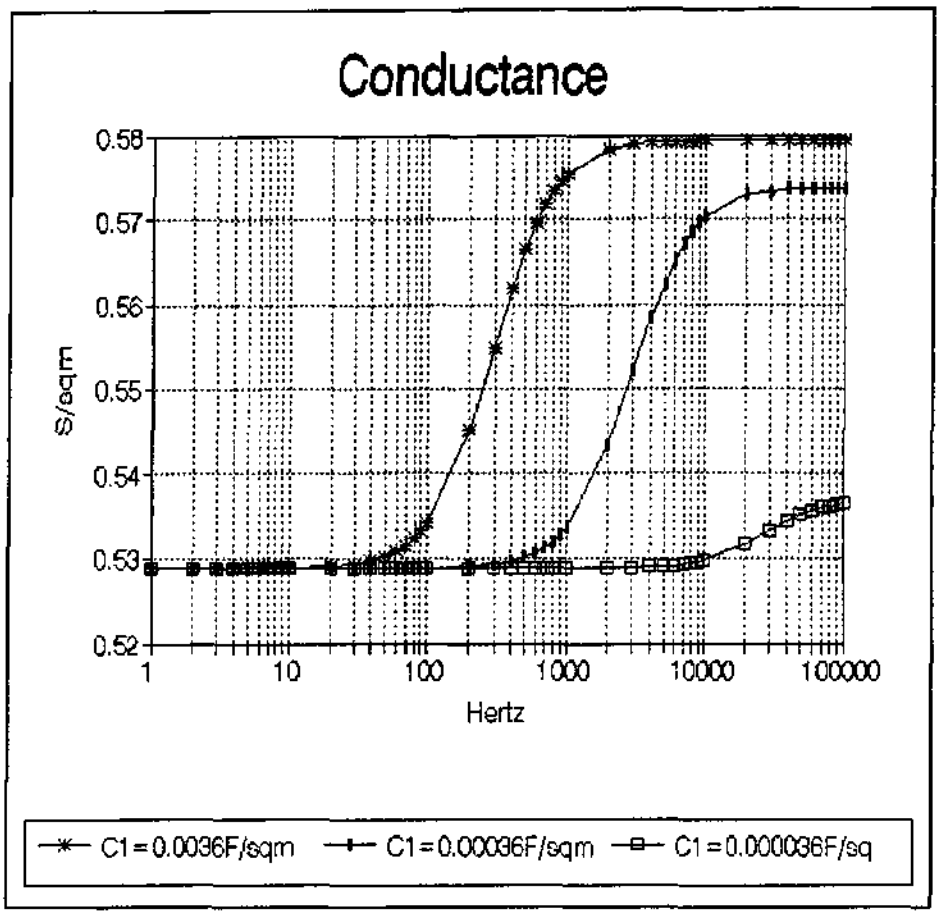

Figure 16 The effect of the double layer capacitance on the conductance of the phases at the interface. Values of C_1 as shown for a 15 mg/l KCl solution at 25 °C. C_2 = 2 μF/m², G_1=0.58 S/m², G_2 = 6.0 S/m².

The effect on the conductance is more dramatic than that of the capacitance of the interface. Very little change is observed for 36 μF/m² in the conductance which is constant from 1 to 3 000 Hz after which just a small increase is noted. As the value of C_1 increases there is a corresponding increase in conductance from 0.53 to 0.58 S/m².

The initial threshold frequency at which the conductance rises rapidly is a function of frequency, the greater the values of C_1, the lower the threshold frequency. Once again high and low frequency values of conductance of the interface are constant.

A feature of the conductance-frequency curves is that the low and high frequency values of limiting conductance are invariant with changes in the values of both C_1 and C_2.

Figure 17 and 18 illustrate this. In Figure 17 for a value for C_1 of 3600 $\mu F/m^2$ and a value for C_1 of 36 000 $\mu F/m^2$ (the double layer capacity at 25 °C for 15 mg/ℓ KCl solution) in Figure 18 is used, which shows that only at C_2 = 200 $\mu F/m^2$ a noticeable difference in conductance is observed. At values from 0.2 to 20 $\mu F/m^2$ there is no calculated effect on the magnitude of the conductance which are all fitting on the same curve.

In Figure 17, with a lower value of C_1 at 3600 $\mu F/m^2$ there is a more pronounced variation of the conductance at frequencies greater than 100 Hz.

Having examined the model of the KCl//membrane interface theoretically, now enables a fit of the model to experimentally obtained data to be attempted.

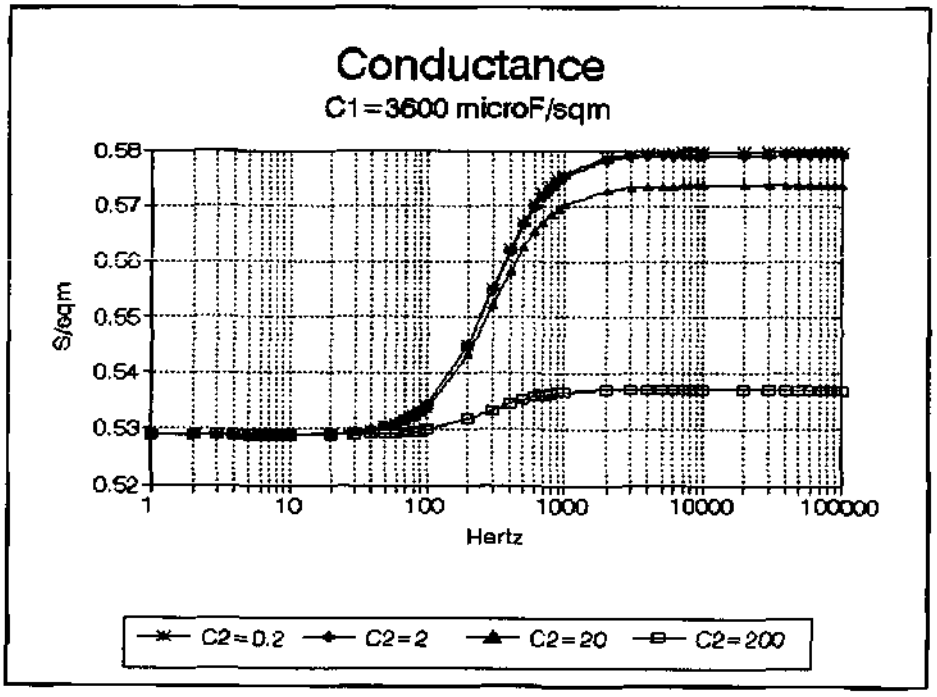

Figure 17 The effect of membrane capacitance variation on the interfacial conductance of the phases for a 15 mg/l KCl concentration. C_1 = 3600 $\mu F/m^2$.

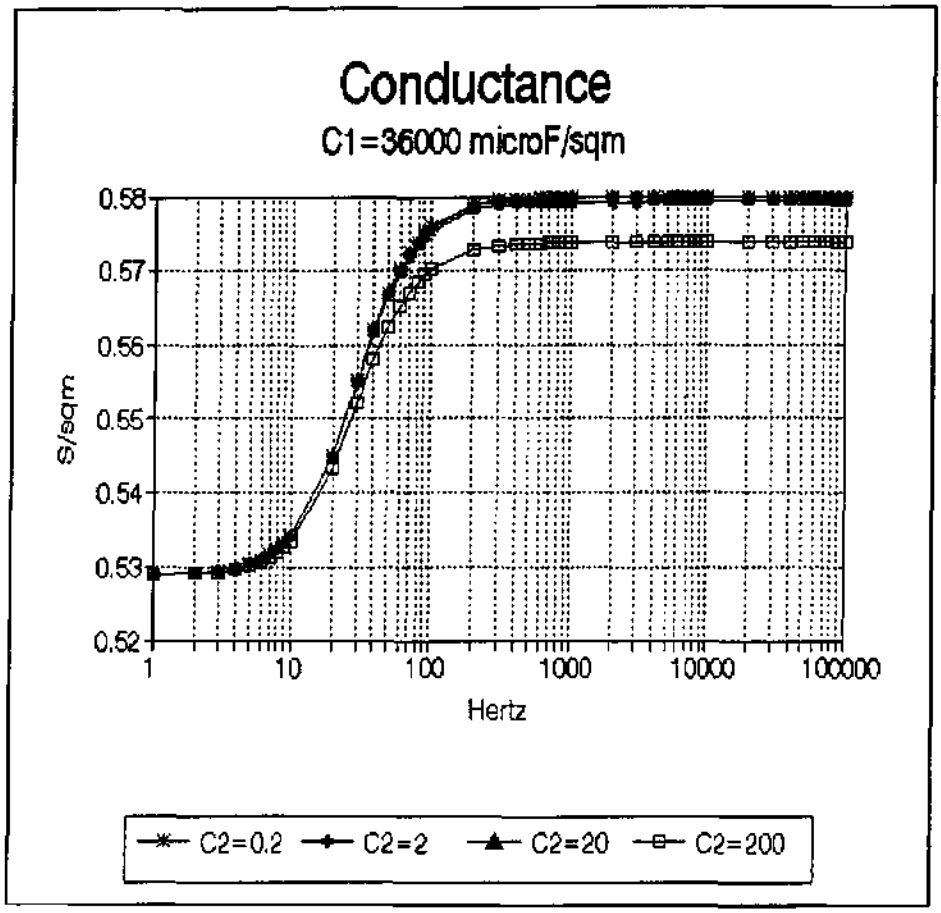

Figure 18 The effect of membrane capacitance variation on the interfacial conductance of the phases for a 15 mg/l KCl concentration with $C_1 = 36\,000\ \mu F/m^2$.

B.2.3.11 TEST OF THE KCl/MEMBRANE THEORY.

Although the method of calculating the total capacity of the interface C_T and the conductance of the double layer was detailed in the report of May 1994 a brief mention of the calculation principles for easy reference will not be out of place.

Figure 19 shows a Nyquist plot of the RC-network as follows.

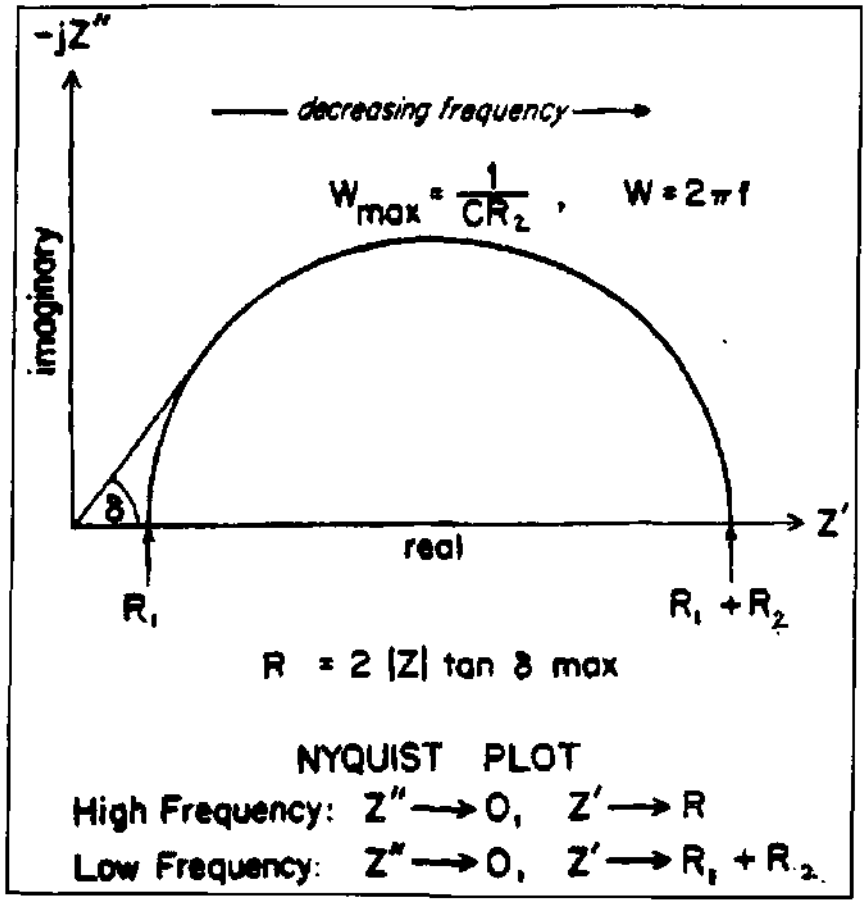

Figure 19 Electrochemical impedance profile for a simple electrochemical system.

A typical computer-fitted curve to the experimentally obtained points is shown in Figure 20 for a 15 mg/ℓ KC*l* solution Celgard 4510 Hydrophobic membrane at 25 °C.

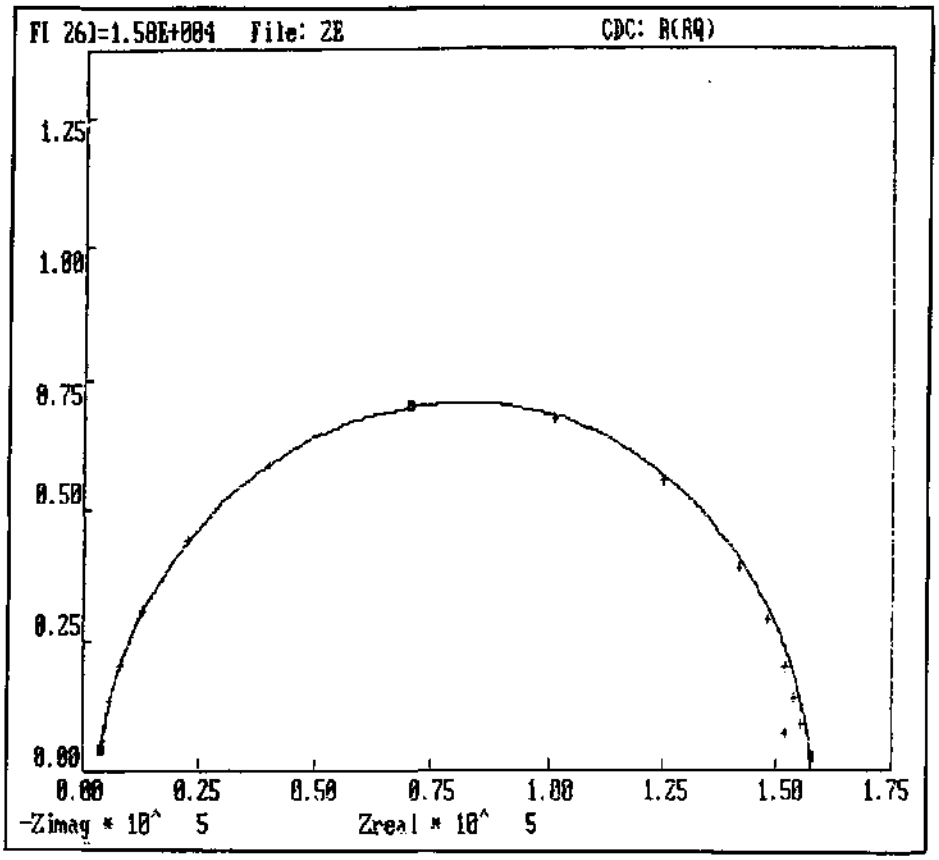

Resistance 1 = 3.157E+03 7.21% [ohm]
Resistance 2 = 1.521E+05 3.40% [ohm]
Capacitance 3 = 2.820E-09 4.79% [Farad]

Figure 20 Computer plotted Nyquist diagram for 15 mg/l KCl at 25 °C / Celgard 4510 Hydrophobic membrane where the capacitance C_T has been calculated. Resistances R_1 and R_2 are calculated in addition.

The following data were obtained from Figure 20

$R_1 = 3.157 \times 10^3$ ohms

$R_2 = 1.521 \times 10^5$ ohms

$C_T = 2.82 \times 10^{-9}$ farads.

Area of membrane = 51.6×10^{-4} m^2 = 51.6 cm^2

thus $C_T = 0.546$ μF/m^2

How does the experimentally measured value of C_T compare with the model of the KCl/membrane interface where the two phase model is used?

At 25 °C the value of C_1 in the KCl/membrane system, was calculated from data to be 36 000 $\mu F/m^2$ with the membrane capacitance being in the range ± 2 $\mu F/m^2$ from literature [2].

The larger capacity is expected to be on the solution side of the membrane because it is more conducting.

It may already be seen that temperature is not the dominating variable in the model. Values of C_1 and C_2, however, dictate the magnitude of C_T.

Referring to Figures 11 and 15 where C_1 and C_2 are varied respectively, it is clear that a value of 36 000 $\mu F/m^2$ together with a low value (Figure 13) of C_2 will never be able to yield a low value for C_T of 0.546 $\mu F/m^2$ thus the calculated double layer capacitance of 36 000 $\mu F/m^2$ is far two high to combine with 2 $\mu F/cm^2$ for the membrane capacitance. To obtain a value for C_1 that does fit the data, Figure 11 must be consulted where a value of $C_1 = 36\ \mu F/cm^2$ combined with $C_2 = 2\ \mu F/cm^2$ yields a value of C_T of the order of 2 to 3 $\mu F/cm^2$.

It has previously been shown that the high frequency value of C_2 is always constant and in this model C_1 is greater than C_2 . Accordingly, the value of C_2 must be less than 2 $\mu F/cm^2$ so that C_T can be experimentally determined as 0.546 $\mu F/m^2$.

An important feature is that the EIS spectrum is not recording the interface double layer/membrane but from the values measured the two phases that are being probed have capacities that belong to the more restricted phases which could be one of the following:-

(i) the interface is a composite of electrolyte film and skin layer of the membrane since the capacity C_T is more membrane-like than double layer-like or

(ii) the Celgard membrane possesses a skin and bulk capacitance and that the EIS technique is probing the membrane rather than the double layer.

The latter statement should be proven by changing the electrolyte in various ways to establish the sensitivity of the EIS technique to the nature of the electrolyte composition and concentration.

An effect of the compact double layer, as the phase that has a much smaller capacity than predicted, needs to be considered in the conductance part of the EIS spectrum which has yet to be discussed in more detail.

Considering the model (ii) mentioned above which is more membrane-like, a few calculations were made to see if the value of $C_T = 0.565\ \mu F/cm^2$ could be arrived at with the two phases differing in that $C_1 > C_2$.

In a previous preliminary report to the WRC (EIS techniques for membrane characterisation, J.J. Smit, O.J. Van der Shijff, F.A. Hawkins and A.F. Van der Merwe, April 1994) the value of C_T obtained for a Celgard Membrane 4510 (hydrophobic), was estimated to be between 0.68 and 2.44 $\mu F/m^2$.

Thus a suitable value for C_2 was deemed to be 2 $\mu F/m^2$, using the two phase model, C_1 at 200 $\mu F/cm^2$ and $G_1 = 0.58\ S/m^2$, $G_2 = 6.0\ S/m^2$.

A capacitance-frequency curve shown in Figure 31 results where a value of $C_T = 3.2\ \mu F/m^2$ was obtained. Although not close to $C_T = 0.565\ \mu F/m^2$, this model and values of C_1 and C_2 are approaching the right order of magnitude required to fit the experimental data.

In the event that it is not possible to distinguish between a model in which two phases are a layer adjacent to the membrane or electrolyte and the membrane surface or a skin and bulk membrane layer, further experiments were done using sodium fluoride to examine the solution side of the electrolyte/membrane interface.

In summary: The EIS spectrum "sees" two layers which have two different capacity values. The value C_2 which is membrane-like is less than 2 $\mu F/m^2$ whereas the adjacent layer has a larger value in the range 20 to 200 $\mu F/m^2$ and exhibits a measure of electrolyte character. The layers cannot be ascribed to a pure electrolytic double layer/membrane interface or phenomenon.

B.2.3.12 STUDY OF THE ELECTROLYTE SIDE OF THE INTERFACE

As mentioned earlier the capacity of the cation does not vary to any marked extent although the capacity of the halide anions follows a trend. Accordingly there should be a difference between fluoride and chloride. The transport numbers of K^+ and Cl^- are about equal as are Na^+ and F^- which is why KF was not selected for the experimental work.

A summary of the data R_1, R_2 and C_T is shown in the following tables. Table 5 was drawn up from a series of Nyquist curves at various times from the commencement of the experiments with a new piece of membrane in each case.

The main feature of the data is that R_1 and R_2 decrease with time until a limiting value is reached after several hours equilibrium and as might be anticipated, the values of R_1 and R_2 decrease with increasing KCl concentration. Values of the capacitance C_T lie in the range 1.92×10^{-9} to 3.54×10^{-9} F/area.

The actual area used was 51.6 cm^2 in each case. Whether the apparent maxima in the capacity as the KCl concentration increases are real, requires more statistical verification.

For a 150 mg/ℓ KCl solution the value of C_T is about 3.0×10^{-9} F/area. In the case of a 150 mg/ℓ NaF solution (Table 6) the corresponding value is 3.6×10^{-9} F/area. This value is not sufficiently different to be significant unless one uses the fact that the double layer capacity of fluoride (the inner layer value is 46.8 $\mu F/cm^2$) is greater than that of chloride at 35.2 $\mu F/cm^2$.

TABLE 5
EIS RESULTS OF CELGARD 4510 HYDROPHOBIC MEMBRANE
KCl SYSTEM at ±25°C

mg/l KCl		0 hr	1 hr	2 hr	3 hr	4 hr
1.5	R1	19378	13179	7253	4590	3328
	R2	10466840	7719731	5329004	3106044	2590252
	C	1.92E-09	1.82E-09	1.92E-09	1.94E-09	2.00E-09
3	R1	14432	9273	6342	4668	3918
	R2	5464485	6715648	7090338	3133836	2822569
	C	2.44E-09	2.66E-09	2.74E-09	2.68E-09	2.69E-09
5	R1	12463	8504	3969	3874	3397
	R2	5361868	4765489	2901058	2707657	2467250
	C	2.96E-09	2.99E-09	3.02E-09	2.98E-09	3.02E-09
7.5	R1	9713	8323	5812	4768	3790
	R2	2526223	3510894	3581407	2578700	2214518
	C	3.11E-09	3.33E-09	3.33E-09	3.32E-09	3.33E-09
10	R1	6574	6327	4918	3921	3383
	R2	3206644	3184574	3242305	2572994	2347749
	C	3.42E-09	3.55E-09	3.55E-09	3.56E-09	3.54E-09
15	R1	4197	4070	3567	2915	1450
	R2	1186787	827180	635104	505016	486098
	C	2.74E-09	2.8E-09	2.86E-09	2.94E-09	3.02E-09
50	R1	1539	1607	1478	1365	1272
	R2	3351305	2037158	1330177	1245519	1029742
	C	2.23E-09	2.52E-09	2.56E-09	2.55E-09	2.57E-09
100	R1	903	914	866	841	805
	R2	589948	257347	255934	249282	243277
	C	2.43E-09	2.58E-09	2.64E-09	2.66E-09	2.70E-09
150	R1	489	657	646	636	620
	R2	278652	149001	143392	136574	130698
	C	2.73E-09	2.98E-09	2.97E-09	2.97E-09	2.97E-09

TABLE 6
EIS RESULTS OF CELGARD 4510 HYDROPHOBIC MEMBRANE
NaF SYSTEM at ±25°C

mg/l NaF		0 hr	1 hr	2 hr	3 hr	4 hr
1.5	R1	12340	8457	6177	4727	3680
	R2	1224416	1631486	2070783	2228691	2062126
	C	1.65E-09	1.83E-09	1.97E-09	2.02E-09	2.09E-09
3	R1	9245	8267	5925	4650	3872
	R2	3602966	4427085	3626345	3343446	2893960
	C	2.26E-09	2.26E-09	2.26E-09	2.29E-09	2.30E-09
5	R1	6354	5055	3674	3750	3188
	R2	3760005	3993256	3288138	3143123	2975619
	C	2.25E-09	2.30E-09	2.33E-09	2.29E-09	2.33E-09
7.5	R1	2237	2212	2008	1788	1646
	R2	2641891	2281189	1899002	1757216	1668481
	C	2.45E-09	2.44E-09	2.46E-09	2.47E-09	2.46E-09
10	R1	3680	3756	3292	2938	2564
	R2	1445420	1666269	1966024	2021489	1841152
	C	2.47E-09	2.55E-09	2.59E-09	2.63E-09	2.66E-09
15	R1	4009	3854	3618	3214	2824
	R2	2548274	2581375	2558102	2476873	2161111
	C	2.63E-09	2.67E-09	2.67E-09	2.72E-09	2.71E-09
50	R1	1223	1379	1360	1300	1266
	R2	1909681	1972031	1819476	1782242	1679117
	C	2.44E-09	2.76E-09	2.77E-09	2.72E-09	2.74E-09
100	R1	722	793	783	739	707
	R2	931880	850103	789182	759340	754739
	C	3.13E-09	3.28E-09	3.27E-09	3.28E-09	3.30E-09
150	R1	503	602	580	551	528
	R2	314626	280192	267176	257234	255832
	C	3.40E-09	3.62E-09	3.62E-09	3.64E-09	3.64E-09

Curiously enough, if the ratio 3.6/3.0 = 1.2 from the C_T values obtained experimentally is compared with the electrochemically obtained ratio 46.8/35.2 above, this is equal to 1.3, which is close.

Additional information may support or contradict the apparent difference of anion seen in the EIS technique.

It has already been stated that the model of the double layer/membrane is not the one seen by the EIS method. Insufficient data with the dilute solutions studied to date is part of the problem. What can be said, however, is that the membrane which is possibly the important part of the interface is emphasised at the expense of the electrolyte.

Analysis of the resistance and subsequent conductance of the system has not yet been attempted as it involves even more calculation and this is currently in progress.

The value of the Tables 5 to 7 is that important characterisation of membranes is clearly verified as supporting data to the early experiments. The characterisation of membranes into two categories which may be achieved when experimentally obtained C_T and R_1, R_2 is referred to and properly correlated.

TABLE 7

EIS RESULTS OF CELGARD 5511 HYDROPHILIC MEMBRANE

KCl SYSTEM at ±25°C

mg/l KCl		0 hr	1 hr	2 hr	3 hr	4 hr
1.5	R1	4286	3229	2242	1748	1079
	R2	7109	4885	3715	3545	3965
	C	1.00E-09	9.94E-10	1.04E-09	8.49E-10	5.85E-10
3	R1	3689	2820	2202	1814	1626
	R2	5715	4383	3338	2664	2340
	C	1.13E-09	1.14E-09	1.23E-09	1.36E-09	1.47E-09
5	R1	5884	4423	3280	2569	2039
	R2	9632	7220	5098	3738	2774
	C	1.29E-09	9.88E-10	1.04E-09	1.17E-09	1.36E-09
7.5	R1	4192	3295	2729	2332	2079
	R2	5554	4321	3501	2800	2410
	C	1.44E-09	1.33E-09	1.41E-09	1.61E-09	1.89E-09
10	R1	3714	3003	2309	2036	1661
	R2	5478	4422	3175	2557	2006
	C	1.83E-09	1.30E-09	1.46E-09	1.50E-09	1.63E-09

According to M.A. Devanathan [6] the capacities of the inner layer and outer layer were calculated and tabulated to be the following:-

TABLE 8
INNER- and OUTER LAYER CAPACITIES

ION	C INNER LAYER ($\mu F/cm^2$)	C DIFFUSE LAYER ($\mu F/cm^2$)
potassium	47.9	26.6
fluoride	46.8	27.0
chloride	35.2	33.3
bromide	32.6	36.0
iodide	29.5	40.8
water	17.1	17.1

Depending on the relative concentrations of each ion in the diffuse and compact layers, capacities may be calculated. This type of analysis has not been applied in this report yet and subsequent experiments have to be done to elucidate this.

B.2.4 CHARACTERISATION OF MEMBRANES ACCORDING TO R_1, R_2 AND C_T.

Results of experiments with Celgard membranes revealed two sets of data depending on the hydrophobic or hydrophilic character of the membrane. It remained to be seen whether membranes selected at random would fit the two categories outlined or alternatively an intermediate type. The extent to which several membranes have been characterised is discussed in the following sections.

The Celgard type of membrane yield the data in Table 5 for the hydrophobic type and data for the hydrophilic type.

Values of R_2 are orders of magnitude smaller in the case of the hydrophilic compared to

the hydrophobic membrane. This may be illustrated by the following data after 4 hours of conditioning.

TABLE 9

COMPARISON OF HYDROPHOBIC AND HYDROPHILIC MEMBRANES

Membrane Type	Electrolyte	R_1 (Ω)	R_2 (Ω)	C_T ($F.m^{-2}$)
Celgard 4510 (hydrophobic)	10 mg/ℓ KCl	3382	2347749	3.54×10^{-9}
Celgard 4510 (hydrophobic)	10 mg/ℓ NaF	2823	2161111	2.71×10^{-9}
Celgard 5510 (hydrophilic)	10 mg/ℓ KCl	1660	2006	1.63×10^{-9}

There is a 1000 times increase in R_2 when the membrane is hydrophobic in 10 mg/ℓ KCl solution. At other concentrations R_2 is still always greater for the hydrophobic compared with the hydrophilic membrane. As the resistance of the R_2 parameter decreases with increasing electrolyte solution the contrast is less marked at concentrations of 150 mg/ℓ and higher (R_1 = 619 Ω and R_2 = 130697 Ω after 4 hours in 150 mg/ℓ KCl solution).

The capacity at 2.97×10^{-9} F/area is not very different from the 10 mg/ℓ KCl solution which was 3.54×10^{-9} F/area. In order to test the R_2 rule above, a series of 10 different ultrafiltration and reverse osmosis membranes all of the same surface area were tested.

In addition to the R_2 criteria mentioned above, in dilute electrolyte solutions a further identifying feature is present to distinguish between hydrophobic and hydrophilic membranes.

This is that where as the Nyquist plot is complete for any hydrophobic membrane over the frequency range 1 Hz to 10^5 Hz, the hydrophilic membranes only yield a partial Nyquist plot and R_1 never intercepts the x - axis but must be estimated by extrapolation using a

computer fitted curve. These features may be seen in the following Figures 21 - 30. Data for R_1, R_2 and C_T are summarised in Table 10 with the membranes numbered. These numbers correspond to the following membranes:

TABLE 10B

MEMBRANES OF RUSSIAN ORIGIN CHARACTERISED BY EIS

No	Type	Pore Size(μ)	Flux $l.m^{-2}hr^{-1}$	Temp °C	Rejec-tion(%)	P(MPa)	Medium %NaCl	HL/HB
1	MF(PVDF)	0.4	15000	< 80				HL
2	MF(PVDF)	0.15		< 80				HB
3	UF(PA)	kD/50	60-1560		> 95			HL
4	RO(PA)		100	50	90	3	0.5	HL
5	UF(PA)	kD/10	60-1560		95			HL
6	UF(PS)	kD/100						HL
7	UF(PVDF)		1000	< 80				HB
8	UF(PVDF)	0.09	35					HL
9	UF(PSA)	kD/50	120		99.7			HL
10	UF(PSA)		100		95			HL

PVDF Polyvinylideneflouride

MF Micro filtration

UF Ultrafiltration

PA Polyamide

PSA Polysulphonamide

RO Reverse Osmosis

HL Hydrophilic

HB Hydrophobic

TABLE 10

EIS RESULTS OF RUSSIAN MEMBRANES

NO STIRRING

	Time (hr)	0	1		2		3	
1	25 °C						26 °C	
	R1	2370	R1	2140	R1	1942	R1	1900
	R2	3575	R2	3363	R2	3161	R2	2776
	C	6.297E-10	C	5.358E-10	C	4.933E-10	C	5.375E-10
2	25°C						26°C	
	R1	4370	R1	3896	R1	3872	R1	3804
	R2	10363869	R2	18959232	R2	20048608	R2	21606399
	C	9.897E-10	C	1.059E-09	C	1.109E-09	C	1.136E-09
3	25°C						26°C	
	R1	2492	R1	2273	R1	2260	R1	2110
	R2	2967	R2	2993	R2	2752	R2	2706
	C	7.353E-10	C	6.441E-10	C	6.933E-10	C	6.774E-10
4	25°C						26°C	
	R1	2736	R1	2185	R1	2119	R1	2041
	R2	3287	R2	3170	R2	2836	R2	2720
	C	8.495E-10	C	5.328E-10	C	6.118E-10	C	6.182E-10
5	25°C						26°C	
	R1	2555	R1	2288	R1	2184	R1	2161
	R2	3912	R2	3641	R2	3440	R2	3377
	C	5.984E-10	C	5.249E-10	C	5.166E-10	C	5.312E-10

TABLE 10 (Continue)

EIS RESULTS OF RUSSIAN MEMBRANES

NO STIRRING

	Time (hr)	0	1		2		3	
6	24°C						25°C	
	R1	2589	R1	2516	R1	2421	R1	1131
	R2	3837	R2	3636	R2	3507	R2	4569
	C	6.91E-10	C	6.609E-10	C	6.398E-10	C	6.196E-10
7	25°C						25°C	
	R1	5647	R1	5036	R1	5059	R1	4993
	R2	2118183	R2	1520873	R2	1659073	R2	1741057
	C	1.926E-09	C	1.999E-09	C	2.046E-09	C	2.084E-09
8	24°C						25°C	
	R1	2548	R1	2490	R1	2425	R1	2352
	R2	3341	R2	3015	R2	2897	R2	2792
	C	8.33E-10	C	7.572E-10	C	7.706E-10	C	7.271E-10
9	23°C						25°C	
	R1	2687	R1	2548	R1	2354	R1	2431
	R2	3463	R2	3334	R2	3391	R2	3177
	C	1.113E-09	C	9.885E-10	C	8.112E-10	C	8.729E-10
10	25°C						26°C	
	R1	2819	R1	2515	R1	2597	R1	2463
	R2	3043	R2	2916	R2	2712	R2	2657
	C	8.416E-10	C	8.367E-10	C	9.193E-10	C	8.785E-10

TABLE 10 (Continue)

EIS RESULTS OF RUSSIAN MEMBRANES

STIRRING 135 r.p.m.

	Time (hr)	0	1		2		3	
1	26°C						31°C	
	R1	1627	R1	1476	R1	1384	R1	1285
	R2	2827	R2	2610	R2	2390	R2	2159
	C	9.686E-10	C	9.69E-10	C	1.011E-09	C	1.032E-09
2	26°C						32°C	
	R1	3455	R1	3261	R1	3049	R1	3028
	R2	9108536	R2	8731632	R2	8360625	R2	7417223
	C	1.165E-09	C	2.229E-09	C	2.676E-09	C	2.7E-09
3	26°C						32°C	
	R1	2003	R1	1743	R1	1608	R1	1471
	R2	2806	R2	2528	R2	2257	R2	1996
	C	1.331E-09	C	1.081E-09	C	1.068E-09	C	1.071E-09
4	26°C						32°C	
	R1	2047	R1	1964	R1	1774	R1	1668
	R2	2937	R2	2740	R2	2442	R2	2243
	C	1.138E-09	C	1.077E-09	C	1.046E-09	C	1.07E-09
5	26°C						30°C	
	R1	2289	R1	2145	R1	2036	R1	1974
	R2	3345	R2	3177	R2	2898	R2	2753
	C	1.115E-09	C	1.084E-09	C	1.104E-09	C	1.133E-09

TABLE 10 (Continue)

EIS RESULTS OF RUSSIAN MEMBRANES

STIRRING 135 r.p.m.

	Time (hr)	0	1		2		3	
6	25°C						30°C	
	R1	2226	R1	2082	R1	1504	R1	1570
	R2	3662	R2	3512	R2	3299	R2	2927
	C	1.135E-09	C	1.061E-09	C	1.585E-09	C	1.365E-09
7	25°C						30°C	
	R1	3757	R1	3981	R1	4010	R1	3862
	R2	1877623	R2	803806	R2	269521	R2	214122
	C	2.075E-09	C	4.181E-09	C	7.028E-09	C	7.814E-09
8	25°C						30°C	
	R1	2258	R1	1908	R1	1741	R1	1609
	R2	2927	R2	2532	R2	2270	R2	2057
	C	1.388E-09	C	1.132E-09	C	1.144E-09	C	1.168E-09
9	25°C						30°C	
	R1	2302	R1	2188	R1	2149	R1	2047
	R2	3527	R2	3291	R2	2997	R2	2866
	C	1.406E-09	C	1.128E-09	C	1.574E-09	C	1.234E-09
10	26°C						30°C	
	R1	2313	R1	2120	R1	1907	R1	1780
	R2	3035	R2	2888	R2	2495	R2	2272
	C	1.274E-09	C	1.153E-09	C	1.251E-09	C	1.214E-09

Table 11 supplies the details of each membrane tested in 15 mg/ℓ KC*l* solution. In Figure 21 the Nyquist plot of membrane No.1, after equilibrium of 4 hours in 15 mg/ℓ KC*l*, is shown. It is apparent that the plot is incomplete and that only R_2 intercepts. In addition R_2 is low at ± 2776 ohms with no stirring. The membrane is thus identified as a hydrophilic type which is indeed the case.

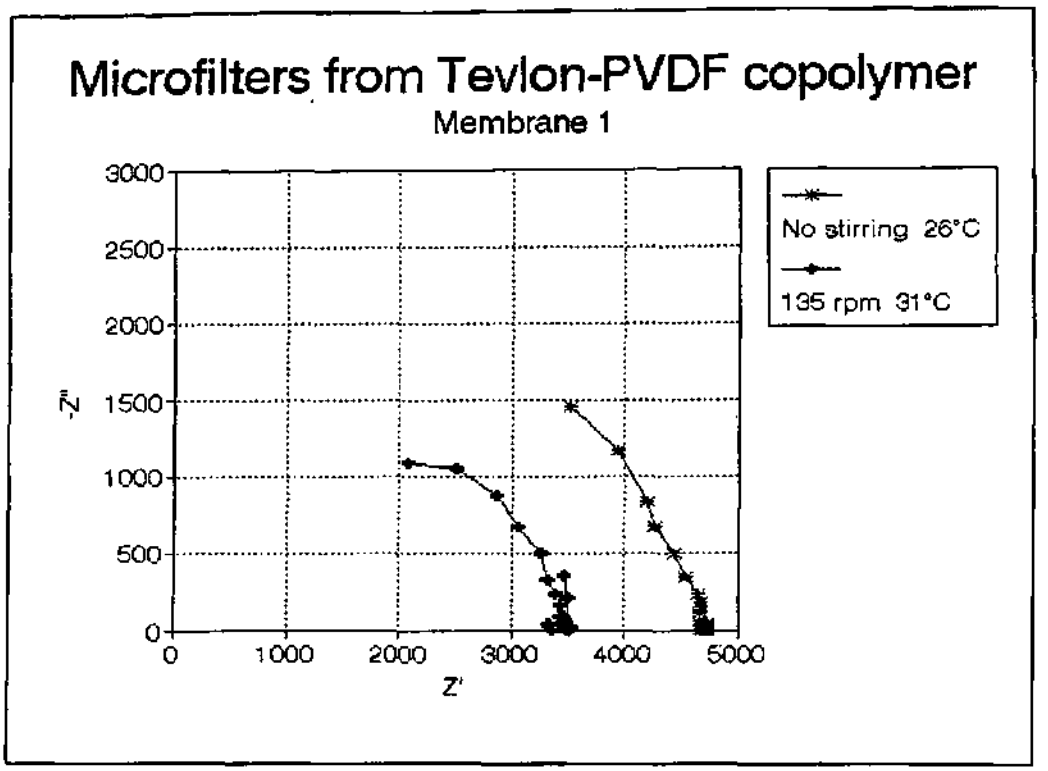

Figure 21 EIS spectrum of membrane 1

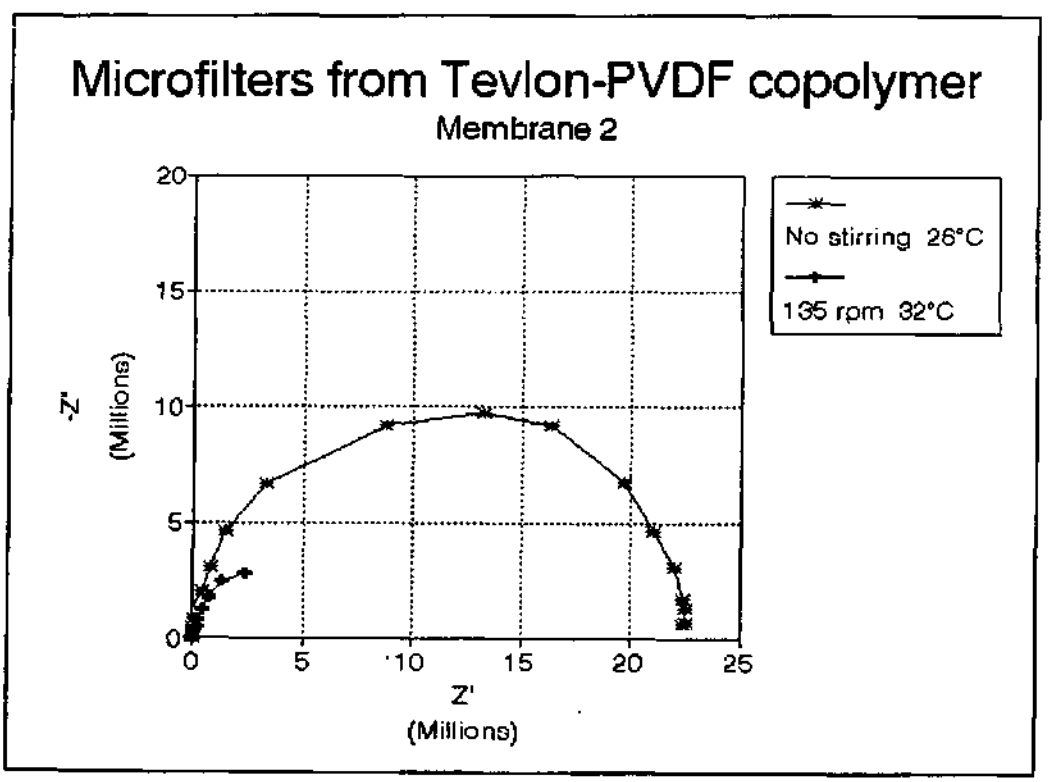

Figure 22 EIS spectrum of membrane 2

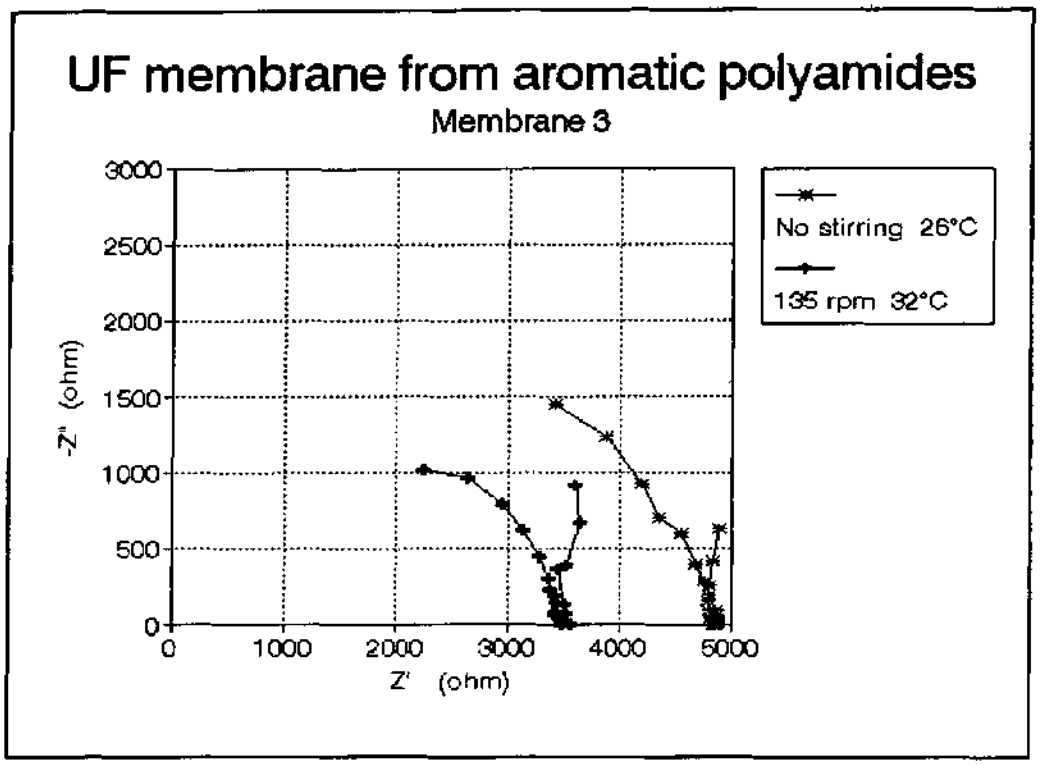

Figure 23 EIS spectrum of membrane 3

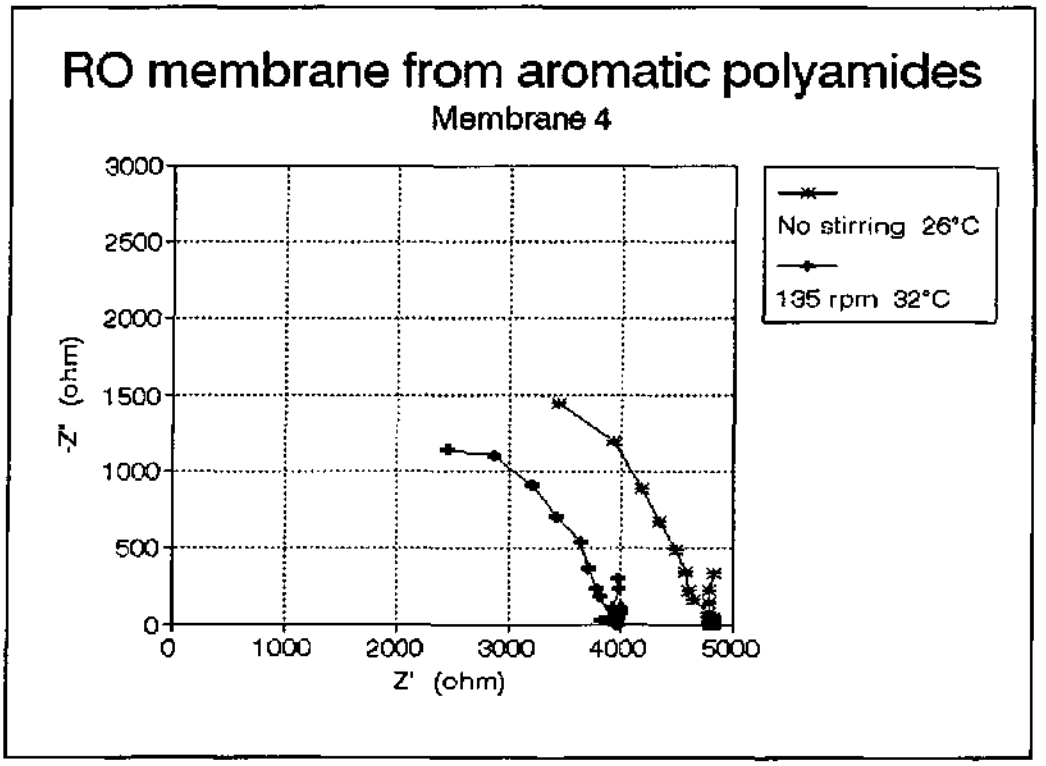

Figure 24 EIS spectrum for membrane 4

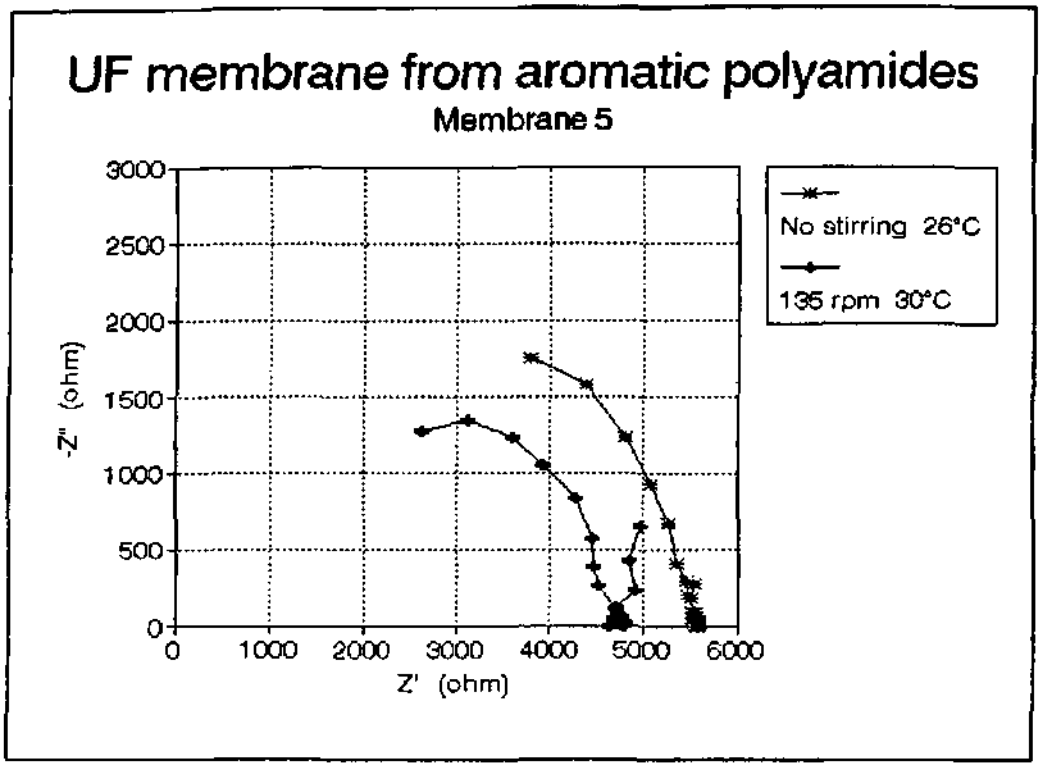

Figure 25 EIS spectrum of membrane 5

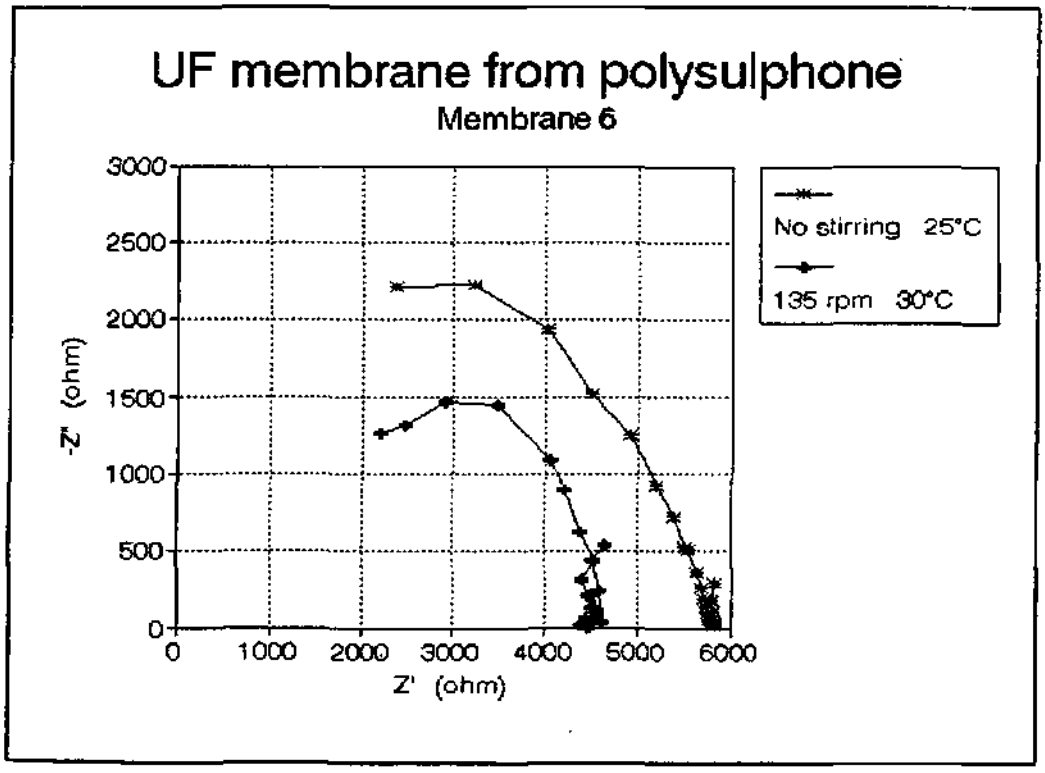

Figure 26 EIS spectrum of membrane 6

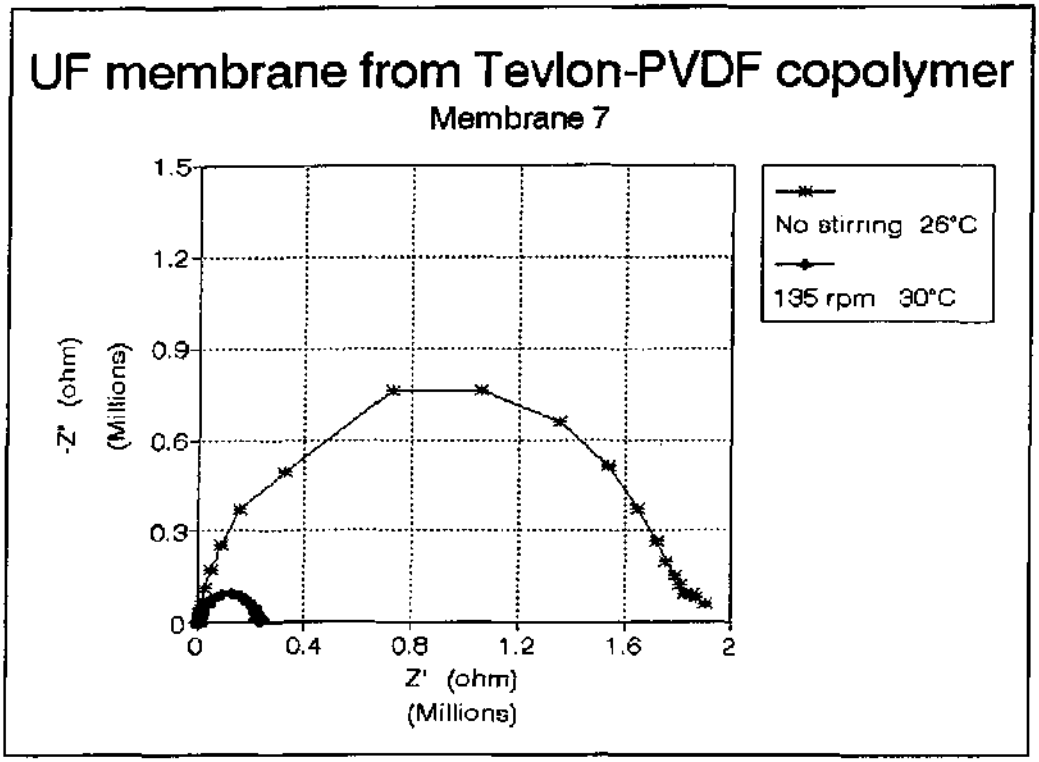

Figure 27 EIS spectrum of membrane 7

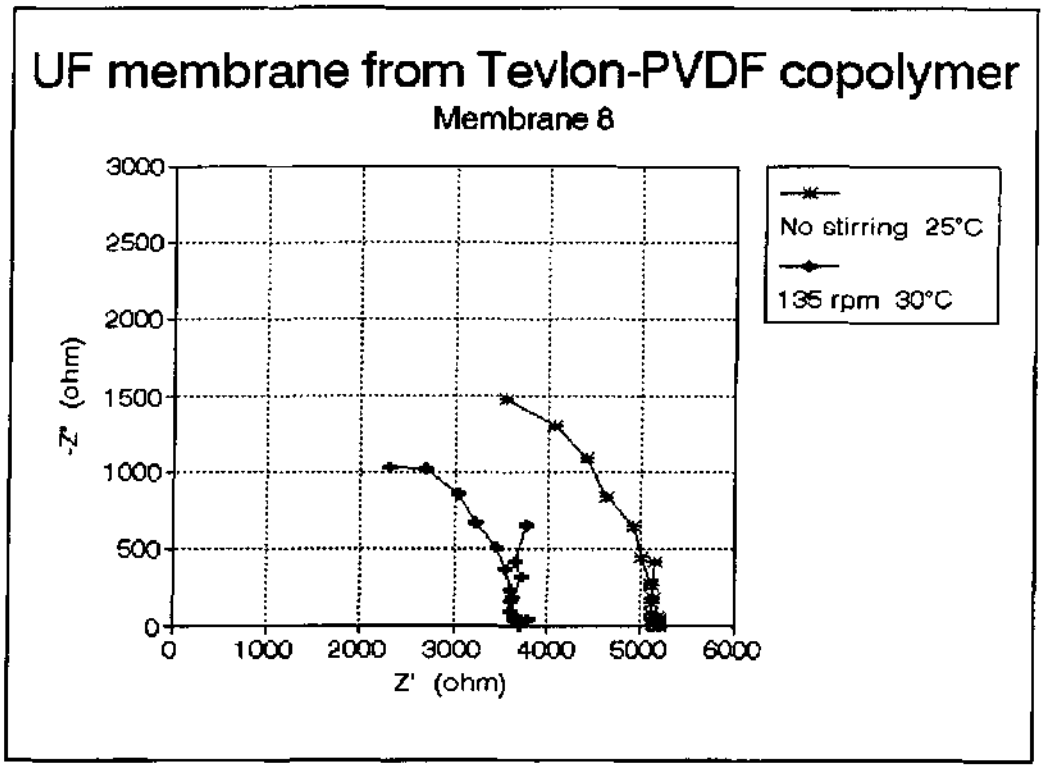

Figure 28 EIS spectrum of membrane 8

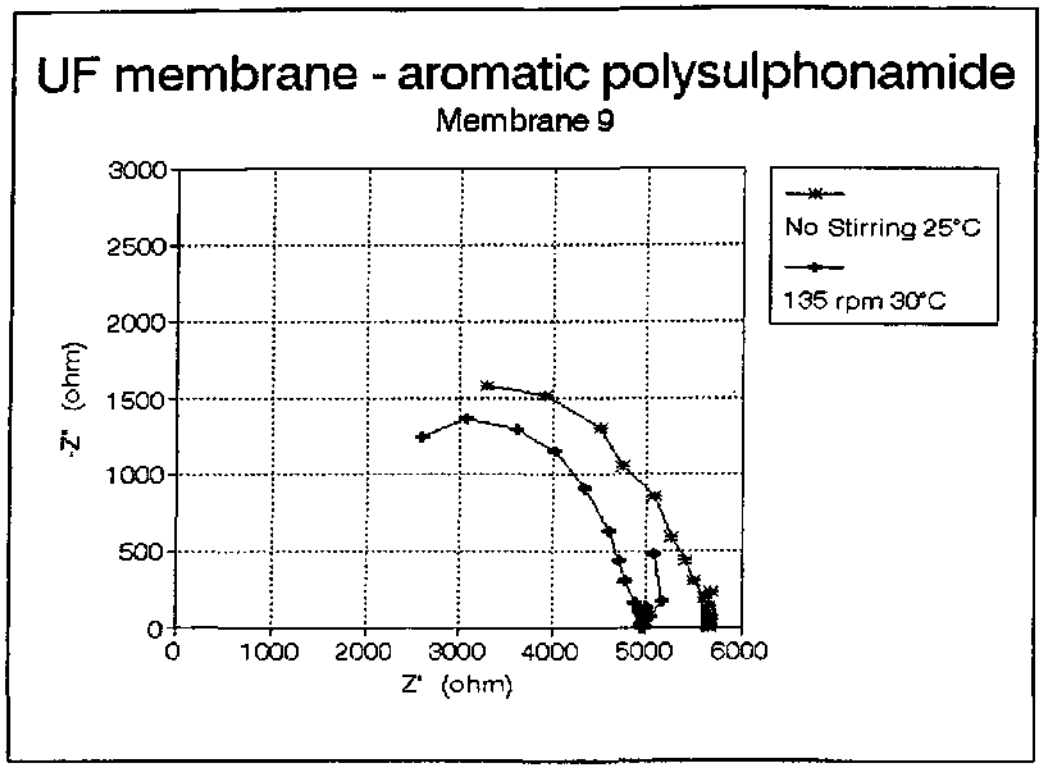

Figure 29 EIS spectrum of membrane 9

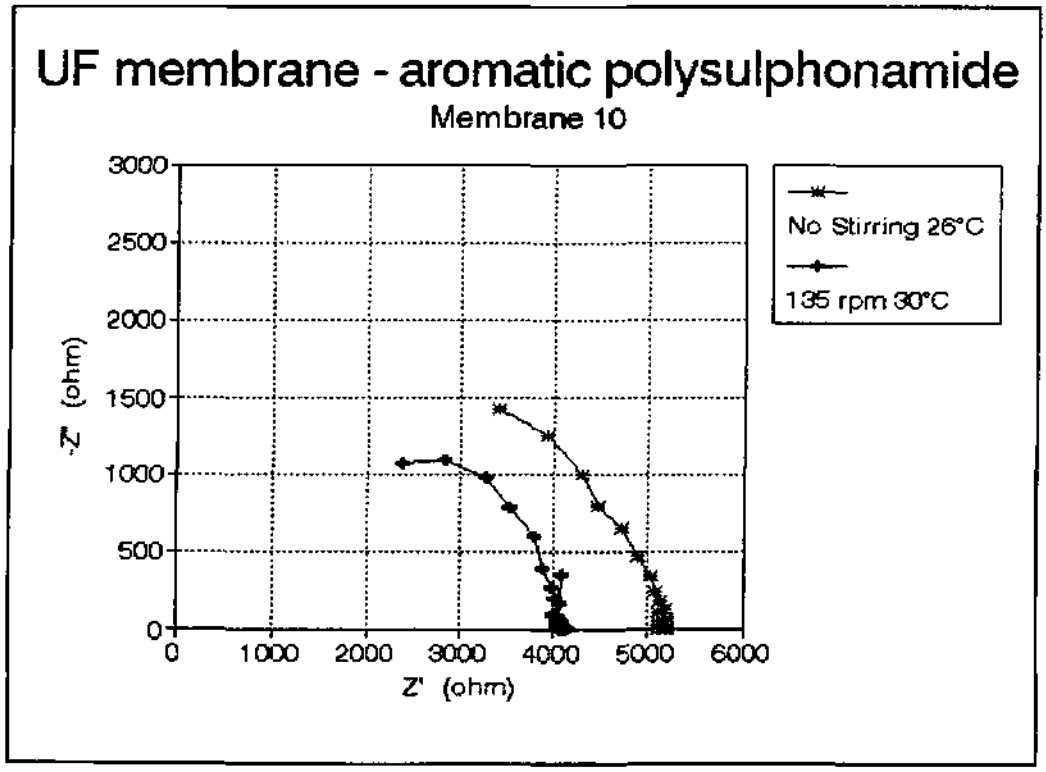

Figure 30 EIS spectrum of membrane 10

In Figure 22 the contrast is marked; not only do R_1 and R_2 intercept the x - axis but R_2 is of the order of $23 \times 10^6\ \Omega$. From Figures 23 - 26 it is deduced that these are hydrophilic, exhibiting some differences in the magnitude of R_2 and the impedance curve shape with and without stirring. The origin of the slight differences in shape has not been investigated at this stage. Figures 27, 28, 29 and 30 also fall into line with the criteria required to distinguish hydrophobic from hydrophilic membranes.

As Table 10 contains much detail, a brief summary is required to clarify the general trends.

Firstly, the time dependence of the quantities R_1, R_2 and C_T are shown each hour starting from 0.

TABLE 11

RANGE OF VALUES FOR EACH MEMBRANE TYPE IN 15 mg/ℓ KCl

Membrane Type	R_1 (Ω)	R_2 (Ω)	C_T ($F.m^{-2}$)
Hydrophobic (7 hr)	3027 - 3862	214121 - 7417223	2.7×10^{-9} - 7.8×10^{-9}
Hydrophilic (7 hr)	1285 - 2047	1996 - 2927	1.03×10^{-9} - 1.3×10^{-9}

From Table 11, in general, R_1 is lower for the hydrophilic than for the hydrophobic membrane and impedance R_2 is orders of magnitude lower, while the capacitance for the hydrophilic is much less than for the hydrophobic membrane by a factor of 2.7 to 6.

These are the trends emerging from a study of different membranes. There is scope for more detailed analysis on these graphs in Figure 21 - 30.

B.2.5 CONCLUSION

A two phase model of the membrane/electrolyte interface with Celgard hydrophobic and hydrophilic membranes shows that the EIS spectra are not monitoring the pure double layer/membrane structure but a less conducting phase adjacent to the membrane.

This was thought to be a membrane skin/membrane bulk model but not the double layer itself. Other models may be needed to fit the data. The double layer capacity was far too large to fit the model.

Definitive identification of membranes into hydrophobic or hydrophilic types has been proven on the trends of the EIS spectra yielded in dilute electrolyte solutions.

The temperature dependence of the two phase model where the double layer is adjacent to the membrane has been determined for NaF and KCl solutions.

B.2.5.1. DISCRIMINATION BETWEEN LAYERS CONSTITUTING THE MEMBRANE CAPACITY

From the capacitance of the interface C_T, the capacitances C_1 and C_2 lead to the porosity of the membrane from calculation. The following analysis shows how the porosity is calculated. If, adjacent to the membrane, there is a layer in contact with the electrolyte then

$$C_p = \frac{A_{pore}\epsilon_\omega\epsilon_0}{d} \qquad (1.1)$$

where C_p is the capacitance of the electrolyte filled pores. Here d is the thickness, ϵ_0 is the permittivity of free space while ϵ_ω is the dielectric constant for water.

A_{pore} = total area of the pores and A_{pore} = (A)(p) where p is the porosity and A is the area

of the membrane.

The conductance of the membrane bulk (phase 2) is taken as approaching zero.

Phase 1 has a capacitance $C_{(skin)}$.

Then

$$C_{(skin)} = \frac{(A_{skin})(\epsilon_m)(\epsilon_0)}{d} \qquad (1.2)$$

where A_{skin} = A = total skin area and ϵ_m is the dielectric constant for the polymer membrane.

The total skin area, excluding pores, will be given by (1-p)(A).

Total capacitance

$$C_1 = C_p + C_{skin} = \frac{[(\epsilon_\omega)(\epsilon_0)(A)(p)] + [(\epsilon_m)(\epsilon_0)(1 - p)A]}{d} \qquad (1.3)$$

Calculation of the porosity, p (in %), is from:

$$p = \frac{\left(\frac{dC_1}{\epsilon_0 A} - \epsilon_m\right)}{(\epsilon_\omega - \epsilon_m)} \qquad (1.4)$$

B.2.5.2 TWO PHASE MODEL OF AN INTERFACE - FREQUENCY DEPENDENCE OF THE CAPACITY AND CONDUCTANCE

A general model of an interface, consisting of these adjacent phases may be represented by a parallel combination of these RC-networks.

These two phases may be either the bulk solution/double layer, the double layer/membrane or the membrane surface/membrane bulk when one is considering the

electrolyte/membrane system. The sketch below shows the type of model used in most of the calculations of the frequency dependence of the system.

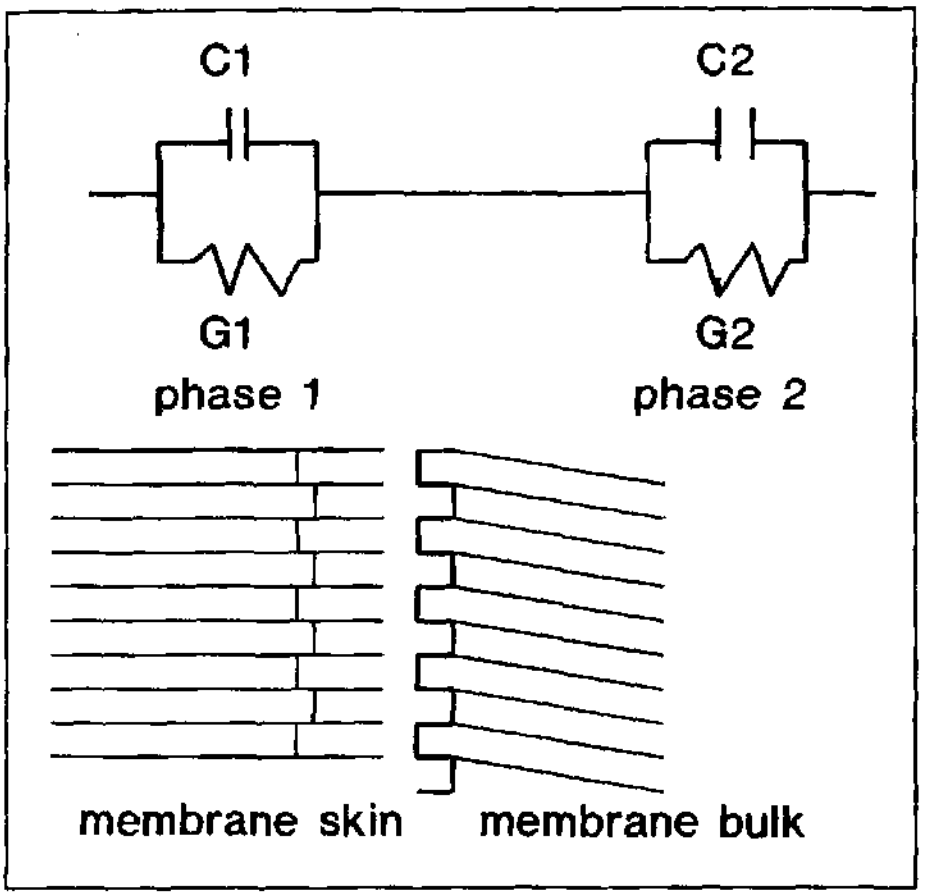

Figure 33 Resistance of membrane.

The subscripts 1 and 2 refer to phase 1 and phase 2 respectively. In the membrane/electrolyte system C_m = capacitance of the membrane while G_m = conductance of the membrane.

An expression for the frequency (ω) dependence of C_m is as follows :

$$C_m(\omega) = \frac{\omega^2 C_1 C_2 (C_1 + C_2) + G_2^2 C_1 + G_1^2 C_2}{(G_1 + G_2)^2 + \omega^2 (C_1 + C_2)^2} \qquad (2.40)$$

For G_m (ω) the corresponding equation is:-

$$G_m(\omega) = \frac{G_1 G_2(G_1 + G_2) + \omega^2\left(C_1^2 G_2 + C_2^2 G_1\right)}{(G_1 + G_2)^2 + \omega^2(C_1 + C_2)^2} \tag{2.41}$$

A total capacitance of the system C_T may be defined using G_e the conductivity of the bulk electrolyte.

$$C_T(\omega) = \frac{C_m G_e^2}{(G_m + G_e)^2 + \omega^2 C_m^2} \tag{2.42}$$

similarly,

$$G_T(\omega) = \frac{G_m G_e(G_m + G_e) + \omega^2 C_m^2 G_e}{(G_m + G_e)^2 + \omega^2 C_m^2} \tag{2.43}$$

Typical examples of the capacitance and conductance frequency variation of this model are shown in figures 1 and 2 respectively. It is of interest to note that at very low and very high frequencies this model leads to constant values for both capacitance and conductance.

These constant values are close to C_2 at high frequency where the values used in Figures 31 and 32 were respective $C_1 = 200\ \mu F/m^2$, $C_2 = 2\ \mu F/m_2$, $G_1 = 6\ S/m^2$ and $G_2 = 0.58 S/m^2$.

To obtain values for porosity, one first needs to study the two phase model and the conductances and capacitances obtained subsequently.

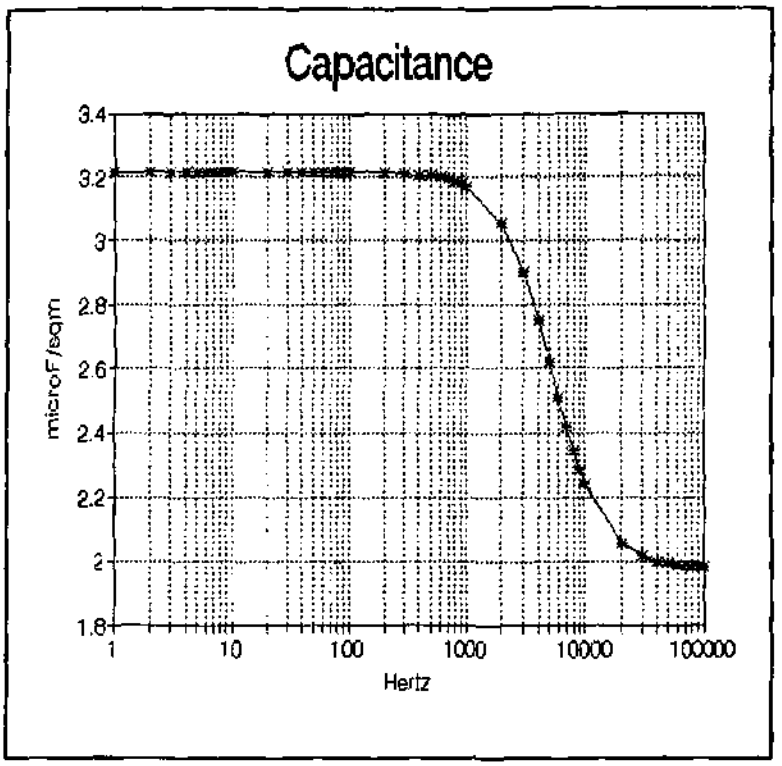

Figure 31 Capacitance vs frequency for 15 mg/l KCl solution.

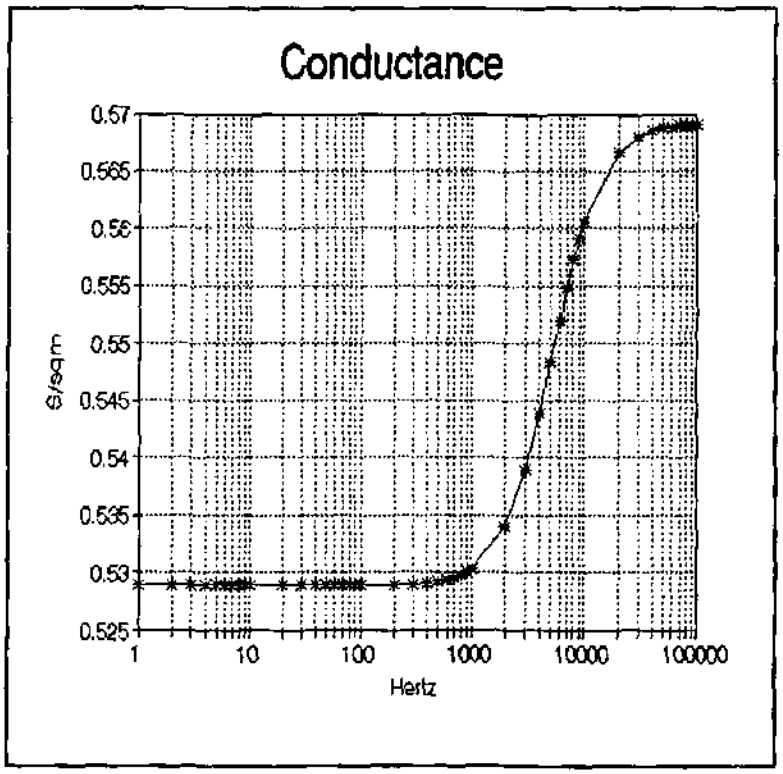

Figure 32 Conductance vs frequency for 15 mg/l KCl, $C_1 = 200\ \mu F/m^2$, $C_2 = 2\ \mu F/m^2$.

B.3 NUMERICAL MODEL FOR THE PREDICTION OF THE TRANSFER PROCESSES IN A CYLINDRICAL MEMBRANE

B.3.1. INTRODUCTION

A cylindrical membrane is a separation device that can be described as a tube with a porous wall. High pressure water with a certain concentration of salt enters the tube at the one end and as the solution moves in the axial direction a certain fraction of clean water is forced radially through the porous wall while the salt is retained on the inside.

The transfer processes in the membrane are very complex and various interdependent mechanisms play a role in the transfer of mass through the membrane. These mechanisms will be briefly discussed.

The flow rate through the membrane wall is a function of the porosity of the wall and the effective pressure difference across the wall which is defined as $(p_i - p_o - p_m)$ where p_i is the inside pressure, p_o is the outside pressure and p_m is the osmotic pressure. The flow rate inside the tube, Q_i, on the other hand is a function of the pressure gradient in the axial direction $(\partial p_i/\partial x)$. A change in the flow rate Q_i will therefore affect the inside pressure gradient which will in turn affect the effective pressure gradient across the wall and therefore also the flow rate through the wall.

The pressure difference across the wall also affects the tube diameter and wall thickness due to the fact that the membrane is elastic. Because the pressure difference across the wall varies in the axial direction the diameter and wall thickness will also vary in the axial direction. This variation results in a variation of cross flow area and thus also the axial velocity. One will therefore have to solve a coupled fluid/structure problem in order to predict velocities and flow rates in the membrane.

The ion concentration also plays a role in the transfer of mass and momentum in the membrane. Due to the fact that the ions are retained on the inside the concentration of

ions inside the tube increases in the axial direction. The concentration also varies radially due to the radial movement of the water through the wall. This influences the osmotic pressure which is a function of the ion concentration at the wall. As explained before the osmotic pressure in turn influences the wall mass flux. A model which can predict the transfer processes in a membrane, will therefore have to take all these effects into consideration.

B.3.2 PURPOSE

The purpose of this project is to develop a computer model to simulate the transfer processes in a cylindrical membrane. The model should take all the mechanisms explained in the previous section into account and must predict inside pressure, diameter, mass flux (axial and radial) and concentration profiles as functions of axial distance.

B.3.3. GOVERNING EQUATIONS.

B.3.3.1. ASSUMPTIONS

The following assumptions will be made:

(a) The length-to-diameter ratio of the tube is very large.

(b) Constant outside pressure.

(c) The Reynolds number is very small which means that the flow is laminar.

(d) The flow is axially symmetric.

(e) The axial variation of flow properties is much smaller than the radial variation.

(f) The pressure doesn't vary across the radius of the tube. Variations in the axial

direction are, however, taken into account.

(g) The viscosity and ion transfer coefficient are constant.

(h) The flow is isothermal.

(i) The flow is incompressible. Density variation due to variations in ion concentration will, however, be taken into consideration.

B.3.3.2. COORDINATE SYSTEM

Figure 3.1 illustrates the orthogonal curvilinear axi-symmetrical coordinate system which we shall use. Although this coordinate system is more complex than a Cartesian or cylindrical coordinate system it is more suitable for the present problem. The reason for this is that a curvilinear coordinate system can be "bend" to fit the varying inside diameter of the tube which simplifies the formulation of boundary conditions at the wall.

A detailed description of the orthogonal axi-symmetrical coordinate system can be found in elsewhere (Gosman, Pun, Runchal, Spalding & Wolfstein, 1969). Only a brief description will be given here for the sake of convenience. The three coordinates that describe the orthogonal axi-symmetrical coordinate system are ξ_1, ξ_2 and ξ_3. The first two coordinates characterise the members of two orthogonal families of surfaces of revolution while the third represents the angle of revolution about the symmetry axis from a reference plane. The left-hand diagram of Figure 3.1 represents the intersection of the constant-ξ_1 and constant-ξ_2 surfaces with a plane through the symmetry axis; this plane is a constant-ξ_3 surface. The right-hand diagram of Figure 3.1 represents a plane of constant ξ_3 appearing as straight lines radiating from the point of symmetry, while circles drawn with this point as centre are lines along which both ξ_1 and ξ_2 are constant.

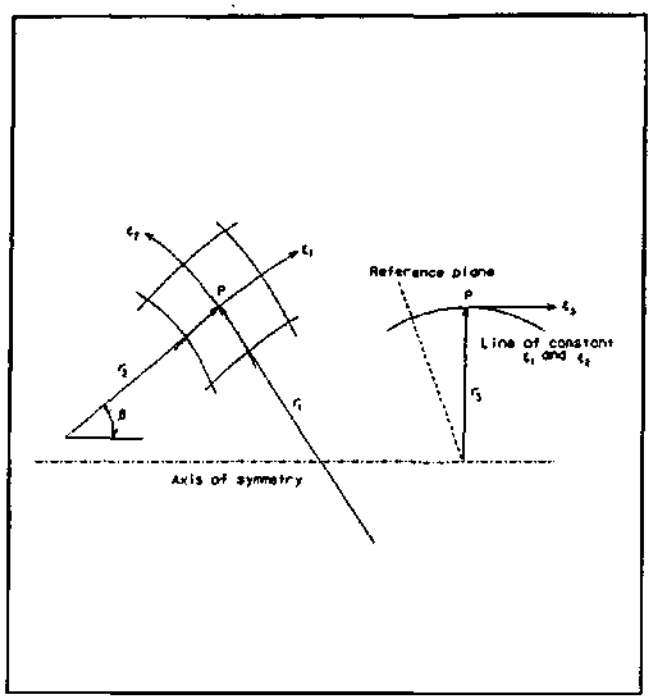

Figure 34 The orthogonal curvilinear axi-symmetrical coordinate system.

The metric coefficients ℓ_1, ℓ_2 and ℓ_3 are defined such that the distance *ds* between two nearby points is related to the increments in ξ_1, ξ_2 and ξ_3 by

$$(ds)^2 = (\ell_1 d\xi_1)^2 + (\ell_2 d\xi_2)^2 + (\ell_3 d\xi_3)^2 \qquad (3.1)$$

If ξ_3 is measured in radians ℓ_3 is identical to the radius of curvature r_3.

B.3.3.3. PARTIAL DIFFERENTIAL EQUATIONS.

The following partial differential equations describe the conservation of mass, momentum and mass fraction in an orthogonal axi-symmetric co-ordinate system (Gosman, Pun, Runchal, Spalding & Wolfstein, 1969):

Mass conservation or continuity equation:

$$\frac{\partial}{\partial \xi_1}(r\ell_2 \rho V_1) + \frac{\partial}{\partial \xi_2}(r\ell_1 \rho V_2) = 0 \tag{3.2}$$

In the above equation r = r_3 the distance along a normal to the axis of symmetry.

Direction -1 momentum conservation equation:

$$-(r\ell_2 \rho V_1^2) + \frac{\partial}{\partial \xi_2}(r\ell_1 \rho V_1 V_2) = -\ell_2 r\frac{\partial p}{\partial \xi_1} + \frac{\partial}{\partial \xi_1}\left(r\mu\frac{\ell_2}{\ell_1}\frac{\partial V_1}{\partial \xi_1}\right) + \frac{\partial}{\partial \xi_2}\left(r\mu\frac{\ell_1}{\ell_2}- \right. \tag{3.3}$$

The above equation applies to incompressible flows and cases where r_1 and r_2 are very large.

Direction -2 momentum conservation equation:

$$\frac{\partial}{\partial \xi_1}(r\ell_2 \rho V_1 V_2) + \frac{\partial}{\partial \xi_2}(r\ell_1 \rho V_2^2) = -\ell_1 r\frac{\partial p}{\partial \xi_2} + \frac{\partial}{\partial \xi_1}\left(r\mu\frac{\ell_2}{\ell_1}\frac{\partial V_2}{\partial \xi_1}\right) + \frac{\partial}{\partial \xi_2}\left(r\mu\frac{\ell_1}{\ell_2}\frac{\partial V_2}{\partial \xi_2}\right) + \frac{\ell_1 \ell_2 \mu V_2}{r} \tag{3.4}$$

The same assumptions which apply to Eq. (3.3) also apply to Eq. (3.4).

Conservation of mass fraction:

$$\frac{\partial}{\partial \xi_1}(r\ell_2 \rho V_1 \phi) + \frac{\partial}{\partial \xi_2}(r\ell_1 \rho V_2 \phi) = \frac{\partial}{\partial \xi_1}\left(r\Gamma \frac{\ell_2}{\ell_1}\frac{\partial \phi}{\partial \xi_1}\right) + \frac{\partial}{\partial \xi_2}\left(r\Gamma \frac{\ell_1}{\ell_2}\frac{\partial \phi}{\partial \xi_2}\right) \qquad (3.5)$$

B.3.3.4. SIMPLIFIED PARTIAL DIFFERENTIAL EQUATIONS

Consider a varying diameter tube with boundary fitting axi-symmetrical orthogonal co-ordinate system as shown in Figure 3.2.

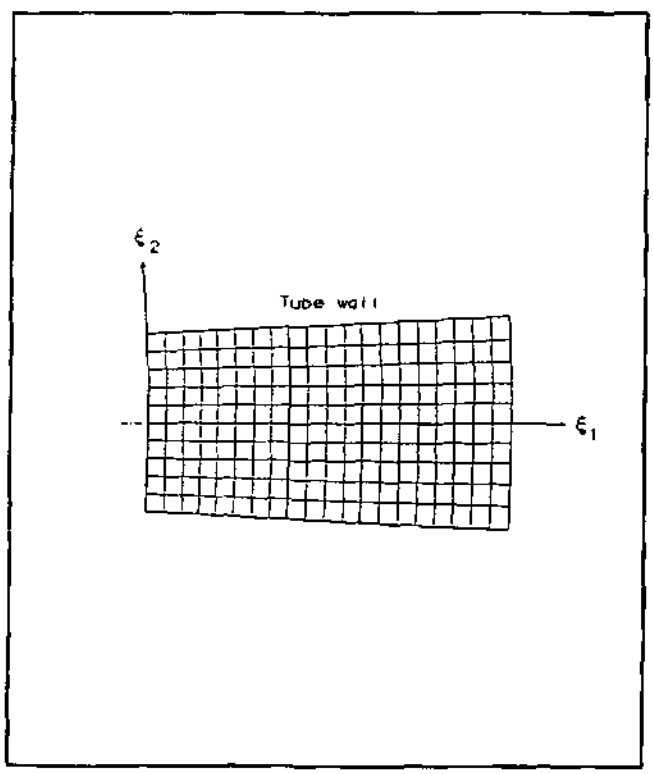

Figure 3.2 Varying diameter tube with boundary fitting orthogonal curvilinear axi-symmetrical grid.

If $\partial R/\partial x << 1$ we can define ξ_1, as

$$\xi_1 = x \tag{3.6}$$

which implies that

$$\ell_1 = 1 \tag{3.7}$$

We can also define ξ_2 as

$$\xi_2 = \xi = r/R \tag{3.8}$$

which implies that

$$\ell_2 = R \tag{3.9}$$

It follows from (3.8) that $\xi_2 = 0$ on the axis of symmetry and $\xi_2 = 1$ on the wall.

In order to simplify the notation we will write that

$$u = V_1 \text{ and} \tag{3.10}$$

$$v = V_2 \tag{3.11}$$

Substitution of (3.6) to (3.11) into (3.2) to (3.5) and applying the boundary layer assumptions $v << u$, $\partial p/\partial r = 0$ and $\partial u/\partial x << \partial u/\partial \xi$ leads to the following set of equations:

Continuity:

$$\frac{\partial}{\partial x}(\xi R^2 \rho u) + \frac{\partial}{\partial \xi}(\xi R \rho v) = 0 \tag{3.12}$$

Direction -1 momentum:

$$\frac{\partial}{\partial x}(\xi R^2 \rho u^2) + \frac{\partial}{\partial \xi}(\xi R \rho v u) = -\xi R^2 \frac{\partial p}{\partial x} + \frac{\partial}{\partial \xi}\left(\xi \mu \frac{\partial u}{\partial \xi}\right) \tag{3.13}$$

Mass fraction

$$\frac{\partial}{\partial x}(\xi R^2 \rho u \phi) + \frac{\partial}{\partial \xi}(\xi R \rho v \phi) = \frac{\partial}{\partial \xi}\left(\xi \Gamma \frac{\partial \phi}{\partial \xi}\right) \tag{3.14}$$

Equations (3.13) and (3.14) are written in the so-called conservative form (Roache, 1972). The equations can also be written in the non-conservative form by applying the continuity equation. The results are

$$\xi R^2 \rho u \frac{\partial u}{\partial x} + \xi R \rho v \frac{\partial u}{\partial y} = -\xi R^2 \frac{\partial p}{\partial x} + \frac{\partial}{\partial \xi}\left(\xi \mu \frac{\partial u}{\partial \xi}\right) \tag{3.15}$$

$$\xi R^2 \rho u \frac{\partial \phi}{\partial x} + \xi R \rho v \frac{\partial \phi}{\partial y} = -\xi R^2 \frac{\partial p}{\partial x} + \frac{\partial}{\partial \xi}\left(\xi \Gamma \frac{\partial \phi}{\partial \xi}\right) \tag{3.16}$$

The reader will notice that the direction-2 momentum equation has been dropped from the set of partial differential equations. This is due to the assumptions that $v \ll u$ and $\partial p/\partial r = 0$. Equations (3.12), (3.13) and (3.14) or (3.12), (3.15) and (3.16) together with the overall continuity equation given in the next section are sufficient to solve for the independent hydrodynamic variables u, v, p and the mass fraction ϕ.

B.3.3.5. OVERALL CONTINUITY EQUATION AND DENSITY.

Equation (3.2) was derived by considering the conservation of mass over an elemental control volume. The overall continuity equation can be derived by considering conservation of mass over the total cross flow area of the tube. This equation is given by

$$\frac{\partial}{\partial x}\int_0^R \rho r V_x \, dr + R\rho_C V_R = 0 \qquad (3.17)$$

where

V_x = velocity component in the axial direction,
V_R = radial velocity through the porous wall and
ρ_C = density of the water flowing through the wall.

If the angle between the axis of symmetry and the direction of ξ_1 is very small as is the case in the present situation, Eq. (3.17) can be approximated by

$$\frac{\partial}{\partial x}\int_0^R \rho r u \, dr + R\rho_C v_R = 0 \qquad (3.18)$$

The density in Equations (3.12) to (3.18) is not constant but vary due to variations in ion concentration. The density is a function of the density of the carrier fluid and the ion concentration. Therefore

$$\rho = \rho(\rho_C, \phi) \qquad (3.19)$$

The density of aqueous sodium chloride solutions are given in Table 3.1.

Mass fraction (%)	Density (k/m^3)
1	1,00409
2	1,01112
4	1,02530
8	1,05412
12	1,08365
16	1,11401
20	1,14523
24	1,17776
26	1,19443

TABLE 3.1 Density of Sodium Chloride solutions at 25°C (Perry & Chilton, 1973:3-78).

B.3.3.6. EQUATION FOR THE WALL VELOCITY.

The wall velocity is given by

$$v_R = A(p_i - p_o - p_m) \tag{3.20}$$

where

p_i = inside pressure,

p_o = outside pressure,

p_m = osmotic pressure and

A = empirical constants that depend on the characteristics of the porous wall.

The osmotic pressure is a function of ion concentration at the wall. Therefore

$$p_m = f(\phi) \tag{3.21}$$

The osmotic pressure for different water salinities is given in Table 3.2.

Mass fraction (%)	**Osmotic pressure, atm at 25°C**
0,00585	0,05
0,05845	0,47
0,2941	2,31
0,5824	4,56
1,1611	9,04
2,3053	18,02
3,4278	27,12
4,5333	36,37
5,6270	45,80
10,8535	96,20
15,7346	153,2

Mass fraction (%)	Osmotic pressure, atm at 25°C
20,3200	218,9
24,6414	295,2

TABLE 3.2 Osmotic pressure of Sodium Chloride Solutions (Perry & Chilton, 1973:17-41).

B.3.3.7. TRANSPORT COEFFICIENT FOR THE MASS FRACTION EQUATION.

The transport coefficient in the mass fraction equation is given by

$$\Gamma = \rho D$$

where D is the diffusion coefficient. The units of D is $m^2\ s^{-1}$ while that of Γ is $kg\ m^{-1}\ s^{-1}$.

In general D varies somewhat with concentration. The values listed below are for an aqueous solution of sodium chloride (from Weast & Astle, 1982:F-51):

Mass fraction (%)	Diffusion coefficient (m^2/s)
0,0585	$1,545 \times 10^{-12}$
0,582	$1,483 \times 10^{-12}$
5,627	$1,484 \times 10^{-12}$

B.3.3.8. DETERMINATION OF INSIDE TUBE DIAMETER.

The radial displacement Δr of any point on a thick-walled cylinder is given by (Popov,1978)

$$\Delta r = A_1 r + A_2/r \tag{3.22}$$

The coefficients A_1 and A_2 are given by

$$A_1 = \frac{(1+\nu)(1-2\nu)}{E}\left(\frac{p_i r_i^2 - p_o r_o^2}{r_o^2 - r_i^2}\right) \tag{3.23}$$

$$A_2 = \frac{(1+\nu)}{E}\left(\frac{p_i - p_o r_o^2}{r_o^2 - r_i^2}\right) r_i^2 r_o^2 \tag{3.24}$$

where

E = elastic modulus

V = Poisson modulus

B.3.4. NUMERICAL MODEL

B.3.4.1. INTRODUCTION.

Equations (3.13) to (3.16) are parabolic differential equations which allows us to solve the set of equations with a space marching boundary layer type finite-difference method.

The advantages of a marching method are that it is very fast and that it requires much less computer storage compared to full elliptic methods.

First the derivation of the finite-difference equations will be discussed after which the solution procedure will be discussed.

B.3.4.2. DISCRETIZATION OF THE MOMENTUM EQUATION.

Consider the following form of Eq. (3.15):

$$\rho u \frac{\partial u}{\partial x} + \frac{\rho v}{R} \frac{\partial u}{\partial y} = - \frac{\partial p}{\partial x} + \frac{1}{\xi R^2} \frac{\partial}{\partial \xi} \left(\xi \mu \frac{\partial u}{\partial \xi} \right) \tag{4.1}$$

Eq. (4.1) can be discretized by integrating it over the control volume shown in Figure 4.1 on the next page. The result is

$$\begin{aligned} &\tfrac{1}{2}[(\rho u)_P + (\rho u)_W](u_P + u_W)\Delta\xi + \tfrac{1}{2}\left[\frac{(\rho v)_P}{R_P} + \frac{(\rho v)_W}{R_W}\right](u_n - u_s)\Delta x = \\ &-\left(\frac{\partial p}{\partial x}\right)_P \Delta x \Delta\xi + \frac{1}{(\xi R^2)_P}\left(\frac{\xi_n \mu_n (u_N - u_P)}{\Delta\xi_n} - \frac{\xi_s \mu_s (u_P - u_S)}{\Delta\xi_s}\right)\Delta x \end{aligned} \tag{4.2}$$

Substitution of

$$u_n = \tfrac{1}{2}(u_N + u_P) \qquad and \qquad u_s = \tfrac{1}{2}(u_S + u_P) \tag{4.3}$$

into (4.2) and rearrangement leads to

$$c_P u_P = c_N u_N + c_S u_S + c_E u_E + c_W u_W + b_P \tag{4.4}$$

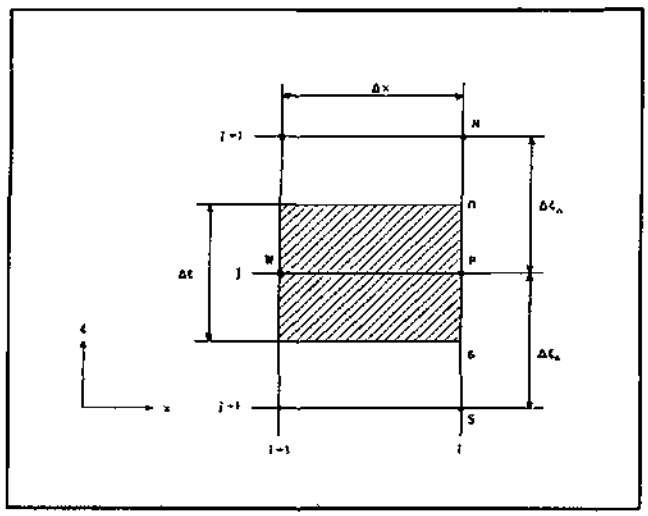

Figure 4.1 Control volume for the discretization of the momentum equation.

where

$$c_N = \frac{\xi_n \mu_n}{\xi_P R_P^2 \Delta\xi_n \Delta\xi} - \frac{1}{4\Delta\xi}\left[\frac{(\rho v)_P}{R_P} + \frac{(\rho v)_W}{R_W}\right]$$

$$c_S = \frac{\xi_s \mu_s}{\xi_P R_P^2 \Delta\xi_s \Delta\xi} + \frac{1}{4\Delta\xi}\left[\frac{(\rho v)_P}{R_P} + \frac{(\rho v)_W}{R_W}\right] \tag{4.5}$$

$$c_W = \frac{(\rho u)_P + (\rho u)_W}{2\Delta x} \tag{4.6}$$

$$b_P = -\left(\frac{\partial p}{\partial x}\right)_P \tag{4.7}$$

and

$$c_P = c_N + c_S + c_W \tag{4.8}$$

If the v-velocities become too large c_N and c_S can become negative which will lead to instabilities. This can be rectified by using the following approximation for u_n and u_s instead of (4.3):

(4.9)

where

$$g = \frac{1}{2\,\Delta\xi}\left[\frac{(\rho v)_P}{R_P} + \frac{(\rho v)_W}{R_W}\right] \tag{4.10}$$

Substitution of (4.9) into (4.2) results in the following modified coefficients for Eq. (4.4):

$$\begin{aligned} c_N' &= \frac{\xi_n\,\mu_n}{\xi_P\,R_P^2\,\Delta\xi_n\,\Delta\xi} + \max[-g,0] \\ c_S' &= \frac{\xi_s\,\mu_s}{\xi_P\,R_P^2\,\Delta\xi_s\,\Delta\xi} + \max[g,0] \end{aligned} \tag{4.11}$$

where g is given by (4.10).

It is important to note that c'_N and c'_S can never become negative. Whenever φ_N or φ_S becomes negative both values are replaced by c'_N and c'_S in (4.4) and (4.8).

The reason why we go to the trouble of using Eq. (4.5) is that this equation represents a more accurate approximation of u_n and u_s at low cell Reynold numbers. Although Eqs. (4.9) and (4.11) ensure stability at high cell Reynolds numbers it can lead to a kind of inaccuracy known as numerical diffusion (Patankar, 1980).

Approximation of u_n and u_s according to (4.3) is equivalent to the central difference method while (4.9) is equivalent to the upwind difference method in the finite-difference approach.

B.3.4.3. DISCRETIZED CONTINUITY EQUATION.

Consider the control volume shown in Figure 4.2

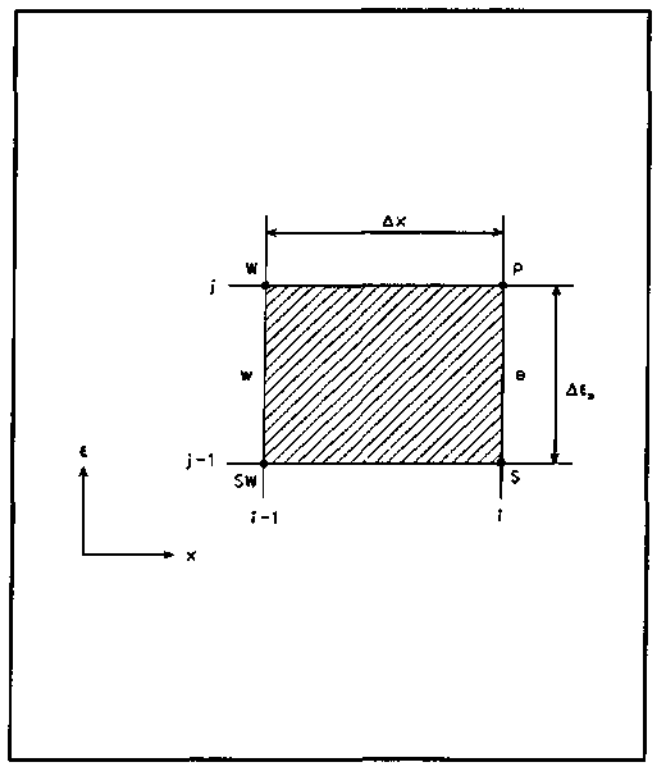

Figure 4.2 Control volume for the discretization of the continuity equation.

Integration of Eq. (3.12) over the control volume shown in Figure 4.2 leads to

$$[(\xi R^2 \rho u)_e - (\xi R^2 \rho u)_w]\Delta\xi_s + [(\xi R \rho v)_P - (\xi R \rho v)_S]\Delta x_w = 0 \qquad (4.12)$$

Values at the midpoints e and w are taken as the mean of the values at P and S and at W and SW respectively. This leads to

$$[(\xi R^2 \rho u)_P + (\xi R^2 \rho u)_S - (\xi R^2 \rho u)_W - (\xi R^2 \rho u)_{SW}]\Delta\xi/2 + [(\xi R \rho v)_P - (\xi R \rho v)_S]\Delta x_w = 0 \qquad (4.13)$$

Solving for v_P

$$= \frac{1}{(\xi R \rho)_P}\left((\xi R \rho v)_S - \frac{\Delta\xi_s}{2\Delta x_w}[(\xi R^2 \rho u)_P + (\xi R^2 \rho u)_S - (\xi R^2 \rho u)_W - (\xi R^2 \rho u)_{SW} \right. \qquad (4.14)$$

B.3.4.4. DISCRETIZED MASS FRACTION EQUATION.

For the mass fraction or concentration equation we shall use a staggered grid where constant ξ grid lines are placed halfway between the regular grid lines as shown in Figure 4.3. The grid is thus formed by the solid constant-x grid lines and the broken constant-ξ grid lines. Points N, P, S and W therefore fall on grid points of the staggered grid while n and s are halfway between N and P and P and S respectively.

Point n and s coincide with grid points (i, j +1) and (i, j -1) of the regular grid.

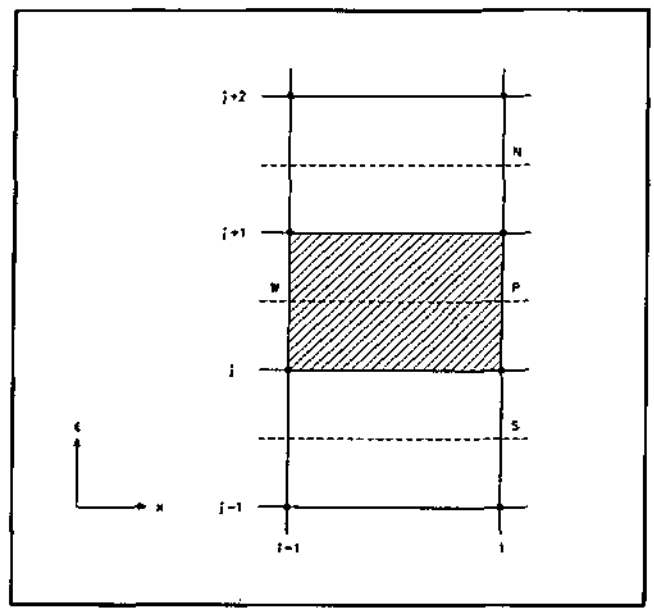

Figure 4.3 Staggered grid with control volume used for the concentration equation.

The reason for this peculiar grid arrangement is to ensure that the same control volume is used as in the case of the continuity equation in order to ensure satisfaction of the conservation principal.

Integration of (3.14) over the control volume shown in Figure 4.3 results in

$$[(\xi R^2 \rho u \phi)_P - (\xi R^2 \rho u \phi)_w]\Delta\xi + [(\xi R \rho v \phi)_n - (\xi R \rho v \phi)_s]\Delta x = \left[\frac{(\xi\Gamma)_n(\phi_N - \phi_P)}{\Delta\xi_n} - \frac{(\xi\Gamma)_s(\phi_P - \phi_S)}{\Delta\xi_s}\right]\Delta x \qquad (4.15)$$

Using central differensing for the terms on the left hand side of (4.15):

$$\begin{aligned} \phi_n &= (\phi_N + \phi_P)/2 \\ \phi_s &= (\phi_S + \phi_P)/2 \end{aligned} \qquad (4.16)$$

After substitution of (4.16) into (4.15) and rearrangement we get

$$c_P \phi_P = c_N \phi_N + c_S \phi_S + c_W \phi_W \qquad (4.17)$$

where

$$\begin{aligned} c_N &= \frac{\xi_n \Gamma_n}{\Delta\xi_n \Delta\xi} - \frac{(\xi R \rho v)_n}{2\Delta\xi} \\ c_S &= \frac{\xi_s \Gamma_s}{\Delta\xi_s \Delta\xi} + \frac{(\xi R \rho v)_s}{2\Delta\xi} \end{aligned} \qquad (4.18)$$

$$c_W = \frac{(\xi R^2 \rho u)_W}{\Delta x} \tag{4.19}$$

$$c_P = c_N + c_S + c_W \tag{4.20}$$

We need a slight different formulation at the wall to ensure that the ions are retained on the inside. Consider the grid arrangement and control volume next to the wall as shown in Figure 4.4.

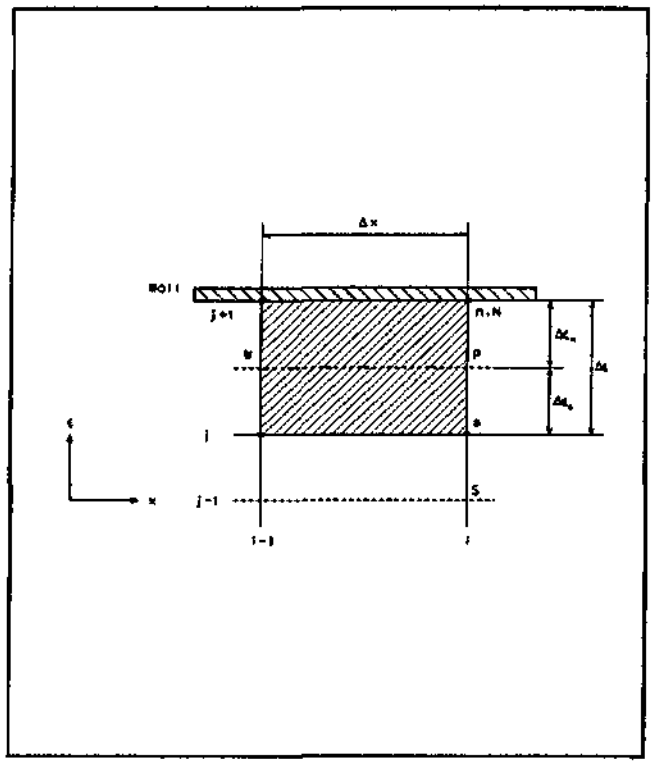

Figure 4.4 Control volume and grid arrangement next to the wall for the concentration equation.

Integration of (3.14) over the control volume shown in Figure 4.4 and applying the condition that no ions are convected through the wall leads to

S
$$[(\xi R^2 \rho u \phi)_P - (\xi R^2 \rho u \phi)_W]\Delta\xi + [(\xi R \rho v \phi)_n - (\xi R \rho v \phi)_s \Delta x = \left[\frac{(\xi\Gamma)_n(\phi_N - \phi_P)}{\Delta\xi_n} - \frac{(\xi\Gamma)_s(\phi_P - \phi_S)}{\Delta\xi_s}\right]\Delta x \quad (4.21)$$

Substitution of (4.16) into (4.21) leads to:

$$c_P \phi_P = c_N \phi_N + c_S \phi_S + c_W \phi_W \quad (4.22)$$

where

(4.23)

$$c_S = \frac{\xi_s \Gamma_s}{\Delta\xi_s \Delta\xi} + \frac{(\xi R \rho v)_s}{2\Delta\xi} \quad (4.24)$$

$$c_W = \frac{(\xi R^2 \rho u)_W}{\Delta x} \quad (4.25)$$

$$c_P = \frac{\xi_n \Gamma_n}{\Delta\xi_n \Delta\xi} + \frac{\xi_s \Gamma_s}{\Delta\xi_s \Delta\xi} + \frac{(\xi R^2 \rho u)_P}{\Delta x} - \frac{(\xi R \rho v)_s}{2\Delta\xi} \quad (4.26)$$

When cell Reynolds numbers are high c_N and c_S in (4.17) and ς and φ in (4.22) can become negative which will cause instabilities. A remedy for this is to use the upwind differencing form for the convective terms in (4.15) and (4.21) whenever the coefficients become negative. The upwind equivalent of (4.16) is

$$\begin{aligned} \phi_n &= \phi_N \quad if \quad v_n < 0 \\ &= \phi_P \quad if \quad v_n \geq 0 \\ \phi_s &= \phi_S \quad if \quad v_s \geq 0 \\ &= \phi_P \quad if \quad v_s < 0 \end{aligned} \tag{4.27}$$

Substitution of (4.27) into (4.15) leads to the following modified form of (4.18)

$$\begin{aligned} c_N' &= \frac{\xi_n \Gamma_n}{\Delta\xi_n \Delta\xi} + \max\left[-\frac{(\xi R \rho v)_n}{\Delta\xi}, 0 \right] \\ c_S' &= \frac{\xi_s \Gamma_s}{\Delta\xi_s \Delta\xi} + \max\left[\frac{(\xi R \rho v)_s}{\Delta\xi}, 0 \right] \end{aligned} \tag{4.28}$$

Substitution of (4.27) into (4.21) leads to the following modified form of (4.24) and (4.26).

$$c_S' = \frac{\xi_s \Gamma_s}{\Delta\xi_s \Delta\xi} + \max\left[\frac{(\xi R \rho v)_s}{\Delta\xi}, 0 \right] \tag{4.29}$$

$$c_P' = \frac{\xi_n \Gamma_n}{\Delta\xi_n \Delta\xi} + \frac{\xi_s \Gamma_s}{\Delta\xi_s \Delta\xi} + \frac{(\xi R^2 \rho u)_P}{\Delta x} + \max\left[-\frac{(\xi R \rho v)_s}{\Delta\xi}, 0 \right] \tag{4.30}$$

B.3.4.5. SOLUTION ALGORITHM.

The solution algorithm can be described as follows:

a) Set values for all variables at the inlet i.e. at i = 1.

b) Calculate the pressure at the next grid position from

$$p_{i+1} = p_i + \left(\frac{\partial p}{\partial x}\right)_{i+\frac{1}{2}} \Delta x \qquad (4.31)$$

Initially $(\partial p/\partial x)_{i+\frac{1}{2}}$ is set equal to $(\partial p/\partial x)_i$ but later a more accurate updated value is calculated from

$$\left(\frac{\partial p}{\partial x}\right)_{i+\frac{1}{2}} = \frac{1}{2}\left[\left(\frac{\partial p}{\partial x}\right)_i + \left(\frac{\partial p}{\partial x}\right)_{i+1}\right]$$

A new value for $(\partial p/\partial x)_{i+1}$ is calculated in Step h). The pressure at (i+½) is calculated as $p_{i+\frac{1}{2}} = (p_i + p_{i+1})/2$.

c) Calculate the radial displacement at (i+1) with (3.22) using the pressure at (i+1) in (3.23) and (3.24). The radius at (i+1) is given by

$$R_{i+1} = R^* + \Delta r_{i+1}$$

where R* is the inside radius under no stress conditions.

The radius at (i+½) is calculated as

$$R_{i+\frac{1}{2}} = (R_i + R_{i+1})/2.$$

d) Calculate the osmotic pressure at (i+½) as

$$p_{m_{i+\frac{1}{2}}} = (p_{m_i} + p_{m_{i+1}})/2$$

Initially $p_{mM_{i+½}}$ is set equal to p_{mM_i} but later the more accurate updated value calculated in Step l) is used.

e) Equation (3.20) is now solved for $v_{RM_{i+½}}$

f) The axial mass flow at (i+1) is now calculated as

$$m_{i+1} = m_i - 2\pi R_{i+½}\,\rho_c\,v_{R_{i+½}}\Delta x \tag{4.32}$$

where ρ_c is the density of the solute.

g) Solve (4.4) simultaneously for all grid points on line (i+1) using the Thomas algorithm (Anderson, Tannehill & Pletcher, 1984). With the first iteration a guessed value of $(\partial p/\partial x)_{i+1}$ is used in Eq. (4.4) and thereafter more accurate updated values determined in the next step are used.

h) Calculate the mass flow across section (i+1) using

$$m_{i+1} = 2\pi\sum_{j=2}^{jm}(\rho\, r\, u)_{i+1,j-½}\,\Delta r \tag{4.33}$$

The mass flow calculated with (4.33) is now compared with the value calculated with (4.32) after which the pressure gradient $(\partial p/\partial x)_{i+1}$ in (4.4) is adjusted with the Newton Correction Method (Stiefel, 1963:79) until the mass flow calculated with (4.33) is equal to the value calculated with (4.32). In the process (4.4) is solved repeatedly.

i) With $(\partial p/\partial x)_{i+1}$ known a new updated value for p_{i+1} is calculated using (4.31).

j) Equation (4.14) is now used to calculate all the v-values on line (i+1).

k) The Thomas algorithm is used to solve (4.17) simultaneously for all grid points on line (i+1).

l) With ϕ_{jm} known a new updated value for $p_{mM_{i+1}}$ is calculated using (3.21).

m) Repeat Steps b) to l) using the updated value of $(\partial p/\partial x)_{i+1}$ in Step b) and the updated value of $p_{m_{i+\frac{1}{2}}}$ in Step d) until convergence is reached.

n) Move to the next axial position and repeat Steps b) to m) until all i-lines have been visited.

B.3.4.6. VERIFICATION OF THE METHOD.

B.3.4.6.1. VELOCITIES AND PRESSURES.

In order to verify the model, developing flow in the entrance region of a constant diameter pipe with impermeable walls was solved. Results were compared to results of the analytical method developed by Langhaar (1942) and experimental results obtained by Nikuradse (as given in Prandtle & Tietjens, 1934:27).

It should be noted that the analytical solution of Langhaar is not an exact solution but an approximate one due to simplifying assumptions that was made in order to obtain a solution.

With the numerical method a grid with 21 grid points equally spaced over the radius of the tube was used in all cases.

Figure 4.5 shows the development of centreline velocities along the axis. The dimensionless axial velocity, $\lambda = u/u_{mean}$, is plotted against the dimensionless axial coordinate, $\sigma = (x/R)R_{ey}$, where R is the radius and R_{ey} is the Reynolds number defined by $R_{ey} = u_{mean}R/\nu$. Although the numerical, analytical and experimental results are in close agreement the numerical results are closer to the experimental results than the analytical results. The number of grid points in the axial direction was 100 and the grid points was uniformly spaced in both directions.

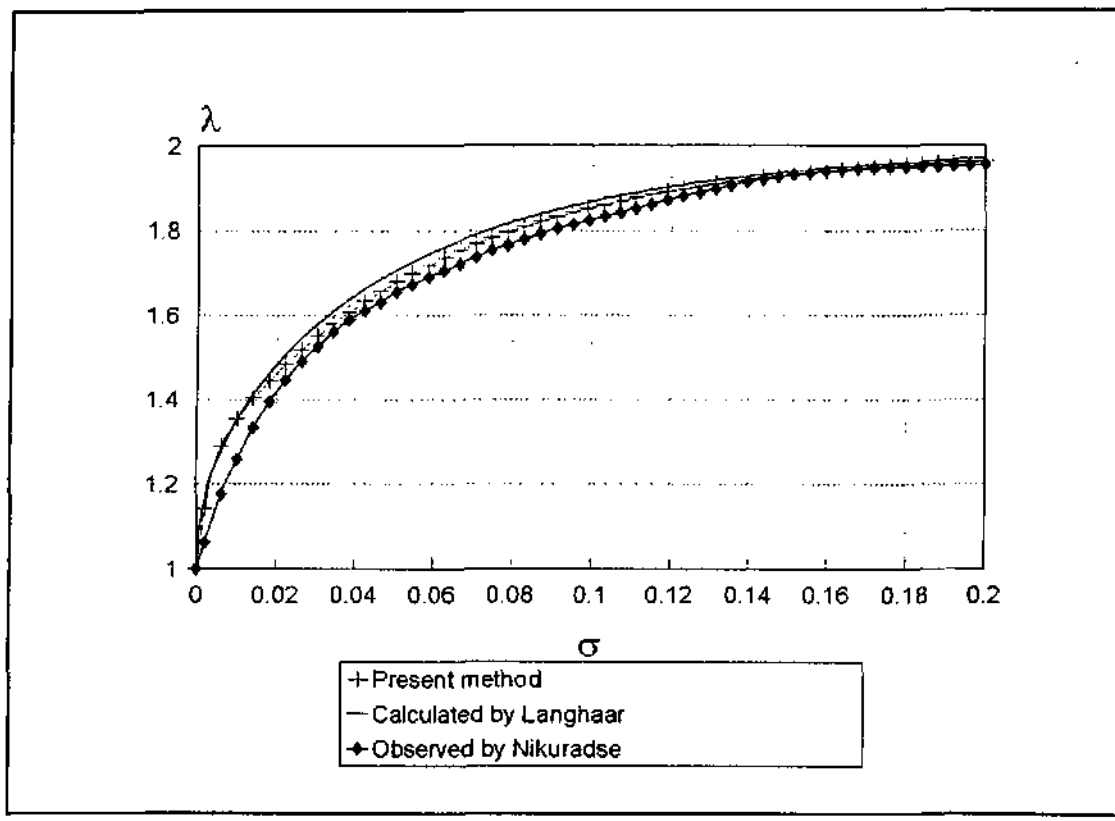

Figure 4.5 Comparison of centreline velocities.

Figure 4.6 compares velocity profiles calculated with the present method and the method of Langhaar at five different axial positions. The numerical results are in close agreement with the analytical results. An uniform grid of 500 x 21 was used.

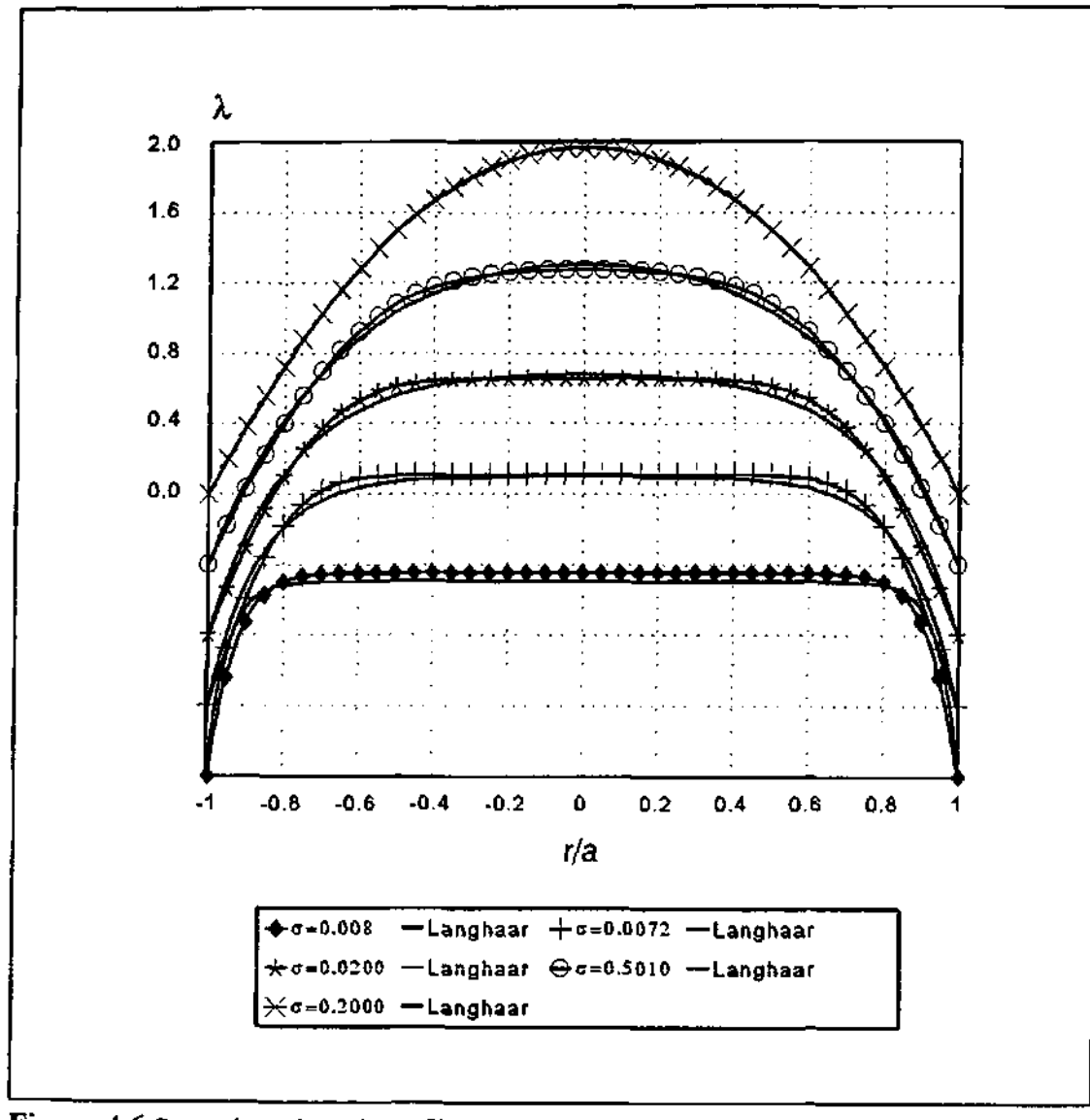

Figure 4.6 Comparison of velocity profiles at different axial positions.

Figure 4.7 shows the variation of pressure along the axis calculated for the present method and the analytical method. The dimensionless pressure drop

$$C_p = 1 + \frac{\Delta p}{\frac{1}{2}\rho u_{mean}^2}$$

is plotted against dimensionless axial distance. Again the numerical results are close to the analytical results. An uniform grid of 100 x 21 was used.

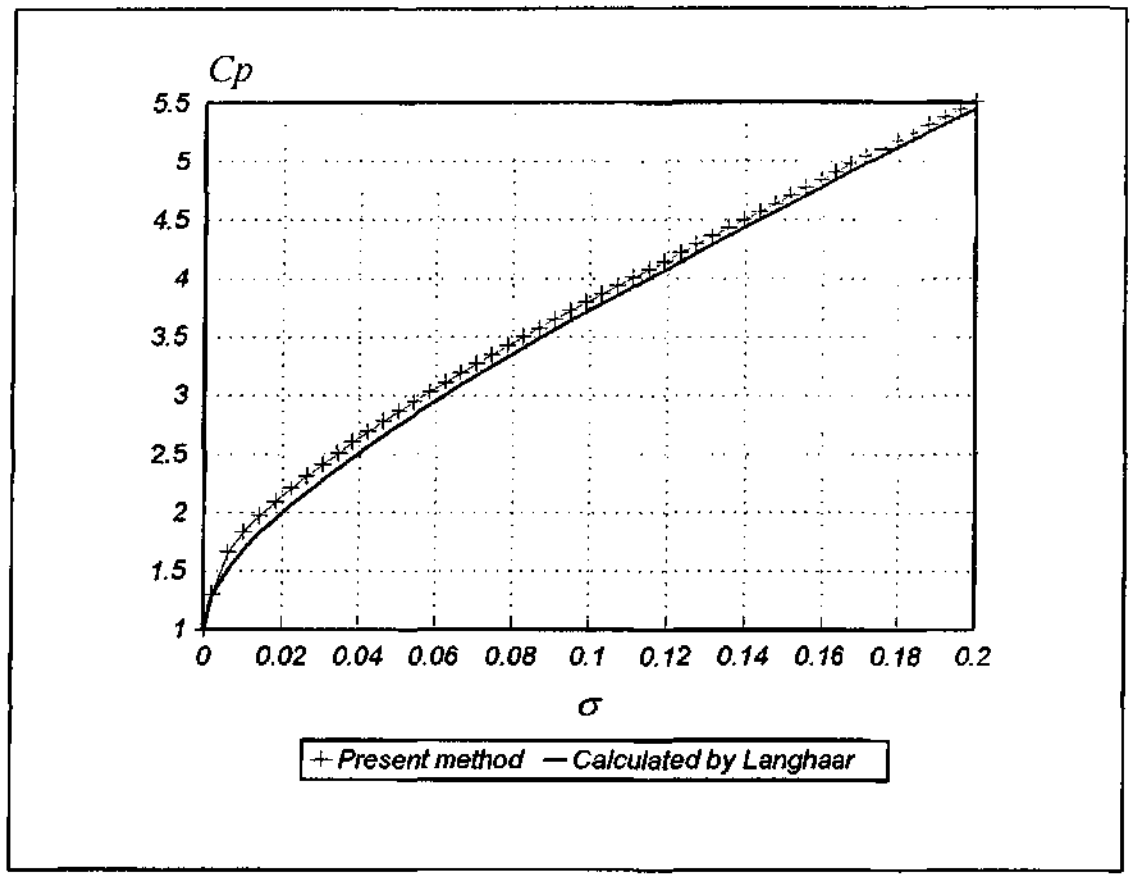

Figure 4.7 Variation of pressure along the axis of the tube.

B.3.4.6.2. CONCENTRATION.

No analytical solution exist for the concentration equation in the entrance region of a pipe. For fully developed flow in a constant diameter pipe Eq. (3.16) however reduces to

$$\rho u \frac{\partial \phi}{\partial x} = \frac{\Gamma}{r} \frac{\partial}{\partial r}\left(r \frac{\partial \phi}{\partial r x} \right) \tag{4.34}$$

Holman (1989) gives the following analytical solution of Eq. (4.34) for the case of a constant wall flux $(\partial\phi/\partial r)_{r=R}$:

$$\phi - \phi_0 = \frac{\Gamma}{\rho} \frac{\partial \phi}{\partial x} \frac{u_0 R^2}{4} \left[\left(\frac{r}{R} \right)^2 - \frac{1}{4} \left(\frac{r}{R} \right)^4 \right] \tag{4.35}$$

where ϕ_0 is the centreline concentration and u_0 the centreline velocity.

Figure 4.8 compares profiles calculated with the present method in the fully developed region with the exact solution given by (4.35). The numerical results are virtually identical to the analytical results. An uniform grid of 100 x 21 was used.

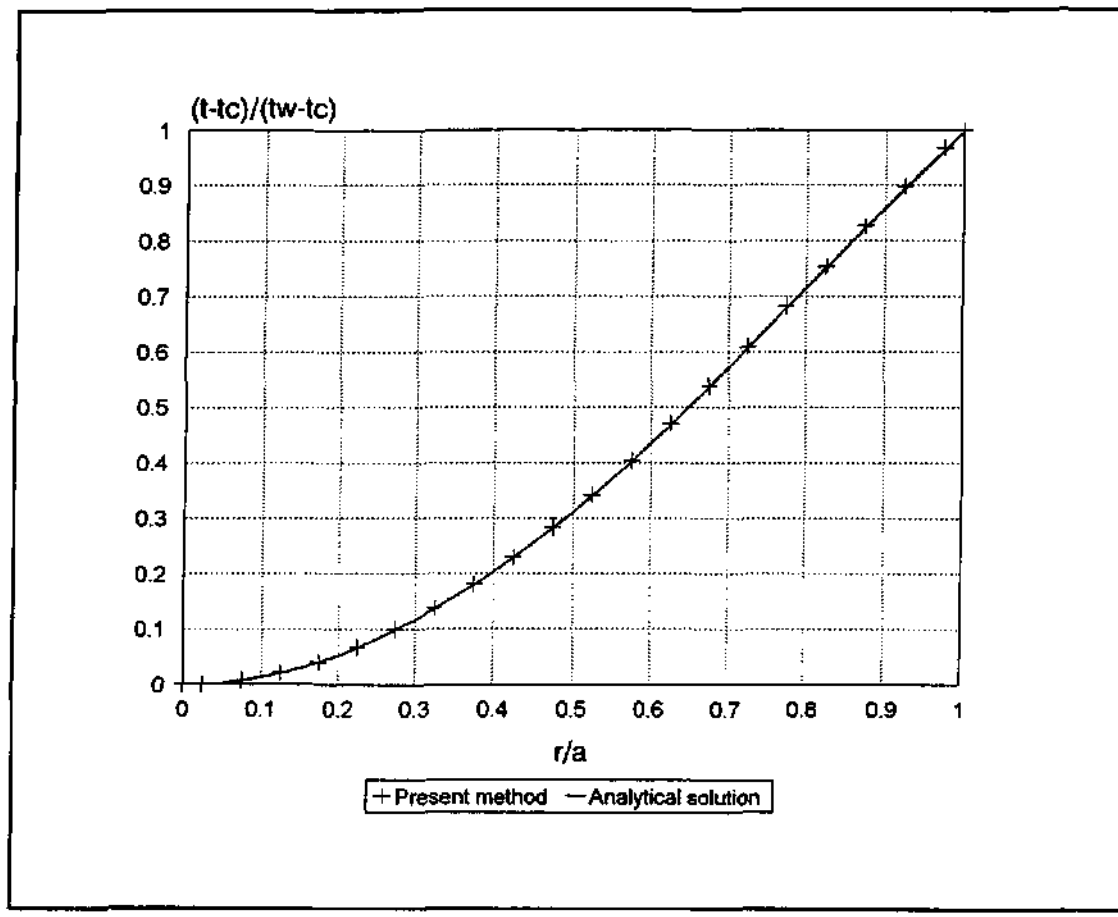

Figure 4.8 Comparison of concentration profiles in the fully developed region.

B.3.5. APPLICATION.

B.3.5.1. INTRODUCTION.

In this chapter the numerical model will be applied to a brackish desalination membrane. First an example calculation will be done to investigate the qualitative behaviour of the model.

After the model has been qualitatively evaluated the effect of inlet pressure, inlet concentration, inlet velocity, diameter and length-to-diameter ratio on separation efficiency will be investigated.

B.3.5.2. EXAMPLE CALCULATION

B.3.5.2.1. DIMENSIONS, OPERATING CONDITIONS AND STRUCTURAL PROPERTIES.

The dimensions of the membrane are as follows:

- Inside diameter = 1,0 mm.
- Outside diameter = 1,2 mm.
- Length = 10 m.

The operating conditions are as follows:

- Inlet velocity = 2 m/s.
- Inlet concentration of NaCl = 1 percent.
- Inlet pressure = 80 Bar.
- Temperature = 25 °C.

The structural properties of the membrane are as follows:

- Young's modulus = 2000 Mpa.
- Poisson ratio = 0,3.

The fluid properties are as follows:

- Density of water = 997,4 kg/m^3.
- Viscosity of water = $9,8 \times 10^{-4}$ kg/m.s.

B.3.5.2.2. MEMBRANE CONSTANTS

The mass flux of water through a membrane can be obtained by multiplying (3.20) with the density of water. The result is

$$j_W = \rho_{Ww} A(\Delta p - p_m) \tag{5.1}$$

where

ρ_W = density of water,
A = membrane constant,
Δp = $p_i - p_o$ i.e. the pressure difference across the membrane and
p_m = osmotic pressure.

Ideally all the salt are retained on the inside but in actual fact a small percentage diffuse across the membrane. The mass flux of salt is given by

$$j_S = B(\rho_{S2} - \rho_{S3}) \tag{5.2}$$

where

ρ_{S2} = density of salt on the inside at the wall,
ρ_{S3} = density of the salt in the permeate and
B = membrane constant.

Parameters A and B are membrane constants which have to be determined by experiment. They are independent of concentrations on both sides of the membrane. The membrane constant A decreases slightly with increasing operating pressure whereas the constant B is almost independent of pressure. Membrane compaction of the active layer is the reason for the pressure dependence of A.

Figure 5.1 shows the membrane constant A for a cellulose acetate reverse osmosis membrane as a function of pressure difference Δp for three different membranes.

For the present study we will use the following linear relationship which is an approximation of the A values of membrane 1 in Figure 5.1:

$$A = 2{,}2 - 0{,}00667\,\Delta p \tag{5.3}$$

The units of A is 10^{-7} $m.s^{-1}$ bar^{-1} and that of Δp is bar.

The rejection coefficient of a membrane is defined as

(5.4)

Equation (5.4) combined with the relationship for the calculation of j_S *and* j_W (Equations 5.1 and 5.2) and the approximation for the permeate concentration

$$\rho_{S3} = \frac{j_S}{(j_S + j_W)/\rho_3} = \frac{j_S}{j_W/\rho_W} = \frac{j_S}{v_R} \tag{5.5}$$

indicate the concentration, pressure and flux dependency of the rejection coefficient:

$$\beta = \left[1 + \frac{B}{A(\Delta p - p_M)}\right]^{-1} \tag{5.6}$$

We will assume a rejection coefficient of 97 percent at a mass concentration of 1 percent and a trans-membrane pressure difference of 30 Bar. Solving (5.6) for B we get

$$B = (1/R - 1)A(\Delta p - p_M)$$
$$= (1/0{,}97 - 1)(2{,}2 - 0{,}00667\times30)(30 - 7{,}9)$$
$$= 1{,}367\times10^{-7}\ m/s$$

With B and v_R known the flux of salt through the membrane can be calculated. Combination of Equations (5.2) and (5.5) gives

$$\rho_{S3} = B(\rho_{S2} - \rho_{S3})/v_R \tag{5.7}$$

Solving of (5.7) for ρ_{S3}:

$$\rho_{S3} = \frac{B\,\rho_{S2}}{v_R + B} \tag{5.8}$$

Substitution of (5.8) into (5.2) gives

$$j_S = B\rho_{S2}\left(1 - \frac{B}{v_R + B}\right) \tag{5.9}$$

The salt density at the inside wall is given by

$$\rho_{S2} = \phi_R\rho_R \tag{5.10}$$

where ϕ_R is the mass fraction at the inside wall and ρ_R is the density of the solution at the inside wall.

Applying Fick's law at the inside membrane wall we get

$$j_S = -\Gamma_R\left(\frac{\partial\phi}{\partial r}\right)_R \tag{5.11}$$

Combination of (5.9), (5.10) and (5.11) gives the boundary condition for mass fraction at the membrane wall

$$\left(\frac{\partial \phi}{\partial r}\right)_R = -\frac{B\,\phi_R \rho_R}{\Gamma_R}\left(1 - \frac{B}{\nu_R + B}\right) \tag{5.12}$$

B.3.5.2.3. GRID SIZE.

A grid with 200 equally spaced grid points in the axial direction and 61 grid points in the radial direction is used. The grid spacing is uniform in the radial direction from j = 1 to j = 30 and then contracts with a ratio of 0,9 from j = 31 to j = 61. This way more grid points are used close to wall to better approximate the steep gradient of mass fraction next to the wall.

B.3.5.2.4. RESULTS.

Figure 5.1 shows the variation of pressure, osmotic pressure and the effective trans-membrane pressure difference with axial distance. The effective trans-membrane pressure difference is defined as ($\Delta p - p_m$) where Δp is the actual pressure difference and p_m is the osmotic pressure. The pressure and effective pressure difference decrease with x while p_m increase with x. The pressure drop from inlet to outlet is 5,68 bar. The increase in osmotic pressure is due to an increase in the salt mass fraction at the wall as can be seen from Figure 5.2

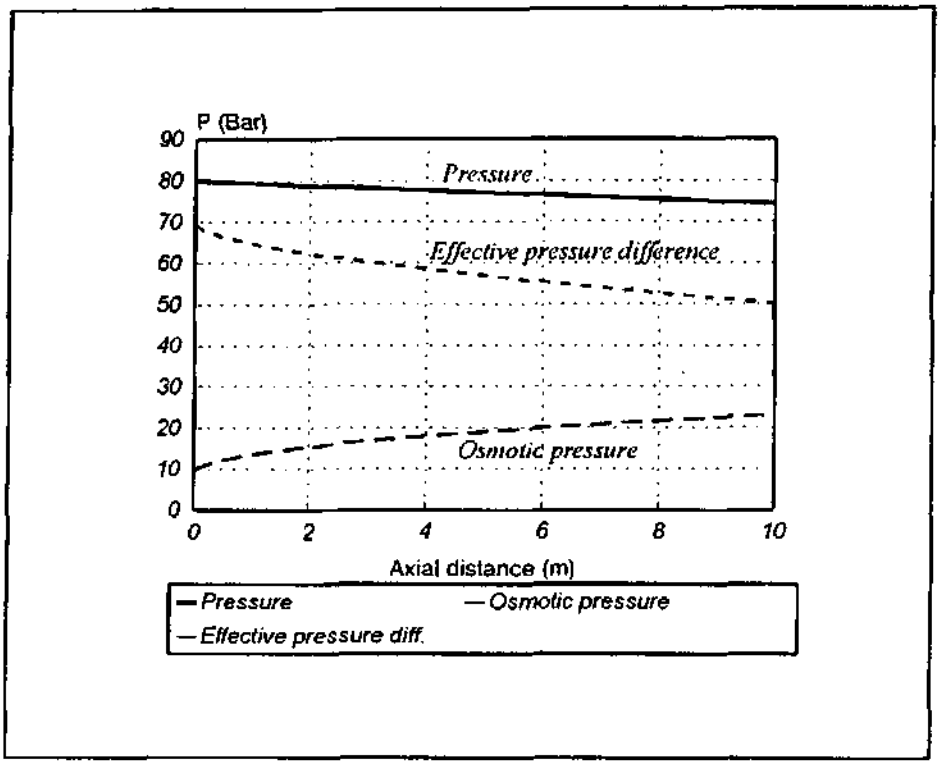

Figure 5.1 Variation of pressure, osmotic pressure and effective pressure difference with axial distance.

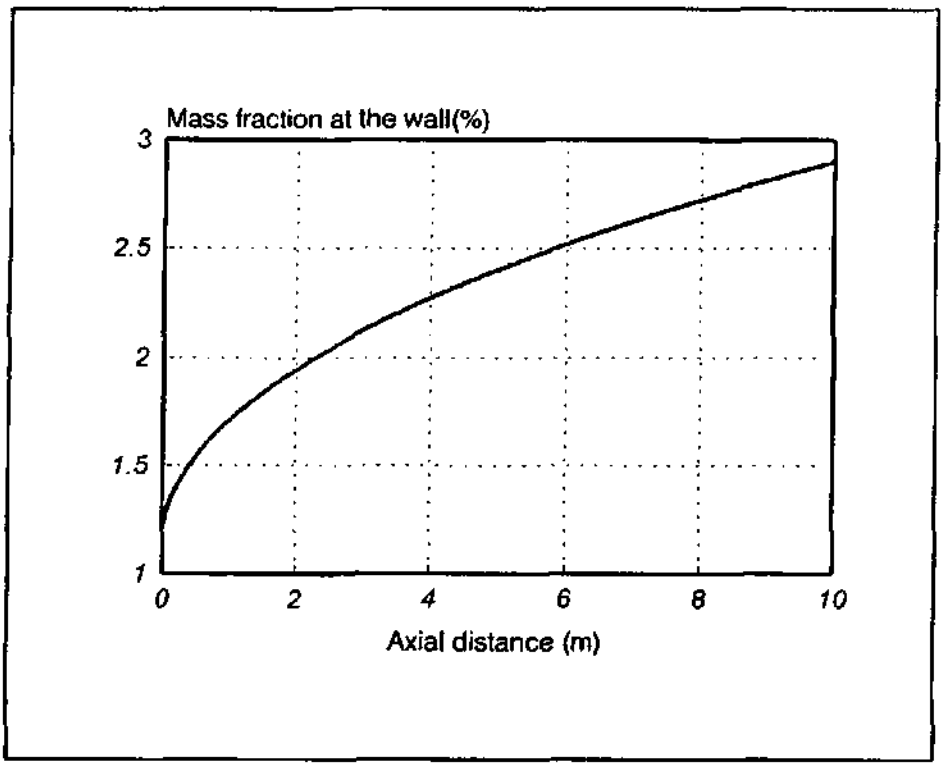

Figure 5.2 Variation of the salt mass fraction at the wall with axial distance.

Figure 5.3 shows the percentage increase of the inside diameter along the length of the tube. The percentage increase is very small (only about 0,45 percent) and the value decreases somewhat along the length. This decrease is due to the decrease of inside pressure.

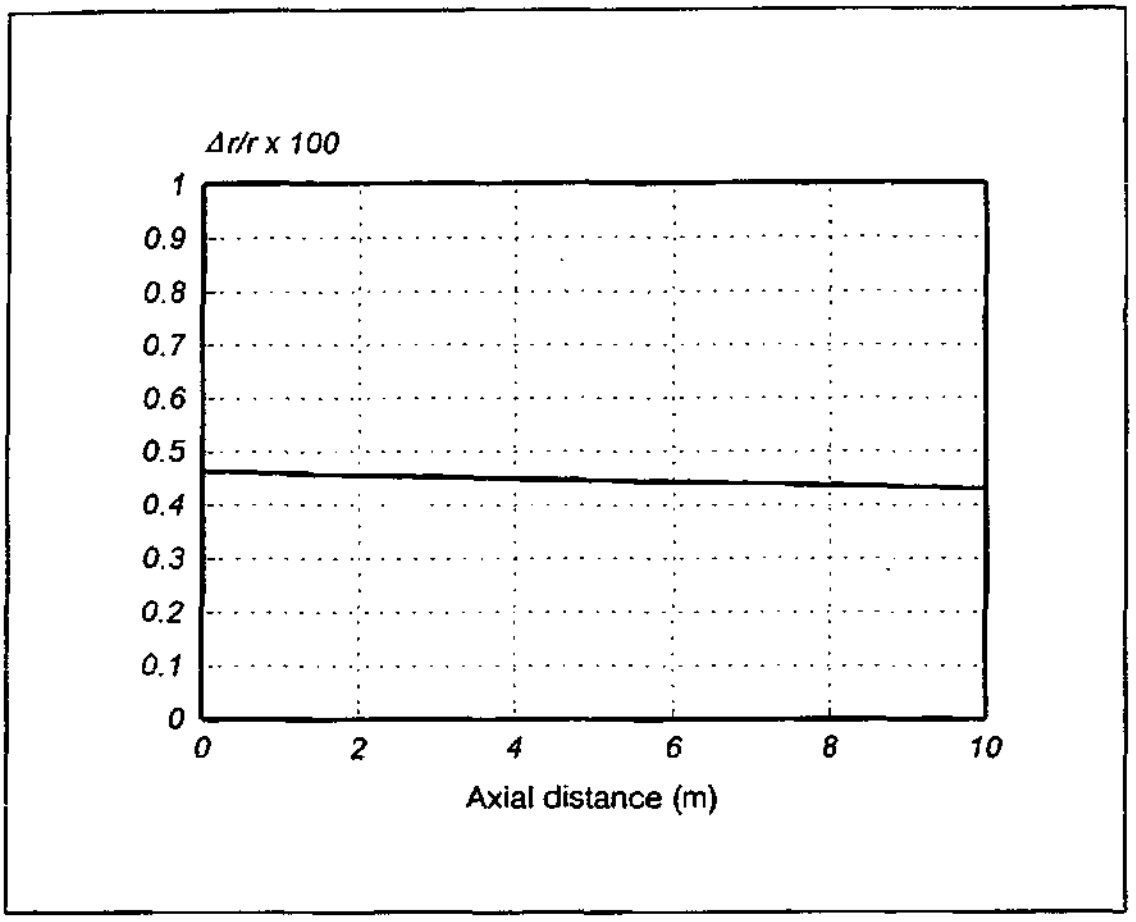

Figure 5.3 Percentage increase in diameter as function of axial distance.

Figure 5.4 shows the variation of wall velocity along the length of the tube. The decrease of wall velocity is due to the decrease of the effective pressure difference as shown in Figure 5.1.

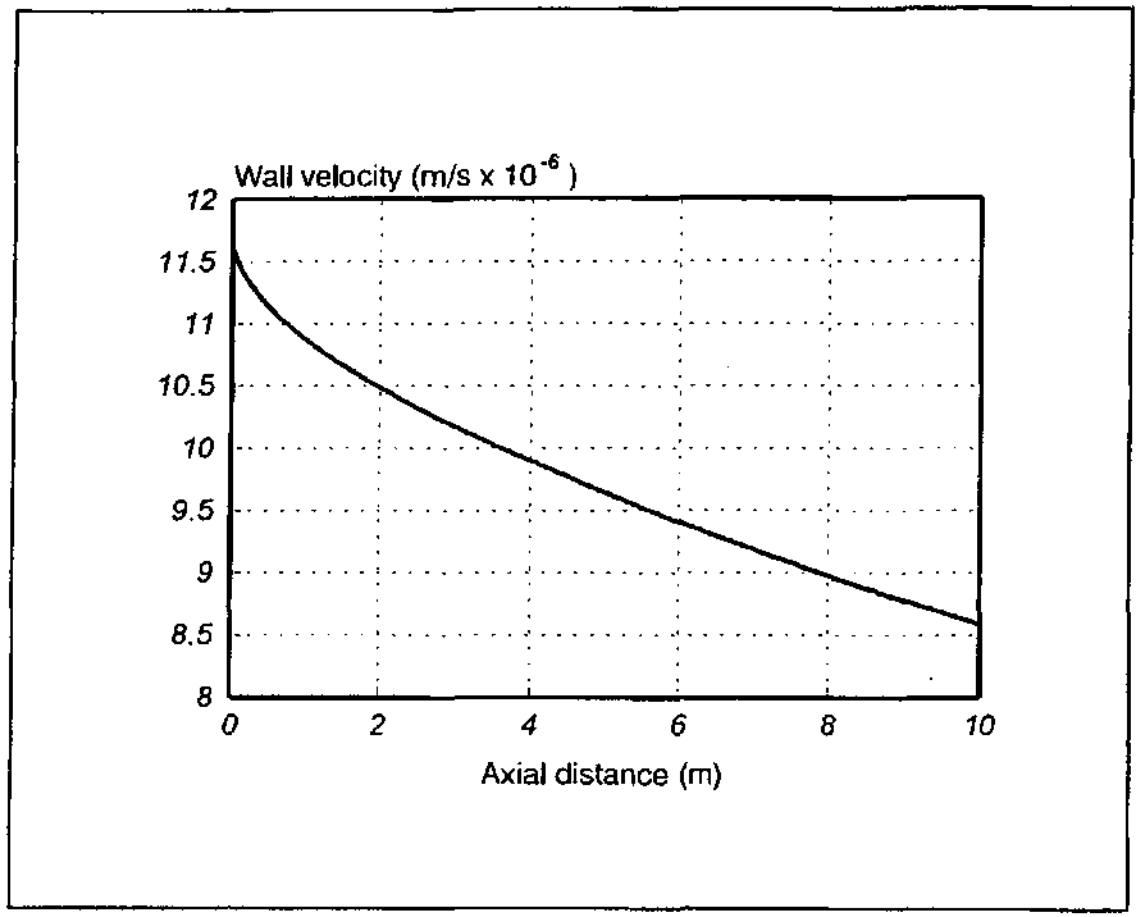

Figure 5.4 Variation of the wall velocity along the length of the tube.

Figure 5.5 shows the variation of axial mass flow along the length of the tube. The ratio of mass flow to inlet mass flow varies from 1 at the inlet to 0,8 at the outlet. This implies that 20 percent of the inlet mass flow moves across the tube wall (membrane).

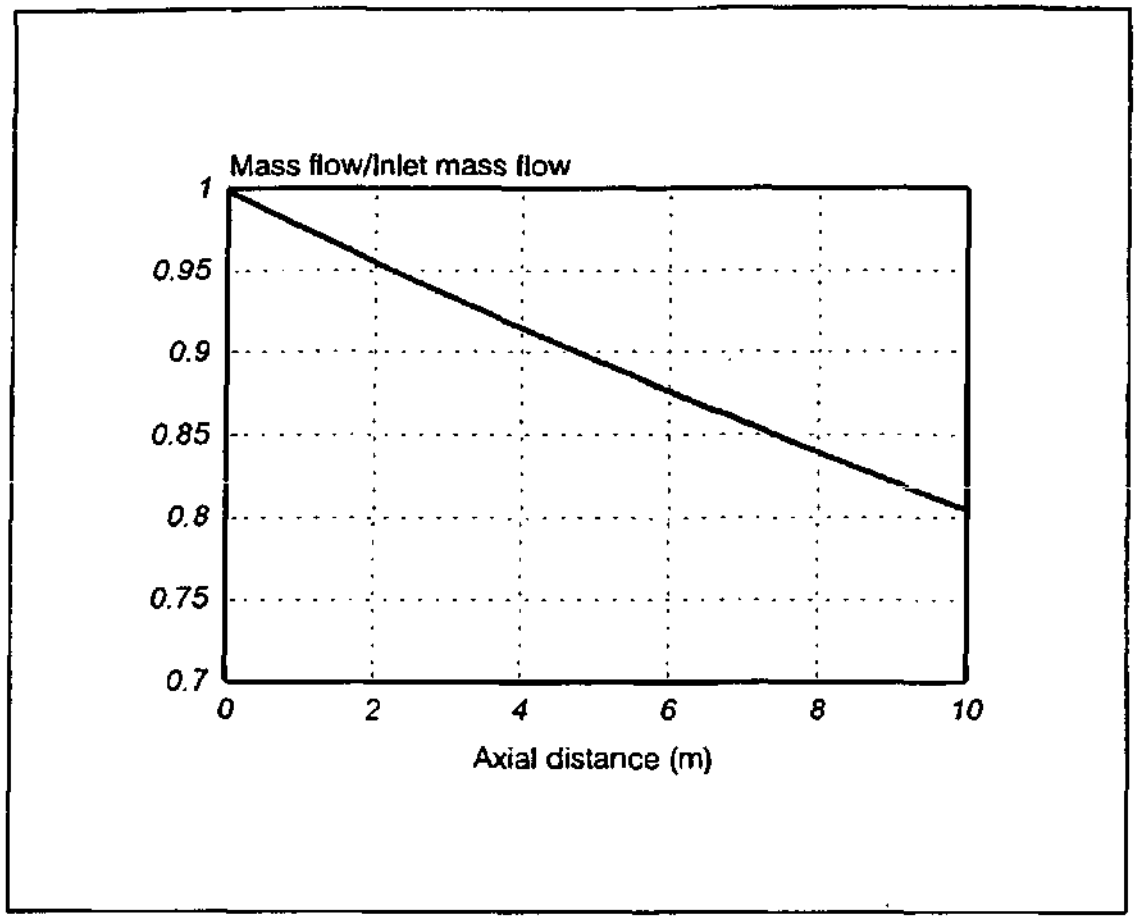

Figure 5.5 Variation of axial mass flow along the length of the tube.

Figure 5.6 shows the variation of rejection coefficient with axial distance. The rejection coefficient varies from 98,8 percent at the inlet to 98,4 percent at the outlet. This decrease is due to the decrease in wall velocity (see Eq. 5.6).

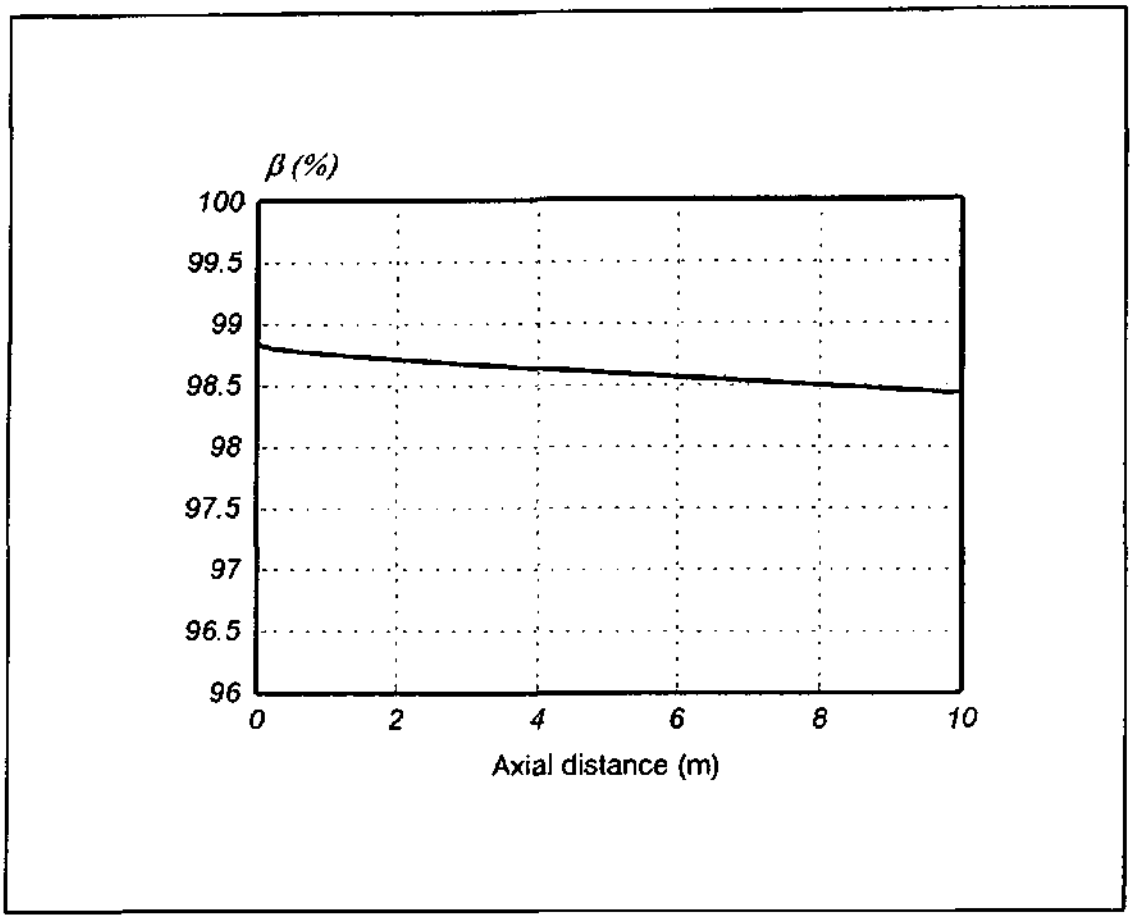

Figure 5.6 Variation of rejection coefficient with axial distance.

Figure 5.7 shows the variation of C/C_{wall}, U/U_c and V/V_{max} over the radius at the outlet where

C = mass fraction,
C_{wall} = mass fraction at the wall,
U = axial velocity,
U_C = centreline velocity,
V = radial velocity and
V_{max} = maximum radial velocity.

The figure shows that C/C_{wall} and V/V_{max} increase from the centreline to the wall while U/U_C decreases.

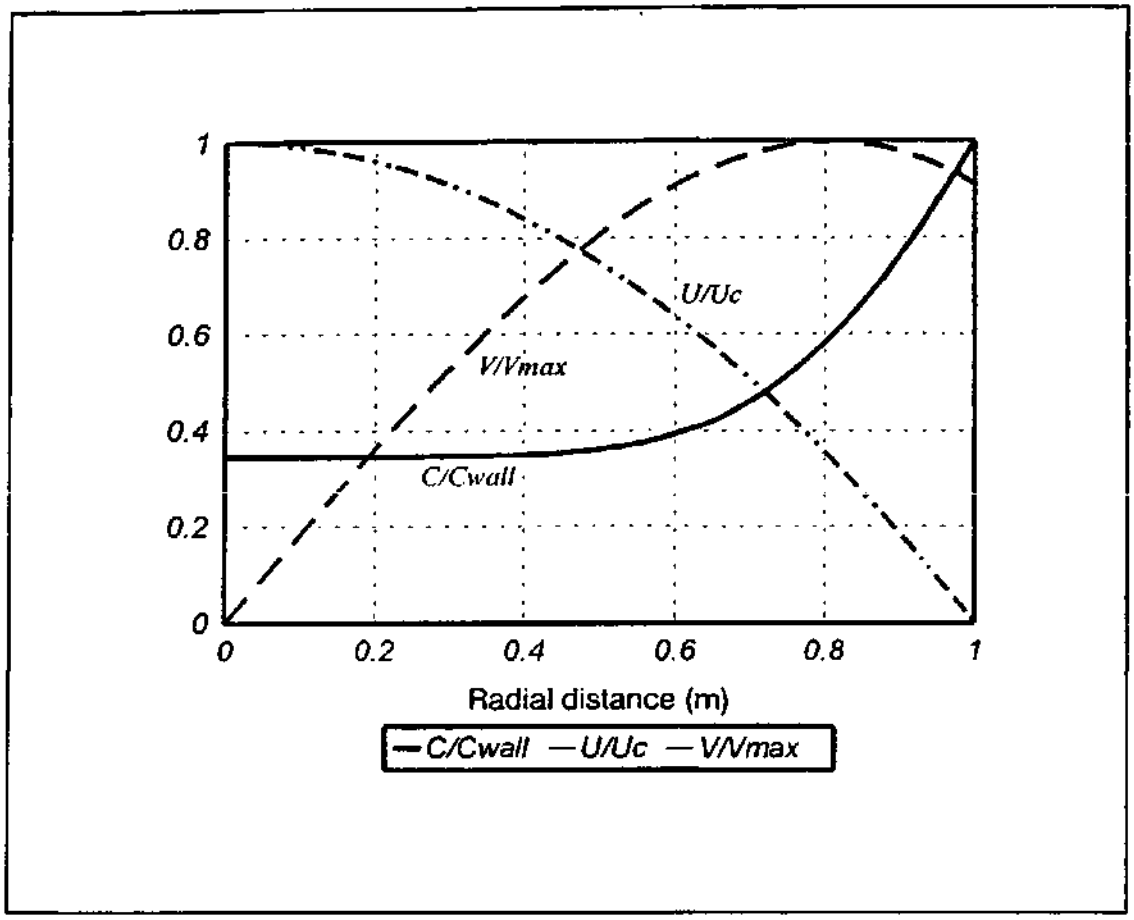

Figure 5.7 Variation of concentration, axial velocity, and radial velocity over the radius at the outlet of the tube.

B.3.5.3. INVESTIGATION INTO THE EFFECT OF GEOMETRY AND OPERATING CONDITIONS ON SEPARATION EFFICIENCY.

B.3.5.3.1. INTRODUCTION.

In this section the effect of length-to-diameter ratio, diameter, inlet pressure, inlet concentration and inlet velocity on the separation efficiency of a desalination membrane is investigated.

The structural properties of the membrane and fluid properties are given in Section 5.2.1. while the membrane constants are given in Section 5.2.2.

A grid with 50 equally spaced grid points in the axial direction and 61 grid points in the radial direction is used. The grid spacing in the radial direction is the same as in Section 5.2.3.

In the next section the separation efficiency is defined after which the results will be discussed.

B.3.5.3.2. SEPARATION EFFICIENCY.

The separation efficiency, ϵ, is defined as the permeate mass flow divided by the energy input. Thus

$$\epsilon = \frac{m_P}{E_{in}} \tag{5.13}$$

The energy input is given by

$$E_{in} = Q_p(p_{in} - p_o) + Q_{out}(p_{in} - p_{out}) \quad (5.14)$$

where

Q_p = permeate volumetric flow rate,
p_{in} = inlet pressure,
p_o = pressure on the outside of the tube,
p_{out} = pressure at the outlet of the tube and
Q_{out} = volumetric flow rate at the outlet of the tube.

B.3.5.3.3. DISCUSSION OF RESULTS.

Figure 5.8 shows separation efficiency , ϵ, versus length-to-diameter ratio for three different diameters at an inlet pressure of 60 Bar, inlet velocity of 1 m/s and an inlet concentration of 2 percent. Separation efficiency is strongly dependent on the diameter and it increases as the diameter decreases. This can be explained as follows: The Peclet number ($\rho UD/\Gamma$), which is the ratio of convective flux to diffusive flux, decreases with diameter. This means that the effect of diffusion increases as the diameter decreases and this causes the wall concentration to decrease. This in turn causes the osmotic pressure to decrease which causes the flux of water through the membrane to increase.

Figure 5.8 also shows that the separation efficiency increases somewhat with length-to-diameter ratio at a constant diameter. This is due to the fact that the area increases with L/D. An increase in length, however, also causes the pressure losses to increase which results in a weaker driving force for reverse osmoses and an increase in energy consumption. This explains why ϵ is a weak function of L/D.

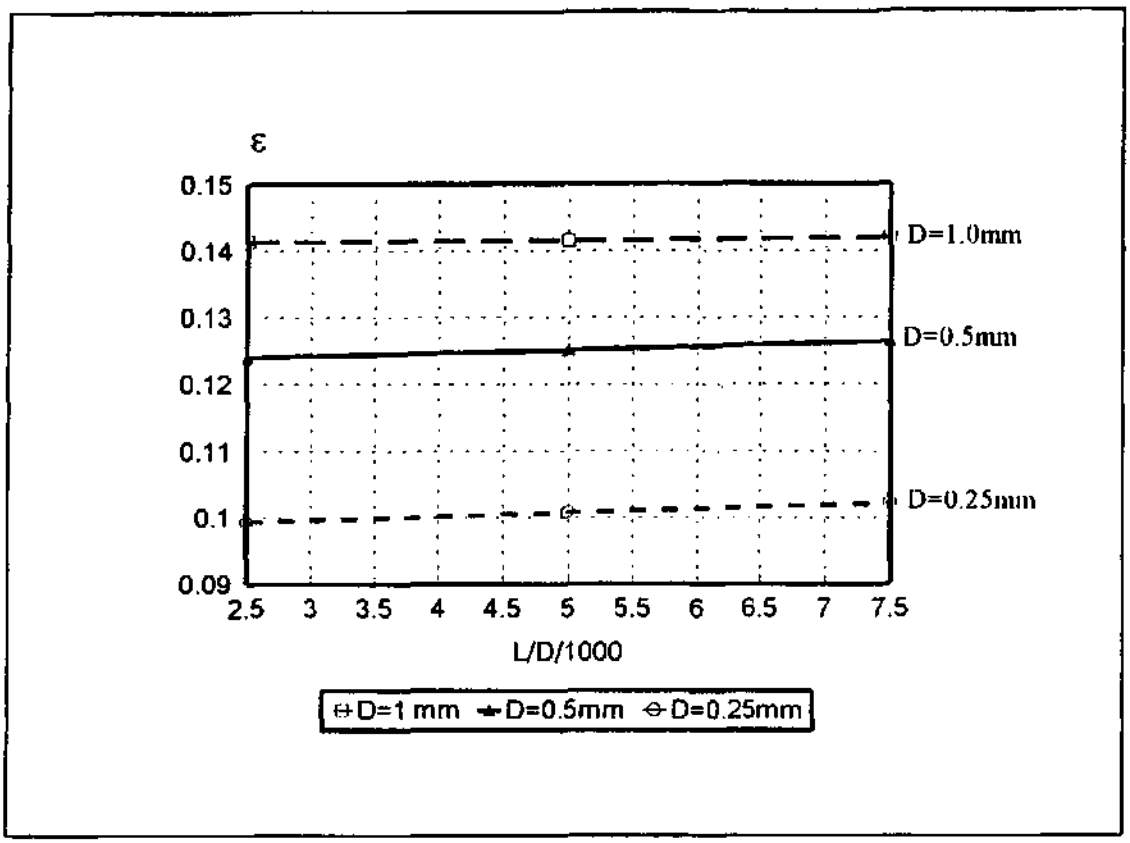

Figure 5.8 Separation efficiency versus L/D for different diameters at p_{in} = 60 Bar, μ = 1 m/s, and ϕ_m = 0.02.

Figure 5.9 shows efficiency versus inlet pressure for an inlet velocity of 1 m/s, an inlet concentration of 2 percent, a diameter of 0,5 mm and a length-to-diameter ratio of 5000. The separation efficiency is maximum at a pressure of 50 Bar and decreases as the pressure moves away from the optimum value.

Both the permeate flux and energy consumption increase with pressure which explains why the separation efficiency, which is the ratio of permeate flux to energy consumption, has an optimum value.

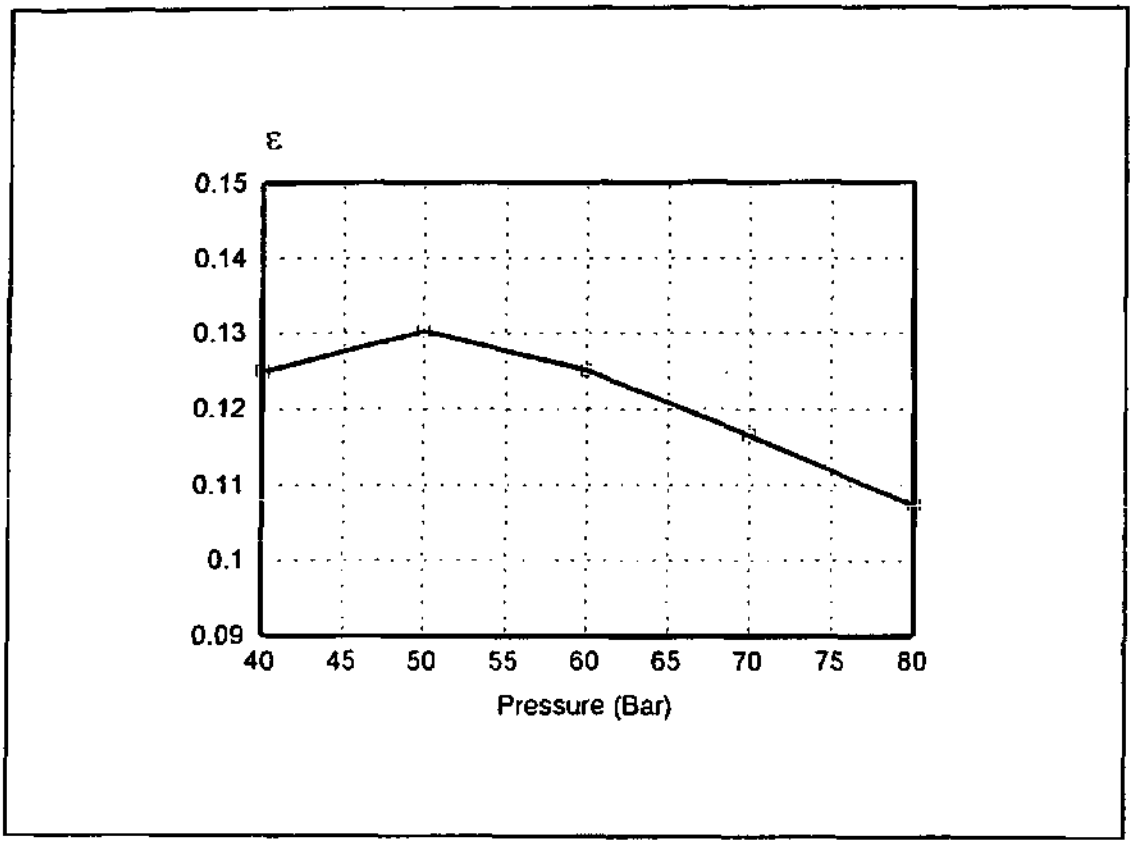

Figure 5.9 Separation efficiency versus inlet pressure for u_m = 1 m/s, ϕ_n = 0,02, D = 0,5 mm and L/D = 5000.

Figure 5.10 shows separation efficiency versus inlet concentration for an inlet pressure of 60 Bar, an inlet velocity of 1 m/s a diameter of 0,5 mm and a length-to-diameter ratio of 5000. Separation efficiency decreases with inlet concentration. Higher inlet concentrations causes the osmotic pressure to increase and thus the driving force for permeate movement through the membrane to decrease.

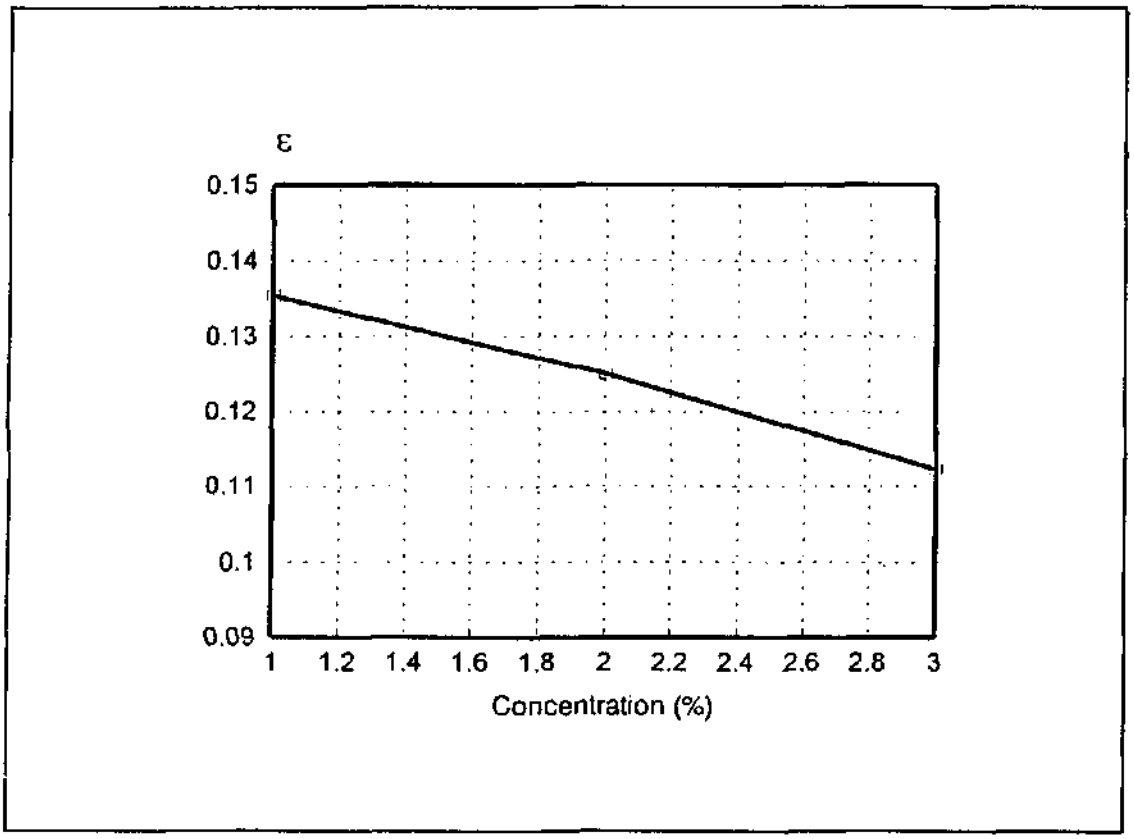

Figure 5.10 Separation efficiency versus inlet concentration for p_{in} = 60 Bar, u_{in} = 1 m/s, D = 0,5 mm and L/D = 5000.

Figure 5.11 shows separation efficiency versus inlet velocity for an inlet pressure of 60 Bar, an inlet concentration of 2 percent a diameter of 0,5 mm and a length-to-diameter ratio of 5000. Separation efficiency decreases with inlet velocity. This is due to the fact that the Peclet number increases with velocity. High Peclet numbers imply small diffusive fluxes and thus higher wall concentration. Higher wall concentrations in turn imply higher osmotic pressures and thus a smaller driving force for permeate movement through the membrane. Higher fluid velocities also imply larger energy losses.

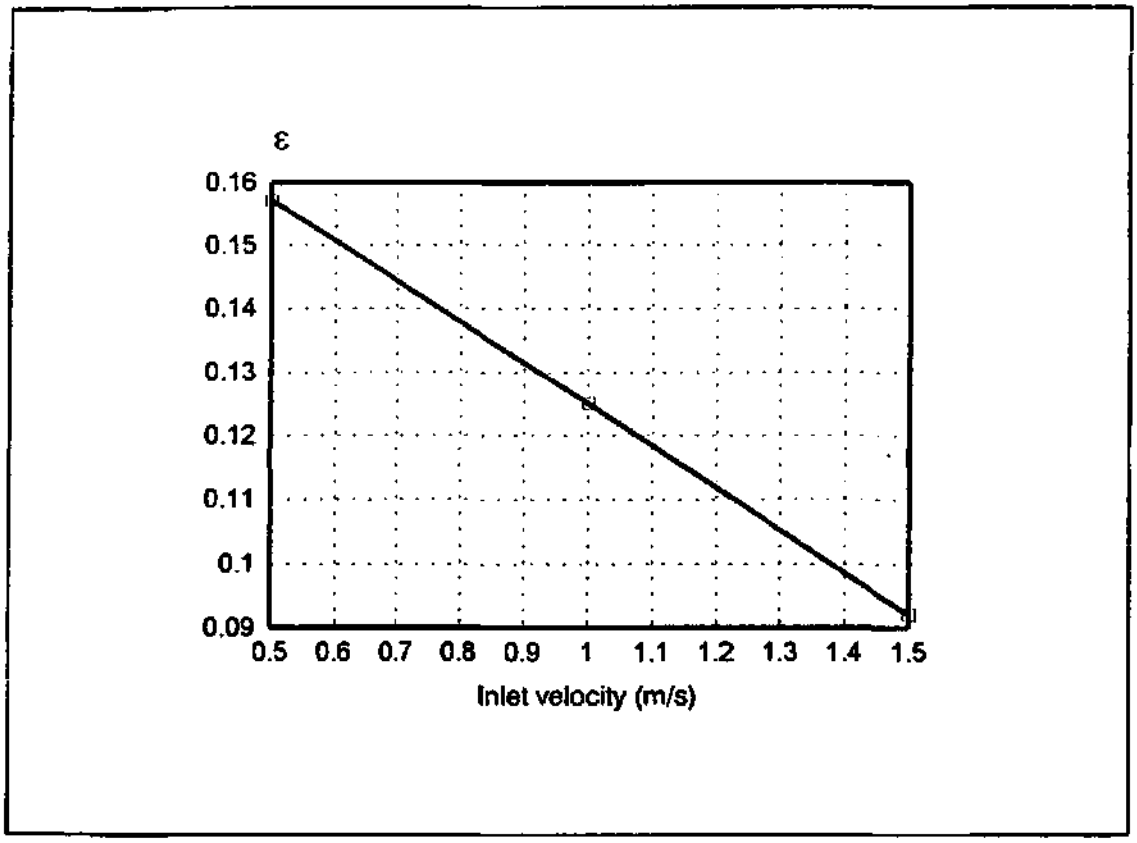

Figure 5.11 Separation efficiency versus inlet velocity for p_{in} = 60 Bar, ϕ_{in} = 0,02, D = 0,5 mm and L/D = 5000.

B.3.6. SUMMARY AND CONCLUSION

B.3.6.1. SUMMARY

A numerical model has been developed to simulate the transfer processes in a cylindrical membrane. The model predicts the radial and axial variations of velocity components and ion concentration as well as the axial variation of pressure. The ion concentration at the wall is used to predict the osmotic pressure which together with the inside and outside pressures, determine the driving force for reverse osmosis. With the driving force known the permeate and ion fluxes through the membrane are calculated. The model also takes the variation in diameter due to the pressure difference across the wall into consideration. The results of the basic numerical model was compared to an approximate analytical solution and the results of the two methods were in close agreement. The model was then applied to a membrane and it was shown that the model behaves qualitatively correct.

Lastly an investigation was done to determine the effect of inlet pressure, inlet concentration, inlet velocity, diameter and length-to-diameter ratio on separation efficiency. It was shown that separation efficiency decreases with diameter, velocity, inlet concentration and increases with length-to-diameter ratio. The separation efficiency is maximum at a specific value of inlet pressure.

The study showed that a numerical model can successfully predict the transfer of mass and momentum in a cylindrical membrane taking all the fundamental mechanisms that play a role into account. The study also showed how the model can be used to optimise geometry and operating parameters.

A limitation of the model is that it only applies to laminar flow. A suggestion for future work is that the model be extended to deal with turbulent flows as well. Another handy feature will be a graphical users interface which will facilitate the use of the program by design engineers.

B.3.6.2. *DETAIL INTERPRETATION OF THE ENHANCEMENTS PROVIDED BY THIS STUDY*

In a previous study Meyer (1993) also solved the transfer processes in a membrane. He used the commercial CFD code STAR-CD to solve the flow field and the finite-element structural analysis code ANSYS to determine the deformation of the tube wall. The couple fluid/structures problem was solved in an iterative way by first solving the flow field and then using the pressures obtained from this solution as boundary conditions for ANSYS in determining the deformation of the tube wall. The CFD grid was then adjusted to take the deformation of the tube into account and the flow field was solved again after which another ANSYS run was made. This process was repeated until convergence.

The procedure described above is very tedious and that because of the following reasons:

a) STAR-CD runs several hours on an expensive UNIX workstation to complete a single simulation. The reason for the long run time is that STAR-CD solves the full three-dimensional Navier-Stokes equations which is unnecessary in the present situation because the flow is only two-dimensional and parabolic (boundary layer type flow). The two-dimensional parabolised Navier-Stokes equations solves much faster and requires much less computer storage than the full three-dimensional Navier-Stokes equation.

b) ANSYS also solves the stresses and strains three-dimensionally. If the assumption is made that the strain doesn't vary strongly in the axial direction, as is the case in the present situation, the structural analysis reduces to a simple set of analytical equations.

c) The fluid/structural coupling is done manually which makes the whole procedure time consuming and expensive.

The tediousness of the procedure made it unsuitable for optimization studies. Another shortcoming of the method as that it didn't take the effect of osmotic pressure on the flow rate through the wall into account.

The present method solves the Navier-Stokes equation in two dimensions using a very fast space marching method. Furthermore the structural analysis is done as an integral part of the solution algorithm which makes the fluid-structure coupling fully automatic. The present method also requires much less computer memory than the previous method which makes it suitable for implementation on low-cost PC type computers. Another advantage of the present method is that all the fundamental transfer mechanisms like convection and diffusion, and deformation of the tube wall are taken into account. This makes the results more useful.

The power and speed of the present method make it ideally suited for optimization studies as was demonstrated in Section 5.3. Large number of simulations can be done in a relatively short time to investigate the effect of parameters such as operating conditions and geometry on the performance of the membrane.

The only shortcoming of the present method is that it only applies to laminar flow which limits the scope of the methods. This can however easily be rectified by incorporation of a suitable turbulence model.

The fact that the source code of the program is available locally will facilitate the extension of the program. There is also no licence fees involved in using the program as is the case with commercial codes like STAR-CD and ANSYS.

REFERENCES Pertaining to CFD.

Anderson, D.A., Tannehill, J.C. and Pletcher, R.H. (1984): *Computational Fluid Mechanics and Heat Transfer,* Hemisphere Publishing Corporation, New York.

Holman, J.P., (1989): *Heat Transfer,* McGraw-Hill, Singapore.

Gosman A.D., Pun W.M., Runchal, A.K., Spalding, D.B. and Wolfstein, M. (1969): *Heat and Mass Transfer in Recirculating flows,* Academic Press, London.

Langhaar, J.L., (1942): Steady Flow in the Transition Length of a Straight Tube, *Journal of Applied Mechanics,* June 1942 pp A55 - A58.

Meyer, J.P. (1993): Membraanoptimering met Berekeningsvloeimeganika, *Progress report for the Water Research Council.*

Prandtle, L. and Tietjens, O.G. (1934): *Applied Hydro- and Aeromechanics*, First Edition, McGraw-Hill, New York.

Patankar, S.V. (1980): *Numerical Heat Transfer and Fluid Flow,* McGraw-Hill, New York.

Perry, R.H. and Chilton, C.H. (1973): *Chemical Engineers Handbook*, Fifth Edition, McGraw-Hill, Johannesburg.

Popov, E.P. (1978): *Mechanics of Materials*, Second Edition, Prentice-Hall, Englewood Cliffs, New Jersey.

Rautenbach, R. and Albrecht, R. (1989): *Membrane Processes,* John Wiley, New York.

Roache, P.J. (1972): *Computational Fluid Dynamics,* Hermosa Publishing, Albuquerque.

Stiefel, E.L. (1963): *An Introduction to Numerical Mathematics*, Academec Press, London.

Weast, R.C. and Astle, M.J. (1982): *Handbook of Chemistry and Physics*, 63 rd Edition, CRC Press, Boca Ratin, Florida.

REFERENCES Pertaining to EIS

1. Mansfield, F., (1981): *Corrosion NACE, 23, No 5*, pp 301-307, May1981.

2. EG&G Princeton Applied Research - Electrochemical Instruments Group, (1985), *Basics of AC impedance measurements.* Application note AC-1.

3. Silverman, D.C., (1986), *Primer on the AC Impedance Technique*, Paper presented at NACE Corrosion/85, Boston, Mass., USA.

4. Vorster, S.W., V.D.Schijff, O.J., (1991), *The corrosion of aluminium alloys by chlorinated hydrocarbons.* Paper presented at the 6th National Meeting of the SA Institude for Chemical Engineers, Durban, RSA.

5. Grahame, D.C., (1954), *J. Am. Chem. Soc.*, Vol 76, pp 4819.

6. Devanathan, M.A.V., Peries, P., (1954), *Trans. Faraday Soc.*, Vol 50, pp 1236-1240.

7. Grahame, D.C., Parsons, R., (1961), *J. Am. Chem. Soc.*, Vol 83, pp 1291-1296.

8. Grahame, D.C., (1951), *J. Electrochem. Soc.*, Vol 98, pp 343.

9. Coster, H.G.L., Kim, K.L., et al, (1992), *J. of Membrane Science,* Vol 66, Characterization of ultrafiltration membranes by impedance spectroscopy. I. Determination of the separate electrical parameters and porosity of the skin and sublayers.

10. Jones, Prendergast, (1937), *J. Amer. Chem. Soc.*, Vol 59, pp 731-736.

PROGRAM LISTING

The program is written in Turbo Pascal and is runs on a IBM PC or compatable.

```
{$r+}
program wnk4;
const
  ymax = 251;
  Maxphys = 100;
  Maxosmot = 20;
  Sentinel = 999;
  s1 : array[1..3] of real = (2500,5000,7000);
  s2 : array[1..3] of real = (1e-3,0.5e-3,0.25e-3);
  s3 : array[1..5] of real = (40e5,50e5,60e5,70e5,80e5);
  s4 : array[1..3] of real = (0.01,0.02,0.03);
  s5 : array[1..3] of real = (0.5,1,1.5);
type
  jrow  =   array[0..ymax] of extended;
  Physvar = (Aphys,Dphys,Mphys,Ephys);
  Osmotvar = (MassOS,PresOS);
  Physarray = array[1..Maxphys,Physvar] of extended;
  Osmotarray = array[1..Maxosmot,Osmotvar] of extended;
var
  Physchar : Physvar;
  Osmotchar : Osmotvar;
  physdat : Physarray;
  osmotdat : Osmotarray;
  Nphys,Nosmot : integer;
  e,f,a,b,c,d,dd,x,y,u,uw,v,vw,fiw,fi,temp              : jrow;
  zeta,rho,rhow,mu,lam,zz,celrey : array[1..ymax] of extended;
  uin,rw,r,dzeta,rhoo,mw,m,dpdx,p,pw,length,dx,grad,mwall,mwalls,fiin,flux,
  influx,inmass,pin,sigg,sum,sumo : extended;
  zetap,zetan,zetas,dzetan,dzetas,mun,mus,dn,ds,muu,con,cn,cs,cw,cp,bp :
      extended;
  j,jm,it,i,im,jmm1,n,mm,nn : integer;
  xx,yy,exrat,vwall,rey,ri,ro,po,bb,jss,wfluxs,wflux,q,di,lopd : extended;
  rout,posmot,vmax : real;
  f1,f2,f4 : text;
  ii,jj : integer;
  ener : array[1..5] of real;
{-------------------------------------------------------------------------
**** Procedure gtri solves a TDM using the Thomas algorithm ****
```

```
{------------------------------------------------------------------------}
Procedure gtri(a,b,c,d : jrow ; var w : jrow; imin,imax,l1,lm : integer;
 a1,q1,am,qm : extended);
{ imin = left boundary, imax = right boundary.
  l1 and lm  are boundary condition option indicators at imin and imax
           respectively with  1 = Dirichlet, 2 = Neumann, 3 = mixed
  Solution is stored in w.
  a1 = lower  boundary value  if l1 = 1
  am = upper  boundary value  if lm = 1
  a1 = (w[imin+1] - w[imin]) if l1 = 2
  am = (w[imax] - w[imax-1]) if lm = 2
}
var
   e,f : jrow;
   den : extended;
   m,mk : integer;
begin
case l1 of
   1: begin
         e[imin] := 0.0;
         f[imin] := a1;
      end;
   2: begin
         e[imin] := 1.0;
         f[imin] := -a1;
      end;
   3: begin
         e[imin] := a1/(a1 - 1.0);
         f[imin] := q1/(1.0 - a1);
      end;
   end;
   for m := imin+1 to imax-1 do
   begin
      den := b[m] - c[m]*e[m-1];
      e[m] := a[m]/den;
      f[m] := (d[m] + c[m]*f[m-1])/den;
   end;
   case lm of
   1: w[imax] := am;
   2: w[imax] := (f[imax-1] + am)/(1.0 - e[imax-1]);
   3: w[imax] := (f[imax-1] + qm/am)/((1.0 + am)/am - e[imax-1]);
   end;
```

```
    for mk := imin to imax-1 do
    begin
       m := imin + imax - 1 - mk;
       w[m] := e[m]*w[m+1] + f[m];
    end;
end;
{-------------------------------------------------------------------------
 **** Function POW returns a to the power of b ****
-------------------------------------------------------------------------}
function POW(a,b: extended) : extended;
begin
   if b = 0.0 then pow := 1
   else if a = 0.0 then pow := 0.0
   else pow := exp(b*ln(a));
end;
{-------------------------------------------------------------------------
 **** Function INTPOW returns a to the power of b. b must be an integer ****
-------------------------------------------------------------------------}
function intpow(a : extended; b : integer) : extended;
var x : extended;
    i : integer;
begin
   x := 1.0;
   for i := 1 to b do x := x*a;
   intpow := x;
end;
{-------------------------------------------------------------------------
 **** Procedure NewtonRaphson calculates the axial pressure gradient
      using the Newton method ****
-------------------------------------------------------------------------}
procedure NewtonRaphson(fact : extended; var t,grad : extended);
{fact = actual function value
 t    = initial guess of independent variable ,input
 t    = independent variable ,output
 grad = initial guess of df/dt}

var
   f,fx,tx,dt : extended;
   i : integer;
function func(t : extended) : extended;
begin
        for j := 2 to jmm1 do d[j] := dd[j] - t;
```

```
          gtri(a,b,c,d,u,1,jm,2,1,0,0,0,0);
          m := 0;
          for j := 1 to jmm1 do
          begin
             dzeta := zeta[j+1] - zeta[j];
             zetap := 0.5*(zeta[j+1] + zeta[j]);
             m := m + 2*pi*zetap*dzeta*r*r*(u[j] + u[j+1])*(rho[j] +
                  rho[j+1])/4;
          end;
          func := m;
end;
{-----------------------------------}
begin
   f := func(t);
   i := 0;
   if grad = 0 then grad := -1.0e5;
   dt := (fact-f)/grad;
   repeat
       i := i + 1;
       fx := f; tx := t;
       t := t + dt;
       f := func(t);
       if abs(tx - t) < 1.0e-7 then dt := 0 else
       begin
          if (fx-f)/(tx-t) <> 0 then grad := (fx-f)/(tx-t);
          if grad = 0 then dt := 0 else dt := (fact-f)/grad;
       end;
   until (abs(dt/t) < 1.0e-12) or (i = 15);
end;
{-------------------------------------------------------------------------
**** Procedure calcv solves the radial velocity using the continuity eq. ****
-------------------------------------------------------------------------}
procedure calcv;
begin
   for j := 2 to jm do
   begin
      v[j] := (v[j-1]*r*rho[j-1]*zeta[j-1] - (zeta[j] - zeta[j-1])/dx*
     ((zeta[j]+zeta[j-1])/2*r*r*(rho[j]+rho[j-1])/2*(u[j]+u[j-1])/2 -
     (zeta[j]+zeta[j-1])/2*rw*rw*(rhow[j]+rhow[j-1])/2*(uw[j]+uw[j-1])/2))
      /r/rho[j]/zeta[j];
   end;
end;
```

```
{-------------------------------------------------------------------------
**** Procedure calcr solves the radial displacement of the tube wall using
     Eq. (3.22) ****
-------------------------------------------------------------------------}
procedure calcr(ri,ro,pin,po: extended; var r : extended);
var
   a1,a2,nu,e,dr : extended;
begin
   e := 2.0e9;
   nu := 0.3;
   a1 := (1 + nu)*(1 - 2*nu)*(pin*ri*ri - po*ro*ro)/(ro*ro - ri*ri)/e;
   a2 := (1 + nu)*(pin - po)*ri*ri*ro*ro/(ro*ro - ri*ri)/e;
   dr := a1*ri + a2*ri;
   r := ri + dr;
end;
{-------------------------------------------------------------------------
**** Procedure calccoeff calculates the coefficients for the momentum eq. ***
-------------------------------------------------------------------------}
procedure calccoeff;
var
   cnx,csx : extended;
begin
         for j := 2 to jmm1 do
         begin
            zetan := 0.5*(zeta[j] + zeta[j+1]);
            zetas := 0.5*(zeta[j] + zeta[j-1]);
            zetap := zeta[j];
            dzetan := zeta[j+1] - zeta[j];
            dzetas := zeta[j] - zeta[j-1];
            dzeta := 0.5*(zeta[j+1] - zeta[j-1]);
            mun := 0.5*(mu[j] + mu[j+1]);
            mus := 0.5*(mu[j] + mu[j-1]);
            dn := zetan * mun / zetap / r / r / dzetan / dzeta;
            ds := zetas * mus / zetap / r / r / dzetas / dzeta;
            con := rho[j] * (vw[j] + v[j])/ 2 / r / dzeta;
            if v[j] >= 0 then cn := dn else cn := dn - con;
            if v[j] >= 0 then cs := ds + con else cs := ds;

            con := con/2; cnx := dn - con; csx := ds + con;
            if (cnx > 0) and (csx > 0) then
            begin
               cn := cnx;
```

```
            cs := csx;
         end;

         cw := rho[j] * (uw[j] + u[j]) / 2 / dx;
         bp := - dpdx;
         cp := cn + cs + cw;
         c[j] := cs;
         a[j] := cn;
         b[j] := cp;
         dd[j] := cw * uw[j];
      end;
end;
{-------------------------------------------------------------------------
**** Procedure calcfi solves for the ion concentration ****
-------------------------------------------------------------------------}
procedure calcfi;
var
  vn,vs,zetan,zetap,mun,mus,dzetan,dzetas,dn,ds,cn,cs,ce,cw,cp  : extended;
begin
      for j := 1 to jmm1 do
      begin
         zetan := zeta[j+1];
         zetas := zeta[j];
         zetap := 0.5*(zeta[j] + zeta[j+1]);
         if j = jmm1 then dzetan := 0.5*(zeta[j+1] - zeta[j])
                     else dzetan := 0.5*(zeta[j+2] - zeta[j]);
         if j = 1 then dzetas := 0.5*(zeta[2] - zeta[1])
                  else dzetas := 0.5*(zeta[j+1] - zeta[j-1]);
         dzeta := zeta[j+1] - zeta[j];
         mun := lam[j+1];
         mus := lam[j];
         dn := zetan * mun / dzetan / dzeta;
         ds := zetas * mus / dzetas / dzeta;
         vn := v[j+1];
         vs := v[j];

         if j = jmm1 then cn := dn
         else
         begin
            cn := dn - r*zetan*rho[j+1]*vn/dzeta/2;
         end;
         cs := ds + r*zetas*rho[j]*vs/dzeta/2;
```

```
      cw := rw*rw*zetap*(rhow[j+1]+rhow[j])/2*(uw[j+1]+uw[j])/2/dx;
      if j = jmm1 then
      begin
         cp := dn + ds +
                   r*r*zetap*(rho[j+1]+rho[j])/2*(u[j+1]+u[j])/2/dx;
         cp := cp - r*zetas*rho[j]*vs/dzeta/2;
      end
      else
         cp := cn + cs + cw;
      if ds <> 0 then celrey[j] := r*zetas*rho[j]*vs/dzeta/ds;
      if (cn < 0) or (cs < 0) then
      begin
          if j = jmm1 then cn := dn
          else
          begin
               if vn >= 0 then cn := dn
               else cn := dn - r*zetan*rho[j+1]*vn/dzeta;
          end;
          if vs >= 0 then cs := ds + r*zetas*rho[j]*vs/dzeta
                     else cs := ds;

          cw := rw*rw*zetap*(rhow[j+1]+rhow[j])/2*(uw[j+1]+uw[j])
                /2/dx;
          if j = jmm1 then
          begin
          cp := dn + ds + r*r*zetap*(rho[j+1]+rho[j])/2*
              (u[j+1]+u[j])/2/dx;
             if vs < 0 then cp := cp - r*zetas*rho[j]*vs/dzeta;
          end
          else
             cp := cn + cs + cw;
      end;

      zz[j] := r*zetas*rho[j]*vs/dzeta - r*zetan*rho[j+1]*vn/dzeta +
               rw*rw*zetap*(rhow[j+1]+rhow[j])/2*(uw[j+1]+uw[j])/2/dx
               - r*r*zetap*(rho[j+1]+rho[j])/2*(u[j+1]+u[j])/2/dx;

      c[j] := cs;
      a[j] := cn;
      b[j] := cp;
      d[j] := cw * fiw[j];
   end;
```

```
gtri(a,b,c,d,fi,0,jm,2,2,0,0,-jss*r*(zeta[jm]-zeta[jmm1])/2/lam[jm],0);
end;



{-------------------------------------------------------------------------
*** Procedure readphysdat reads the physical data from file 'sodiumch.dat' **
-------------------------------------------------------------------------}
procedure readphysdat;
var
    f1 : text;
    i,j : integer;
    x : extended;
begin
    assign(f1,'sodiumch.dat');
    {$i-}
    Reset(f1);
    {$i+}
    if ioresult <> 0 then
    begin
       writeln('ERROR : Cannot find file sodiumch.dat.');
       halt;
    end;
    Readln(f1);
    I := 0;
    repeat
       I := I+1;
       Read(f1,Physdat[I,Aphys]);
       if (Physdat[I,Aphys] < Sentinel) then
       begin
            for Physchar := Dphys to Ephys do Read(f1,Physdat[I,Physchar]);
            Readln(f1);
            Physdat[I,Aphys] := Physdat[I,Aphys]/100.0;
            Physdat[I,Mphys] := Physdat[I,Mphys]/100.0;
            Physdat[I,Dphys] := Physdat[I,Dphys]*rhoo;
            Physdat[I,Ephys] := Physdat[I,Ephys]*muu;
       end
       else Readln(f1);
    until Physdat[I,Aphys] >= Sentinel;
    Nphys := I-1;
    close(f1);
```

```
end;
{-------------------------------------------------------------------------
*** Procedure readosmotdat reads the osmotic pressures from file 'osmot.dat'
-------------------------------------------------------------------------}
procedure readosmotdat;
var
    f1 : text;
    i,j : integer;
    x : extended;
begin
    assign(f1,'osmot.dat');
    {$i-}
    Reset(f1);
    {$i+}
    if ioresult <> 0 then
    begin
       writeln('ERROR : Cannot find file osmot.dat.');
       halt;
    end;
    Readln(f1);
    I := 0;
    repeat
       I := I+1;
       Read(f1,Osmotdat[I,MassOS]);
       if (Osmotdat[I,MassOS] < Sentinel) then
       begin
          Readln(f1,Osmotdat[I,PresOS]);
          Osmotdat[I,MassOS] := Osmotdat[I,MassOS]/100.0;
          Osmotdat[I,PresOS] := Osmotdat[I,PresOS]*1.01325e5;
       end
       else Readln(f1);
    until Osmotdat[I,MassOS] >= Sentinel;
    Nosmot := I-1;
    close(f1);
end;
{-------------------------------------------------------------------------
*** Function Physint interpolates for the physical properties ****
-------------------------------------------------------------------------}
Function Physint(Outtype,Intype : Physvar ; Inval : extended) : extended;
var
   Max,Min,Mid : Integer;
   Flag : boolean;
```

```
begin
   Max := Nphys;
   Min := 1;
   Flag := false;
   case Intype of
   Aphys,Dphys,Mphys,Ephys :
        begin
           repeat
               Mid := (Max+Min+1) div 2;
               if Inval < Physdat[Mid-1,Intype] then
                  Max := Mid-1
               else if Inval > Physdat[Mid,Intype] then
                  Min := Mid
               else
                  Flag := true;
           until Flag or (Max <= Min);
        end;
   else
        begin
          writeln('ERROR : Property not in table in function Physint');
          halt;
        end;
   end;
   Physint :=(Physdat[Mid,Outtype]-Physdat[Mid-1,Outtype])*
             (Inval-Physdat[Mid-1,Intype])/(Physdat[Mid,Intype]-
             Physdat[Mid-1,Intype])+ Physdat[Mid-1,Outtype];
end;
{-------------------------------------------------------------------------
*** Function Osmotint interpolates for the osmotic pressure ****
-------------------------------------------------------------------------}
Function Osmotint(Outtype,Intype : Osmotvar ; Inval : extended) : extended;
var
   Max,Min,Mid : Integer;
   Flag : boolean;
begin
   Max := Nosmot;
   Min := 1;
   Flag := false;
           repeat
               Mid := (Max+Min+1) div 2;
               if Inval < Osmotdat[Mid-1,Intype] then
                  Max := Mid-1
```

```
                else if Inval > Osmotdat[Mid,Intype] then
                   Min := Mid
                else
                   Flag := true;
             until Flag or (Max <= Min);
    if Max <= Min then writeln('Interpolation out of range in Osmotint');
    Osmotint := (Osmotdat[Mid,Outtype]-Osmotdat[Mid-1,Outtype])*
                (Inval-Osmotdat[Mid-1,Intype])/(Osmotdat[Mid,Intype]-
                Osmotdat[Mid-1,Intype])+Osmotdat[Mid-1,Outtype];
end;
{-------------------------------------------------------------------------
*** Procedure calcmwall calculates the wall velocity using Eq. (3.20) ****
-------------------------------------------------------------------------}
procedure calcmwall(po,p,fiwall,dx,r : extended; var mwall,vwall : extended);
var
   delp,vwallo,posmot,rex : extended;
begin
   rex := 0.5;
   vwallo := vwall;
   posmot := Osmotint(PresOS,MassOS,fiwall);
   delp := p-po;
   vwall := (delp - posmot)*(2.2 - 0.00667*delp*1.0e-5)*1.0e-12;
   if vwall < 0 then vwall := 0;
   vwall := rex*vwall + (1-rex)*vwallo;
   mwall := 2*pi*r*dx*vwall*rhoo;
end;
{-------------------------------------------------------------------------
*** Function Diffint calculates the diffusion coefficient for the
    concentration eq. ****
-------------------------------------------------------------------------}
Function Diffint(x : extended) : extended;
var
   y : extended;
begin
   if x < 0.00582 then y := (1.483 - 1.545)/(0.00582 - 0.000585)*
                            (x - 0.000585) + 1.545
                  else y := (1.484 - 1.483)/(0.05627 - 0.00582)*
                            (x - 0.00582) + 1.483;
   Diffint := y*1.0e-9;
end;
{-------------------------------------------------------------------------
                          *** Main program ****
```

```
------------------------------------------------------------------------}
begin
   assign(f4,'f4.out');
   rewrite(f4);
   rhoo := 997.4;              {density}
   muu := 9.8e-4;              {viscosity of water}
   readphysdat;
   readosmotdat;
   for jj := 1 to 5 do         {repeat simulation for 5 inlet pressures}
   begin
   uin := 1.0;                 {mean inlet velocity}
   di := 0.5e-3;               {tube inside diameter}
   pin := 60.0e5;              {inlet pressure}
   fiin := 0.02;               {inlet concentration}
   lopd := 5000;               {L/D}
   pin := s3[jj];              {inlet pressure}
   ri := di/2;                 {inside radius}
   jm := 61;                   {number of grid points in y-direction}
   mm := round((jm-1)/2);      {constant dzeta increments}
   writeln('jm,mm ',jm:4,mm:4);
   nn := jm - mm - 1;          {variable dzeta increments}
   exrat := 0.9;               {grid contraction ratio}
   ro := ri*6/5;               {outside radius}
   rw := ri;                   {inlet radius}
   po := 1.0e5;                {outside pressure}
   im := 50;                   {number of grid points in x-direction}
   length := 2*ri*lopd;        {length of tube}
   grad := -1.0e-4;            {initial guess of dm/d(dpdx)}

   bb := 1.367e-7;             {membrane constant}
   rey := rhoo*uin*rw*2/muu;
   writeln(' Reynoldsgetal = ',rey:9:2);
   pw := pin;
   jmm1 := jm-1;
   dx := length/(im-1);
   for j := 1 to jm do vw[j] := 0;
   for j := 1 to jm do rhow[j] := Physint(Dphys,Aphys,fiin);
   for j := 1 to jm do mu[j]  :=  Physint(Ephys,Aphys,fiin);
   for j := 1 to jm do lam[j] :=  Diffint(fiin)*rhow[j];
   for j := 0 to jm do fiw[j] :=  fiin;

   if exrat = 1 then
```

```
begin
   dzeta := 1/(jm-1);
   zeta[1] := 0; for j := 2 to jm do zeta[j] := zeta[j-1] + dzeta;
end
else
begin
   dzeta := 1/((pow(exrat,nn) - 1)/(exrat - 1) + mm);
   zeta[1] := 0;
   for j := 2 to mm + 1 do zeta[j] := zeta[j-1] + dzeta;
   for j := mm + 2 to jm do zeta[j] := zeta[j-1] + dzeta*pow(exrat,j-mm-2);
end;

for j := 1 to jm do uw[j] := 2*uin*(1-zeta[j]*zeta[j]);

dpdx := -5e5;
{***** Calculate inlet mass and concentration flux *****}
mw := 0;
flux := 0;
for j := 1 to jmm1 do
begin
   dzeta := zeta[j+1] - zeta[j];
   zetap := 0.5*(zeta[j+1] + zeta[j]);
   flux := flux + 2*pi*zetap*dzeta*rw*rw*(uw[j] + uw[j+1])*(rhow[j]
           + rhow[j+1])/4*fiw[j];
   mw := mw + 2*pi*zetap*dzeta*rw*rw*(uw[j] + uw[j+1])*(rhow[j]
           + rhow[j+1])/4;
end;
influx := flux;
inmass := mw;
writeln('inmass = ',inmass:13,influx:13);
vwall := 0;
{****** Start of integration scheme ******}
n := 0;
wflux := 0;
wfluxs := 0;
for i := 1 to im do
begin
   n := n + 1;
   r := rw;
   p := pw;
   for j := 1 to jm do u[j] := uw[j];
   for j := 1 to jm do v[j] := vw[j];
```

```
      for j := 1 to jm do rho[j] := rhow[j];
      for j := 0 to jm do fi[j] := fiw[j];
      it := 0;
      sum := 1;
      repeat
         it := it + 1; sumo := sum;
         calccoeff;
         calcmwall(po,(p+pw)/2,(fi[jm]+fi[jm])/2,dx,r,mwall,vwall);
         jss := bb*fi[jm]*rho[jm]*(1-bb/(vwall + bb));   {Eq. (5.9)}
         mwalls := 2*pi*r*dx*jss;
         m := mw-mwall-mwalls;
         NewtonRaphson(m,dpdx,grad);
         calcv;
         calcfi;
         p := pw + dpdx*dx;
         calcr(ri,ro,p,po,r);
         sum := 0; for j := 1 to jm do sum := sum + u[j];
         for j := 1 to jm do rho[j] := Physint(Dphys,Aphys,fi[j]);
         for j := 1 to jm do mu[j]  := Physint(Ephys,Aphys,fi[j]);
         for j := 1 to jm do lam[j] := Diffint(fi[j])*rho[j];
      until (it = 30) or (abs((sum - sumo)/sumo) < 1.0e-9);
      rout := (r-ri)/ri*100;
      wfluxs := wfluxs + mwalls;
      wflux := wflux + mwall + mwalls;
      {Calculate concentration flux}
      flux := 0;
      for j := 1 to jmm1 do
      begin
         dzeta := zeta[j+1] - zeta[j];
         zetap := 0.5*(zeta[j+1] + zeta[j]);
         flux := flux + 2*pi*zetap*dzeta*r*r*(u[j] + u[j+1])*(rho[j]
                 + rho[j+1])/4*fi[j];
      end;
      sigg := i*dx/r/(rhoo*uin*r/mu[1]);
      writeln(i:4,sigg:8:4,m+wflux:15,' ',flux+wfluxs:15,'
              ',u[1]/uin:7:3,p:13,it:4,fi[jmm1]*100:12,flux/m:8:5);
      writeln('  j       fi       rho        mu      lam      u/uin          v');
      for j := jm-4 to jm do writeln(j:4,fi[j]*100:11:5,
               ' ',rho[j]:9:4,mu[j]:11:7,lam[j]:13,' ',
                zz[j]:13,celrey[j]:13);
      for j := 1 to jm do uw[j] := u[j];
      for j := 1 to jm do vw[j] := v[j];
```

```
      for j := 1 to jm do rhow[j] := rho[j];
      for j := 0 to jm do fiw[j] := fi[j];
      rw := r;
      mw := m;
      pw := p;
   end;
   vmax := 0; for j := 1 to jm do if v[j] > vmax then vmax := v[j];
   q := 0;
   for j := 1 to jmm1 do
      begin
         dzeta := zeta[j+1] - zeta[j];
         zetap := 0.5*(zeta[j+1] + zeta[j]);
         q := q + 2*pi*zetap*dzeta*r*r*(u[j] + u[j+1])/2;
      end;
   ener[jj] := (inmass - m)/(q*(pin-p) + (inmass - m)*(pin - po)/rhoo);
   writeln(jj:4,ener[jj]*1000:14);
   end; {jj}

   for jj := 1 to 5 do writeln(f4,s3[jj]/1e5:9:2,ener[jj]*1000:9:5);

   close(f4);
   writeln('Done...');readln;
end.
```